FILE COPY

CR 51

AN EXPERIMENTAL STUDY OF SOIL WATER FLOW SYSTEMS INVOLVING HYSTERESIS

by

A. Klute and R.W. Gillham

August 1973

Colorado State University
Fort Collins, Colorado

Completion Report
No.51

AN EXPERIMENTAL STUDY OF SOIL WATER FLOW SYSTEMS INVOLVING HYSTEREISIS

Completion Report

OWRR Project No. A-014-COLO

by

A. Klute and R. W. Gillham
Department of Agronomy
Colorado State University, and
USDA-Agricultural Research Service

Submitted to

Office of Water Resources Research
U. S. Department of Interior
Washington, D. C. 20240

August 1973

The work upon which this report is based was supported (in part) by funds provided by the United States Department of the Interior, Office of Water Resources Research, as authorized by the Water Resources Research Act of 1964, and pursuant to Grant Agreement Nos. 14-31-0001-3206, 14-31-0001-3506, 14-31-0001-3806, and 14-31-0001-4006.

Colorado Water Resources Research Institute
Colorado State University
Fort Collins, Colorado 80523

Norman A. Evans, Director

ABSTRACT

AN EXPERIMENTAL STUDY OF SOIL WATER
FLOW SYSTEMS INVOLVING HYSTERESIS

The hydraulic functions, i.e., hydraulic conductivity-water content and pressure head-water content relationships, were measured in an unsteady state flow situation on a column of sand using gamma absorption for water content measurements and pressure transducer tensiometry for pressure head measurements. Subsequently, the same flow column was subjected to a boundary condition that caused drainage and rewetting of the column. Measurements of pressure head, hydraulic head and water content versus time were made at various positions. These data were compared with the predictions from soil water flow theory which included the effects of hysteresis in the water content-pressure head relationship. Measured and predicted pressure head-time curves were in reasonable agreement, but measured and predicted water content-time curves were not always in good agreement.

Klute, A. and W. R. Gillham
AN EXPERIMENTAL STUDY OF SOIL WATER FLOW SYSTEMS INVOLVING HYSTERESIS
Completion report to Office of Water Resources Research, Department of the Interior, August 1973, Washington, D. C., 105 p.

KEYWORDS: water flow/soil water/unsaturated flow/hysteresis/water retention/gamma attenuation/tensiometry.

INTERPRETIVE SUMMARY

The ability of soils to store water is measured by a property known as a water retention curve, which is a relation between the water content and the soil water pressure. At saturation the soil water pressure is at or near atmospheric, and as the soil becomes desaturated the soil water pressure becomes less than atmospheric. Thus we speak of a water content-soil water pressure relation or function. This function is not single valued, i.e., the function obtained for drainage of a soil differs from that for wetting of the soil. The term hysteresis is applied to this phenomenon. It is one of the goals of soil physics to be able to predict the behavior of water in soil from basic physical principles. In order to accomplish this goal, knowledge of the hysteresis described above is required, and this information must be properly incorporated into the prediction scheme. The work described in this paper reports an attempt to measure the hysteretic relationship for a given porous material and to use this data to predict the behavior of water in the same material under certain imposed conditions. The work has advanced our understanding of the behavior of water in soil.

TABLE OF CONTENTS

Mention of proprietary names of products in this report does not imply endorsement by the U. S. Department of Agriculture or the U. S. Department of the Interior over products not mentioned.

LIST OF FIGURES

Figure | Page

Figure | Page

BACKGROUND:

The water content-pressure head relation for most porous media, including soils, exhibits the phenomenon called hysteresis (Childs, 1969; Miller and Miller, 1956). The water content obtained by drainage to a given pressure head is larger than the water content obtained by wetting to the same pressure head. In addition there is an infinite family of wetting scanning curves and draining scanning curves between the main drainage water content-pressure head curve and the main wetting water content-pressure head curve. In general it is impossible to infer, without ambiguity, the water content from a given value of the pressure head and vice versa. It is necessary to give additional information which will identify the particular scanning curve that is applicable.

The theory for water flow in unsaturated soil which is based on the Darcy equation and the continuity equation, leads to a nonlinear partial differential equation of flow with either the water content or the soil water pressure head as the dependent variable. In the development of this equation it is necessary to introduce a relation between water content and pressure head. This function is hysteretic, and it may also depend on position as in a nonuniform soil profile. The hydraulic conductivity-water content relation, which also appears in the flow equation, may also exhibit some hysteretic behavior but in many cases may be taken as non-hysteretic.

The nonlinear nature of the flow equation has largely precluded analytic solution and numerical and approximate means of solution have had to be used. To avoid the complications introduced by hysteresis it has been customary to restrict analysis to those situations where the flow was of such a nature that all changes of water content, θ, (and pressure head, h)

were monotonic functions of time, i.e., always increasing or always decreasing. In such cases $\frac{\partial \theta}{\partial t}$ does not change algebraic sign during the flow. Analyses of a large number of unsteady state flow systems have been made in this way, e.g., infiltration (both horizontal and vertical), drainage, and evaporation.

In natural situations, i.e. "the field," the commonly occurring flow systems involve some aspect of hysteresis. For example, infiltration, perhaps from rain or ponded water, is followed by a combined period of drainage, redistribution and evaporation at the surface. Thus there will be parts of the flow system in which $\partial\theta/\partial t$ will change sign during the source of the flow and the hysteretic nature of the water content-pressure head function must be utilized in the analysis of such flow.

As will be seen upon reading the more detailed literature review in the following pages, there have been several numerical procedures developed to account for hysteresis (Rubin, 1967; Ibrahim and Brutsaert, 1968; Hanks et al., 1969). However, not much comparison of the results of these procedures has been made with experimental data. There is a definite need for more experimental testing of the predictions of the analyses of hysteric flow. In the course of development of the hysteretic analyses certain simplifying assumptions as to the nature of the hysteresis are usually made. Experimental testing is needed to determine whether or not these approximations are adequate. If significant discrepancies are found, it may be possible, with knowledge of the nature of these discrepancies, to improve upon the method of analysis.

PROJECT OBJECTIVES:

1. To make measurements of the hydraulic conductivity-water content and water content-pressure head relationships for selected soils and porous materials. This will include as much of their hysteretic nature as can be determined.

2. To conduct experimental observations of the behavior of selected hysteretic flow systems in laboratory models.

3. To compare the observed behavior with that predicted by solutions of the flow equation for water in unsaturated soils in which hysteresis is considered, and thus evaluate the predictive value of such analyses.

The text of the main body of a Ph.D. thesis is reproduced in the following pages. The thesis is being submitted to the Graduate School of the University of Illinois at Urbana, Illinois, by R. W. Gillham as part of the requirements for the Ph.D. degree in Agronomy. Mr. Gillham is completing the requirements for the Ph.D. in absentia from the University of Illinois.

COOPERATION:

The research described in this report was carried out in cooperation with and with partial financial support from the USDA, Agricultural Research Service, Colorado-Wyoming Area, Fort Collins, Colorado.

PUBLICATIONS IN PREPARATION:

A paper from this research will be presented at the American Society of Agronomy Annual Meeting in Las Vegas, Nevada, November 11-16, 1973 entitled "Hysteretic flow in a porous medium: Experimental results and theoretical prediction," and a manuscript with this title will be prepared for publication in the Soil Science Society of America Proceedings.

Two other publications are being prepared, one concerning the methods of measurement of the hysteretic properties of a porous medium, and one concerning the effect of various simplifications of the representation of the hysteretic properties upon the numerical predictions of flow system behavior.

HYSTERETIC WATER FLOW IN A POROUS MEDIUM: EXPERIMENTAL STUDY AND NUMERICAL SIMULATION

BY

ROBERT WINSTON GILLHAM

B.S.A., University of Toronto, 1963
M.Sc., University of Guelph, 1968

THESIS

Submitted in partial fulfillment of the requirements
for the degree of Doctor of Philosophy in Agronomy
in the Graduate College of the
University of Illinois at Urbana-Champaign, 1973

Urbana, Illinois

HYSTERETIC WATER FLOW IN A POROUS MEDIUM: EXPERIMENTAL STUDY AND NUMERICAL SIMULATION

Robert Winston Gillham, Ph.D.
Department of Agronomy
University of Illinois at Urbana-Champaign, 1973

A finite difference solution of the flow equation for saturated-unsaturated flow was tested experimentally under conditions of hysteretic flow in a non-uniform medium. The medium used was a column of dune sand 60 cm long, and flow was in the vertical direction. The numerical solution required that the hysteretic water content-pressure head and conductivity-water content relations be specified as a function of the vertical space coordinate. From wetting and drainage cycles performed on the column with simultaneous measurement of water content and pressure head, families of primary wetting and drying scanning curves were measured at 2 cm intervals along the column. Water content was measured by gamma ray attenuation and pressure head by rapid response tensiometry. An efficient means of representing the hysteresis information within the computer by empirical equations was developed. The conductivity-water content functions were measured by transient flow methods and represented by empirical equations.

Boundary conditions resulting in hysteretic flow were imposed on the laboratory column and the numerical solution and the resulting measured and predicted water content and pressure head profiles compared. In the first experiment, the medium was partially drained and rewet at a rate approximately equal to that used during collection of the hysteresis data. Very good agreement was found between the measured and predicted results giving confidence in the flow equation, the numerical solution of the equation and the procedure used for incorporating hysteresis and non-uniformity into the solution. The same flow experiment was simulated using only the main

drainage curve in place of the families of wetting and drying curves. There was no apparent decrease in the accuracy with which the pressure heads were predicted; however, there was considerable error in the predicted water content values.

The second flow experiment was similar to the first, but the drainage and rewet rates were approximately twice as great. The agreement between measured and predicted results was quite good, indicating that under the conditions of this experiment, a rate dependence of the water content-pressure head relation did not cause serious errors in the predicted results.

In the third experiment, a cyclic step change in the pressure head was applied at the lower boundary of the column. The predicted water contents and pressure heads differed appreciably from those measured. There was insufficient data to determine whether the differences were caused by numerical inaccuracies or experimental difficulties. As more cycles were performed the difference between measured and predicted results did not increase. This suggested that secondary and higher order families of scanning curves were not required in the description of the water content-pressure head relation.

ACKNOWLEDGEMENTS

The author would like to thank the members of his Doctoral committee, Dr. Doyle Peters, Dr. Arnold Klute, Dr. Charles Boast, Dr. John Gieseking and Dr. Walter Lembke; and Dr. Richard Millington and Dr. Adrian Schiedegger for serving as committee members at the preliminary examination.

Particular thanks are due Dr. Klute, Department of Agronomy, Colorado State University, Fort Collins, for his valuable advice and assistance throughout the course of the research and manuscript preparation, and Dr. Dale Heermann, Agricultural Research Service, Fort Collins, Colorado, for his assistance with the computer aspects of the project.

The research reported here was conducted in absentia in the Department of Agronomy, Colorado State University. Appreciation is extended to Dr. Robert Whitney, Department Head, for accommodating the author in his department.

The work reported in this thesis was supported in part by funds provided by the United States Department of the Interior, Office of Water Resources Research Act of 1964, Allotment Program Project No. A-014 Colo. Partial support was also provided by the U.S.D.A., A.R.S. Financial support afforded the author by the University of Illinois during the first two years of his Doctoral studies is gratefully acknowledged.

Finally, the author wishes to thank his wife, Virginia, for her continued help and encouragement throughout his Doctoral programme.

I. INTRODUCTION

In principle, the differential equation describing the flow of the solution phase in a partially saturated porous medium can be solved to predict the time and spatial distributions of water content and pressure head which would result from imposed initial and boundary conditions. As a result of the non-linearity in the equation, analytical solutions are available for only a few rather artificial flow systems. A number of steady state flow problems can be solved analytically, and semi-analytical solutions have been derived for the unsteady state problems of horizontal and vertical infiltration [Philip (1969)]. The unsteady state analytical solutions assume a semi-infinite homogeneous medium and require that the boundary conditions be time-invariant, thus imposing severe limitations on their applicability to natural systems.

Natural systems are typified by inhomogeneous media and have time-dependent boundary conditions. In addition, the media must frequently be considered as finite. These complexities have been incorporated into solutions of the flow equation with apparent success by the application of computerized numerical solution techniques [Remson et al (1971)].

The soil surface, or upper boundary of a natural flow system, will generally experience cyclic changes in water content. As a consequence, regions of the medium will go through cycles of wetting and draining. A similar consequence would result from fluctuations in the water table elevation. The result is an hysteretic flow system. The phenomenon of hysteresis will be considered in greater detail in the section to follow. In soil physics the term usually refers to the fact that the water content corresponding to a particular pressure head depends upon the previous wetting and drying history of the medium. To solve the flow equation, the functional relationship

between the water content and pressure head must be specified, thus, as the medium wets, one functional relationship would apply, and as it drains, a different relationship would apply. The appropriate relationship depends upon the water content (or pressure head) at which the reversal (change of sign of $\partial h/\partial t$) occurred. Most porous media appear to have a highly hysteretic water content-pressure head relationship, and since natural boundary conditions induce hysteretic flow systems, hysteresis should be accounted for in solutions of the flow equation. Numerical solutions have been proposed which account for limited forms of hysteresis; however, owing to the difficulty of characterizing the hysteretic nature of a porous material, particularly an inhomogeneous medium, these solutions have not been verified experimentally. In addition to the difficulties associated with measuring the hysteretic nature of an inhomogeneous medium, a major problem is the representation of the hysteretic water content-pressure head function in a form which can be readily stored in the computer and is readily available for use by the computer.

The logical extension of the work which has been done previously is the construction of a numerical solution which is capable of accounting for hysteresis as it occurs in natural flow systems. Since comparable analytical solutions are not available, the validity of such a solution must be tested against experimental results. This solution could, in turn, be used to assess the effect of hysteresis on the solutions and to gain some insight into the amount of detail necessary in describing the hysteretic nature of a material in order for the model to adequately simulate the flow system.

II. REVIEW OF LITERATURE

A. The Flow Equation

Combination of the Darcy equation with the equation of continuity for the solution phase yields the partial differential equation for flow in a partially saturated porous medium:

$$\frac{\partial \theta}{\partial t} = \nabla(K\ (\theta)\ \nabla\ H) \qquad (1)$$

where θ is the volumetric water content, t is time, K the hydraulic conductivity and H hydraulic head. The hydraulic head is the sum of the pressure head h and gravitational head $\bar{z}$ where $\bar{z}$ is considered positive in the upward direction and is the elevation above some arbitrary datum; thus:

$$H = h + \bar{z} \qquad (2)$$

Klute (1971) discussed in considerable detail the assumptions which are made in applying (1). A partial list of these includes the assumptions that the Darcy equation is valid, the porous matrix is rigid, the gas phase has a constant total pressure, and the system is isothermal. In spite of the many assumptions, Klute (1971) observed that the Darcy based flow equation is an adequate model for predicting unsaturated flow behaviour in many instances, and at worst, serves as a point of departure for a modified theory.

Introduction of the water capacity C defined as:

$$C = {}^{\partial h}/_{\partial \theta} \qquad (3)$$

reduces from two to one the number of dependent variables in equation (1). Substituting (2) and (3) into (1) and assuming one dimensional flow in the vertical direction yields the pressure head form of the flow equation:

$$C\ (h)\ \frac{\partial h}{\partial t} = \frac{\partial}{\partial \bar{z}}\ (K\ (h)\ \frac{\partial h}{\partial \bar{z}}\ ) + \frac{\partial k}{\partial \bar{z}}\ (h) \qquad (4)$$

The properties of the medium which control the flow of the solution phase are the water capacity C(h) and the hydraulic conductivity K(h).

In developing equation (4), the water capacity was assumed to be independent of $\partial\theta/\partial t$. Some recent evidence indicates that this may not be the case.

Topp et al (1967) measured the desorption $\theta(h)$ curve for a small rectangular parallelepiped sample of fine sand subjected to unsteady state, steady state and static equilibrium conditions of flow. Three different unsteady flow rates were imposed. The water contents corresponding to a given pressure head were similar for the three unsteady flow cases, but were greater than the water contents for static equilibrium and steady state flow conditions. Rogers and Klute (1971) reported similar results from experiments in which a column of sand was allowed to drain from saturation at different rates.

Smiles et al (1971) tested the uniqueness of the water content-pressure head relationship for a sand medium in a horizontal column under conditions of non-hysteretic flow. Both drainage and wetting soil characteristics were studied. For the medium used, the wetting characteristic curve appeared to be independent of $\partial\theta/\partial t$; however, the drainage curve was dependent upon the rate of drainage. Smiles showed that the rate dependence of the water content-pressure head relationship could cause significant errors when the diffusivity form of the flow equation is applied in the analysis of desorption flow phenomena.

Additional research is required to determine the extent to which the water capacity is dependent upon the rate of flow in a wider range of kinds of soil materials than has heretofore been investigated. The incorporation of the rate dependence into the flow equation should be studied and its significance in various flow situations should be assessed.

The general nature of the hysteresis in the $\theta(h)$ function is shown in Figure 1. If the medium is draining from complete saturation, the applicable water capacity function is obtained from the slope of the "initial drainage curve" (IDC). If the system is wetting from a water content near the residual water content, the water capacity is the slope of the "main wetting curve" (MWC). When a pressure head of zero is reached by proceeding along the main wetting curve, a water content less than that at complete saturation is reached as a result of entrapment of air within a portion of the pore space. If drainage is induced at this point, the water capacity is determined from the "main drainage curve" (MDC). Furthermore, if during drainage the pressure head is reversed before the water content approaches the residual water content, the water content will proceed along a "primary wetting scanning curve" (PWSC). There are an infinite number of primary wetting scanning curves, and similarly, an infinite number of "primary drainage scanning curves" (PDSC). Topp and Miller (1966) described in detail the hysteretic nature of two glass bead media. In addition to the families of primary scanning curves, they measured families of secondary scanning curves. If a reversal occurs while on a primary drainage scanning curve, the water content proceeds along a "secondary wetting scanning curve" (SWSC). Similarly, if a reversal occurs while on a primary wetting scanning curve, the water content proceeds along a "secondary drainage scanning curve" (SDSC). Associated with each primary scanning curve is an infinite number of secondary scanning curves. Higher order scanning curves can similarly be defined.

The hydraulic conductivity within the unsaturated zone is a function of water content, ie $K(\theta)$. Various workers have reported hysteretic $K(\theta)$ relationships. Using the pressure plate outflow technique, Collis-George and Rosenthal (1966) found three coarse-textured materials to exhibit

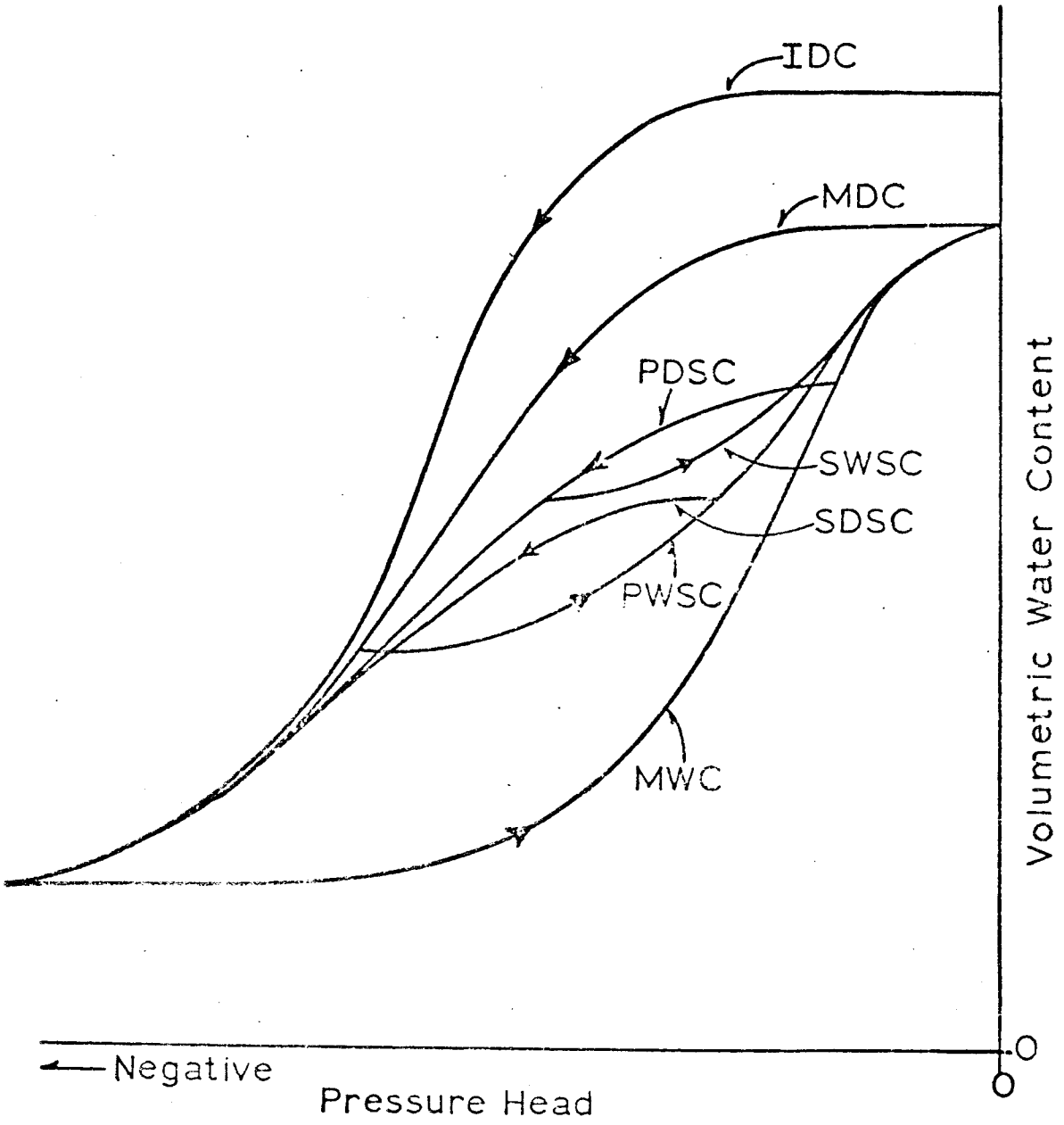

Figure 1. Diagram of typical hysteresis curves, where IDC is the initial drainage curve, MWC and MDC are main wetting and drainage curves respectively, PWSC and PDSC are primary wetting and drainage scanning curves and SWSC and SDSC are secondary wetting and drainage scanning curves.

hysteresis in $K(\theta)$.

Topp and Miller (1966) measured the water content and pressure head simultaneously in a small rectangular sample using gamma ray attenuation and rapid response tensiometry. They reported little or no hysteresis in $K(\theta)$. Similar results were reported for column experiments by Rogers and Klute (1971), and Vachaud and Thony (1971). Although a degree of uncertainty still exists, it appears that the assumption of a single valued functional relationship between the hydraulic conductivity and water content would introduce very slight errors into solutions of the flow equation.

Equation (4) can be written in dimensionless form as:

$$\gamma(\Phi)\frac{\partial\Phi}{\partial\tau} = \frac{\partial}{\partial\zeta}\left(\varkappa(\Phi)\frac{\partial\Phi}{\partial\zeta}\right) + \frac{\partial\varkappa}{\partial\zeta}(\Phi) \qquad (5)$$

The dimensionless variables are defined by:

i) dimensionless pressure head, $\Phi = h/L$

ii) dimensionless conductivity, $\varkappa = K/K_s$

iii) dimensionless position, $\zeta = Z/L$

iv) dimensionless time, $\tau = tK_s/\theta_s L$

v) dimensionless water content, $\Theta = \theta/\theta_s$

vi) dimensionless water capacity, $\gamma = C(h)L/\theta_s$

where L is a characteristic length of the flow system, K_s is the conductivity of the medium at saturation and θ_s is the saturated water content.

B. Solutions of the Flow Equation

The solution of equation (4) requires that the initial condition and two boundary conditions be specified. Since K and C are both functions of pressure head, the equation is non-linear and difficult to solve analytically except in a few cases of simple initial and boundary conditions.

The solutions of idealized problems such as those presented by Philip

(1969) for horizontal and vertical infiltration have been invaluable aids to an understanding of the unsaturated flow process, but, of course, cannot be directly and quantitatively applied to more natural flow systems involving cyclic boundary conditions and inhomogeneous soil materials. The complications of hysteresis, and non-uniform media, can be incorporated into numerical schemes for solution of equation (4). The remainder of this discussion will deal with finite difference solutions of the flow equation; particularly those solutions which have attempted to account for hysteresis.

In finite difference solutions of the flow equation, the space and time axes are divided into finite elements and the spatial and time derivatives of the flow equation are replaced by finite difference approximations. By applying the appropriate boundary and initial conditions, the resulting system of algebraic equations can be solved for the pressure head at each node of the time-space grid.

The effect of hysteresis was introduced into a numerical solution of the flow equation by Whisler and Klute (1965). The finite difference equation used was similar to the Crank-Nicolson equation modified to include gravity. The resulting set of linear equations was solved by the iterative procedure of Richtmyer (1957). The flow problem considered was infiltration into a vertical column at equilibrium under gravity. In draining to equilibrium, regions at different elevations have different equilibrium water contents and thus, upon infiltration, wet up along different wetting scanning curves, requiring a different $h(\theta)$ function at each point (node) in the column. The solution was restricted to a wetting process. There was no provision to allow for sequences of wetting and drying. The conductivities and water capacities used were for two hypothetical soils; therefore, the predicted water content and pressure head profiles could not be compared with experimental results.

The predicted results did appear to be qualitatively reasonable. In three different simulations, the water capacity was determined from: i) the main drainage curve, ii) the main wetting curve, and iii) the family of wetting scanning curves. The three methods resulted in quite different predicted water content distributions suggesting that hysteresis cannot be ignored when solving hysteretic flow problems.

Rubin (1967) developed a numerical solution of the diffusivity form of the flow equation for redistribution after infiltration into a vertical soil column. In such a flow system, regions near the surface of the column continue to drain throughout the redistribution period. Regions at some depth would begin to wet at some time and continue to wet, whereas intermediate regions would wet for a period, then begin to drain. At the start of the redistribution process, all points of the flow system were considered to be somewhere on the main wetting curves. During the course of redistribution, a comparison of the fluxes into and out of each finite element was made to determine whether the element was continuing to wet, or had begun to dry. As drying commenced, the water capacity was determined from the appropriate drying scanning curve. Once an element began to drain, there was no provision for that element to return to a wetting condition. This appears reasonable for a redistribution process, however, the procedure could not be used to analyze flow systems with repeated wetting and drying sequences. Since the diffusivity form of the flow equation was used, the solution is restricted to systems, all parts of which remain at a water content less than saturation. The redistribution patterns predicted by Rubin appeared to be reasonable; however, they were not compared with experimental results.

Ibrahim and Brutsaert (1968) studied the flow system resulting from intermittent infiltration into a homogeneous soil. Such flow systems involve

wetting and drying sequences, thus requiring a consideration of hysteresis. In their solution, the water content and pressure head were both retained as dependent variables. The pressure head-water content function was considered to be hysteretic, and was determined using the independent domain model as proposed by Poulovassilis (1962). The results shown by Ibrahim and Brutsaert appeared to be qualitatively reasonable; however, their analysis was for a hypothetical loam soil and thus could not be compared with experimental results. Furthermore, recent work [Topp (1969)] indicates that the independent domain model may not be applicable in soils.

Staple (1969), considered redistribution in three soils, Uplands sand, Castor loam and Rideau clay. The flow equation was solved using both explicit and implicit finite difference schemes. Computed water contents were compared with experimentally determined water content profiles. Good agreement was found; however, the computed results were fitted to the experimental results in certain regions. The diffusivity in the wetting to drying transition region was adjusted such that the computed flux through that region agreed with the experimentally determined flux. For this reason, the procedure has questionable predictive capability. The conductivity and diffusivity functions were obtained from samples of soil other than those used in the flow experiments. This could have accounted for some of the discrepancies observed. Also, the $h(\theta)$ relationship was determined under static flow conditions and therefore may not be applicable to the unsteady state system which was simulated.

In a similar experiment, Staple (1970), considered second and third cycle wetting as well as the initial infiltration and redistribution cycle for Rideau clay and Uplands sand. Different $K(\theta)$ and $D(\theta)$ functions were required for the second and third cycles than had been determined for the

freshly packed columns. As in the previous paper, the conductivities had to be adjusted in order to get acceptable agreement between measured and predicted results. Staple found that hysteresis had a significant effect on the computed results, i.e., different results were obtained if the main drainage curve was used rather than using the appropriate scanning curves. In the work of Staple, the medium was assumed to be homogeneous and the $K(\theta)$ and $h(\theta)$ information for the soil was stored in the computer in tabular form.

Hanks et al (1969) developed a modification of the Hanks and Bowers (1962) procedure to account for hysteresis. In this procedure, the wetting and drying scanning curves were assumed to be straight lines, and the slope of the wetting curves was assumed to be equal to the slope of the drying curves. The slope of the scanning "line" was considered to be a function of the reversal water content. The water content at each position was calculated from the computed pressure heads. The curve to be used (wetting, drying or scanning) in this calculation was determined from the calculation at the previous time step, i.e., if the moisture content at a point continued to increase, then the moisture content would continue to be determined from the appropriate wetting scanning curve. If a reversal in the sign of $\partial\theta/\partial t$ was observed, θ was calculated from the appropriate drying curve. The computational procedure was compared with experimental results for infiltration, redistribution and evaporation in columns of Nunn clay loam. The computed and measured positions of the wetting front and the average soil water contents above the wetting fronts, were in good agreement.

Freeze (1969) introduced a numerical solution to simulate flow through an integrated saturated-unsaturated system. The solution was applicable to homogeneous, isotropic soils and allowed for hysteresis in the $h(\theta)$ and $K(h)$ functions. The model also allowed for a variety of upper boundary conditions

including constant rate rainfall, ponded water and evaporation. The finite-difference scheme used was similar to that used by Rubin and Steinhardt (1963) but was modified to incorporate the different boundary conditions. The effect of a variety of soil and flow conditions was demonstrated by applying the numerical solution; however, the results were not compared with experimental data.

Freeze and Banner (1970) compared the results of the mathematical model [Freeze (1969)] with the results of flow experiments in laboratory columns. The medium used was a fine to medium sand. The main wetting and main drying curves of the $h(\theta)$ function were determined using steady state procedures on separate samples and the $K(h)$ function was determined on the experimental column using steady state methods. Based upon the experimental evidence, $K(h)$ was assumed to be non-hysteretic, while considerable hysteresis in the $h(\theta)$ function was observed. As discussed previously, there is a considerable body of evidence indicating that $K(\theta)$ is only slightly hysteretic. If this is the case, and if $h(\theta)$ is hysteretic, it follows that $K(h)$ must be hysteretic. Therefore, the $K(h)$ data or its interpretation, as presented by Freeze and Banner, is subject to question. Two flow situations were considered, 1) drainage from steady state downward flow, and 2) infiltration into a column which had previously been draining. In both cases, the water table was located at some initial elevation in the column. The computed time dependence of the water table elevation was compared with the measured fluctuations. The agreement was reasonably good; however, the authors conceded that it was necessary to adjust the $h(\theta)$ functions. Although the water table elevation was predicted with some degree of accuracy, no comparison was shown between the predicted and measured pressure head profiles.

C. Summary and Objectives

Because of the assumptions necessary in deriving the flow equation (4), it is an imperfect model for natural, unsaturated flow processes. However, for many applications, solutions of equation (4) should adequately predict the behaviour of the flow system, and at worst, could be regarded as a reasonable first approximation of most flow systems. Solutions of equation (4) require that the medium be characterized with respect to the hydraulic functions $h(\theta)$ and $K(\theta)$. The pressure head-water content function is hysteretic and appears to be rate dependent; however, the conductivity-water content function appears to be only slightly hysteretic.

In order to incorporate a consideration of hysteresis, non-uniform media, cyclic boundary conditions, or other complexities associated with natural flow systems into solutions of the flow equation, computerized numerical solution techniques are required. Of the solutions proposed, many are limited by the nature of the boundary conditions which can be used. Of those which consider hysteresis, most can account for a limited degree of hysteresis or use a simplified hysteretic model. An adequate method for representing, in the computer, the hysteretic $h(\theta)$ function for an inhomogeneous material has not been developed. Few numerical solutions have been tested against experimental data, and the tests performed have yielded inconclusive results. No solution has been tested experimentally where the medium was considered to be non-uniform.

In view of the foregoing circumstances, the following objectives were set forth:

1) to design and construct an experimental system to measure the hysteretic $h(\theta)$ function as a function of position for a particular column of soil.

2) to gain further evidence regarding the hysteretic nature of $K(\theta)$ and the rate dependence of $\partial\theta/\partial h$.

3) to devise a scheme for entering into the computer, in a form readily usable by the computer, the large amount of data necessary to describe $h(\theta)$ for an inhomogeneous medium.

4) to incorporate hysteresis into a numerical solution, and to test the solution by imposing boundary conditions on a column of soil which will result in hysteretic flow conditions, simulating the same conditions in the mathematical model and comparing the measured and predicted flow patterns.

III. APPARATUS AND PROCEDURES

A major portion of the work involved in this study was associated with the experimental aspects. A flow column was constructed with provision for applying the desired upper and lower boundary conditions. The column was filled with soil and the hydraulic properties of the column of soil were measured for use in the numerical solution. Flow experiments for testing the numerical solution were conducted using the same column.

Collection of the large amount of data necessary to specify h(θ) required rapid nondestructive methods for obtaining simultaneous measurements of pressure head and water content. Water content was measured using gamma radiation attenuation techniques. The pressure head was measured using tensiometers and strain-gauge transducers by modifying the method described by Klute and Peters (1966). The conductivity-water content function was determined using an adaptation of the transient procedure of Watson (1966).

A. Construction of the Flow System

1. Soil Container

The soil container for this study was 60 cm long and had an inside rectangular cross section of 12.8 x 5.65 cm (Figure 2). The back and sides of the container were constructed of lucite, 1.27 cm thick and the front was constructed of lucite 0.635 cm thick. The back and front were fastened to the sides with 10-32 machine screws and silicone sealant. The front plate was milled with 0.635 x 12 cm slots spaced 2.0 cm apart to accept the tensiometers.

The back plate of the column was drilled and tapped to accept two rows of 0.635 cm long, 6-32 machine screws. The rows were positioned 8 cm apart with a pair of screws at each 5 cm interval along the column beginning

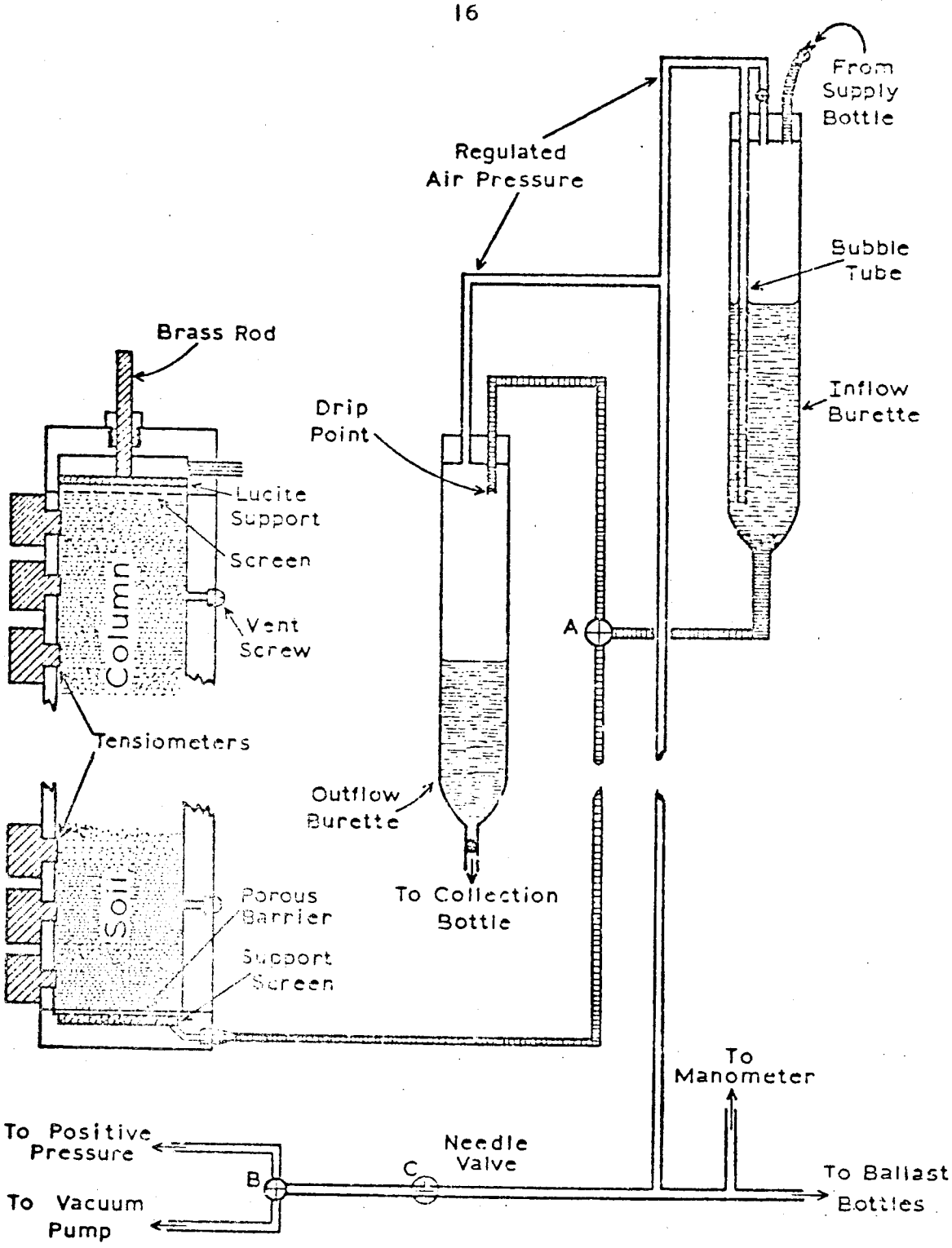

Figure 2. Cross section through the flow column and flow control system.

2.5 cm from either end. The screws were fitted with O-rings and could be removed to ensure that the gas phase pressure within the column was atmospheric. In addition, measurement of the gas phase pressure was facilitated by installing a plastic check-valve at each 10 cm interval along the container, beginning 5 cm from either end.

2. Flow Control System

The purpose of the flow control system was to control and measure the rate at which water was added to or removed from the bottom of the column. Four 250 ml. burettes, two for measuring inflow and two for measuring outflow, were used. (Only one burette of each pair is shown in Figure 2.) The burettes were positioned such that the drip point of the outflow burette and the bubble tube of the inflow burette were at the same elevation as the upper soil surface. The air space of the outflow burette and the bubble tube of the inflow burette were connected to a source of controlled air pressure; thus, the pressure at which water was applied or removed from the lower end of the column was equal to the controlled air pressure plus a gravitational head equal to the length of the column. As a consequence, when the applied air pressure was atmospheric, and there was no inflow or outflow, the water table was positioned at the upper soil surface.

The air space of the flow control system included two 18 litre bottles which acted as a ballast tank and were connected through a needle valve (C) and plug valve (B) to either a source of positive pressure or a vacuum pump. In order to initiate drainage from a saturated condition, valve A was turned such that the outflow burette was connected to the bottom barrier and valve B was set to vacuum. By observing the manometer and adjusting the needle valve, the desired rate of change in the pressure under the barrier could be obtained. By including the ballast bottles in the

system, slower rates of drainage could be attained. Similarly, a controlled rate of inflow could be maintained. Two outflow burettes were used so one could be drained while the other was filling. Similarly, one inflow burette could be refilled while the other was supplying water to the column. In order to prevent sudden changes in the gas phase pressure during the refilling or draining of burettes, the air spaces in the supply bottle and collection bottle were maintained at the applied air pressure (pressure in the ballast bottles). This is not shown in Figure 2.

The barrier at the upper end of the column was constructed from two plates of lucite 1.27 cm thick. The centre of the lower plate was milled out to the approximate inside cross sectional dimensions of the column. A screen supported by a plate of 0.635 cm lucite was held firmly against the soil by two 0.635 cm brass rods passing through flex fittings in the top of the end plate. For the addition of water at the upper end, and in order to ensure that the gas phase pressure at the upper end was atmospheric, a length of 0.635 cm o.d. acrylic tubing was glued into the side of the upper plate.

The bottom barrier was constructed from a plate of 1.27 cm acrylic. A sheet of porous plastic (Porvic) which had a bubbling pressure of approximately 500 cm of water was glued into the plate and supported by two layers of brass screen. The plate was drilled and tapped to accept two brass 0.318 cm tubing adapters. One tubing adapter was connected to the water supply and the other was used for flushing air from beneath the porous plastic barrier.

B. Pressure Measurement

Hydraulic head measurements were made using a system of tensiometers and pressure transducers. A block diagram of the system is shown in Figure 3. The tensiometers were constructed from pieces of lucite 17.5 x 2 x

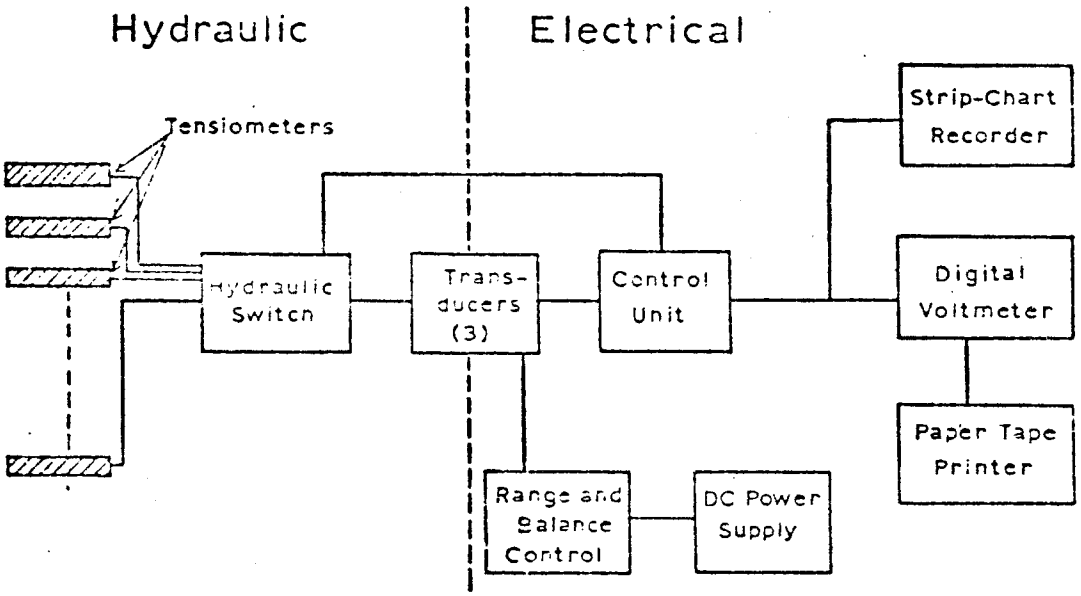

Figure 3. Block diagram of hydraulic head measurement system.

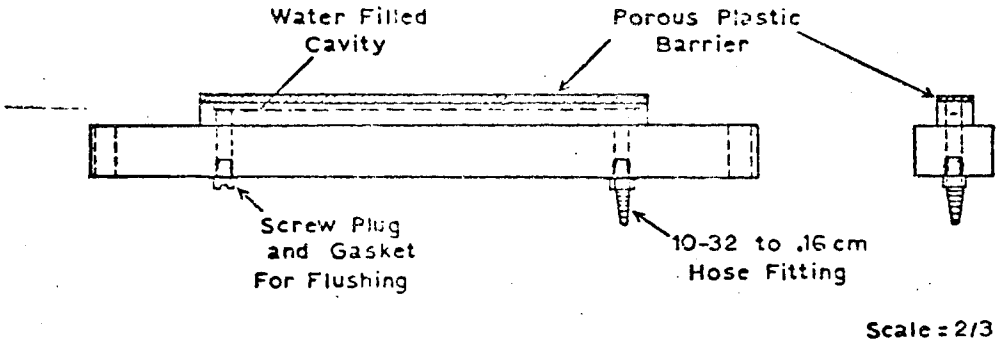

Figure 4. Diagram of a tensiometer.

1.27 cm and 12 x 0.64 x 0.60 cm assembled as shown in Figure 4. The porous barrier of each tensiometer was made from porous plastic (Porvic) which had a bubbling pressure of approximately 500 cm of water. The porous barrier was fastened to the lucite with epoxy cement and had an effective area of approximately 12 x 0.3 cm. Two 10-32 holes were drilled and tapped in each tensiometer. One was fitted with a 10-32 to 0.16 cm hose fitting.[1] The other was closed with a 10-32 screw plug which could be removed to allow for the flushing of air from the tensiometer. Each tensiometer was fastened to the column with two 2.54 cm 8-32 machine screws and sealed with silicone cement.

The geometry of the tensiometer barrier gave a large effective area, thus minimizing the response time while maintaining a small dimension in the direction of flow. Furthermore, the large lateral dimension tended to "average out" the effect of lateral non-uniformities in the porous medium.

Each tensiometer was connected to a 12 position rotary hydraulic switch[2] by 1.59 mm o.d. nylon tubing. Three rotary switches were required; each was connected to 10 tensiometers and two standard water levels. The hydraulic switches were operated by a solenoid drive.[3] The solenoid drive (and thus the hydraulic switch) could be advanced in steps from position to position, but also had the capacity for selective control in that by closing one of 12 contacts, the switch advanced to the appropriate position. The three hydraulic switches were driven by the same solenoid giving, by the electrical analogue, a 3 pole - 12 throw hydraulic switch (Figure 5).

---

[1] Clippard Instrument Laboratory, Inc., 7390 Colerain Rd., Cincinnati, Ohio.

[2] Scanivalve, Inc., P.O. Box 20005, San Diego, California, 92120. Scan Co. #WI/IP - 12 T.

[3] Scanivalve, Inc. Scan Co. #WS5 - 12 - 95 vdc.

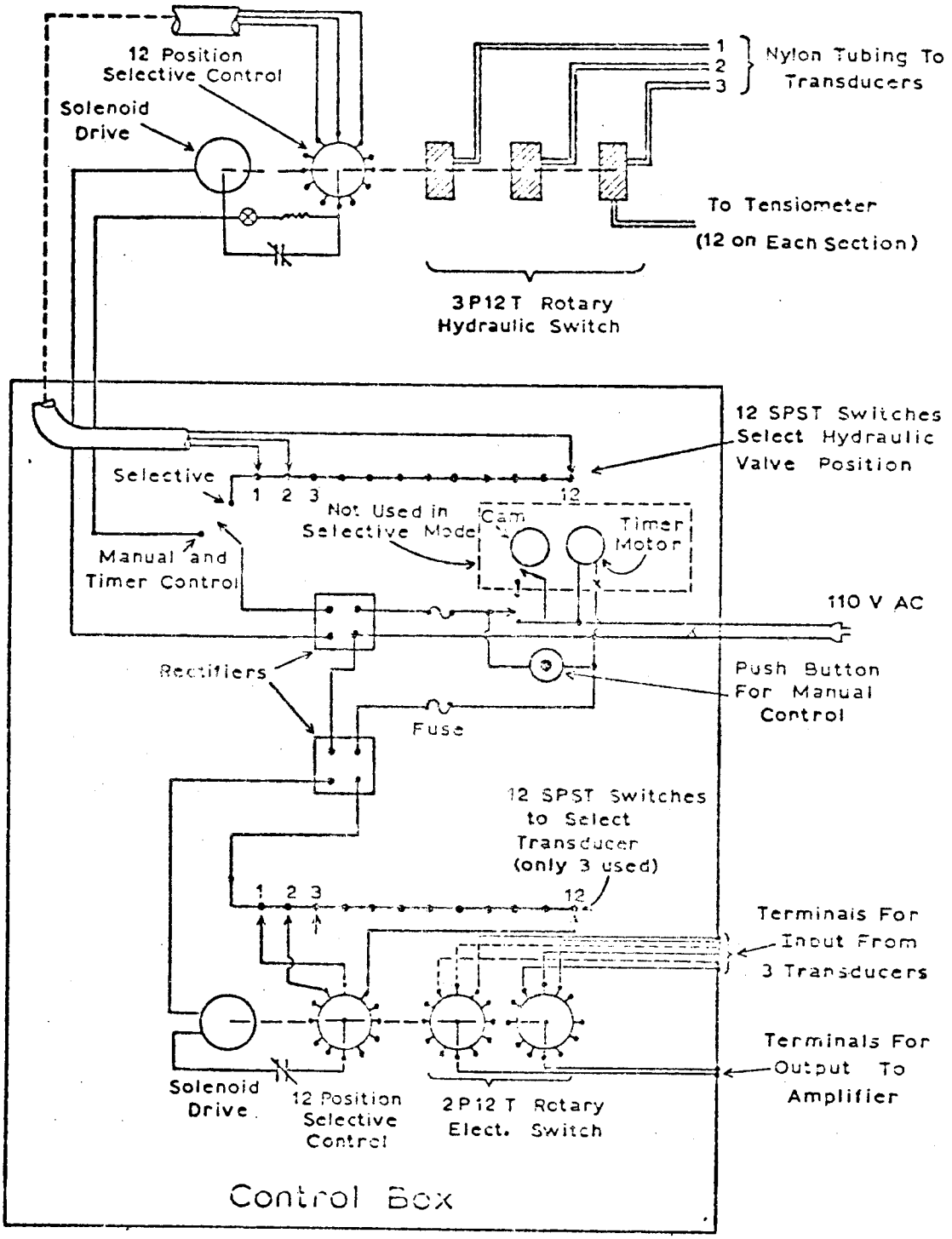

Figure 5. Circuit diagram of the control unit for selecting the tensiometer to be monitored.

The common port of each hydraulic switch was connected by 1.59 mm o.d. nylon tubing to one of three ± 15 PSI strain-gauge pressure transducers.[4]

The electrical output of each transducer was connected through a 2 pole - 12 position rotary electrical switch[5] and amplified to a Hewlett Packard digital volt meter and paper tape printer. A strip chart recorder was connected in parallel with the input of the digital volt meter. As in the case of the solenoid drive for the hydraulic switch, the rotary electrical switch had selective control capability.

A special control box was constructed for selecting the tensiometer to be monitored (Figure 5). In addition to having the capacity to switch almost instantly to any one of 144 tensiometers (only 30 were used in this study), the hydraulic switches could be advanced by use of a manual push-button, or at set time intervals by use of a timer.

The pressure measuring system was calibrated such that values of hydraulic head were printed directly onto the paper tape. In order to minimize the effects of changes in the air temperature on the transducer output, the transducers were mounted in a Styrofoam box. In spite of these precautions, significant drift did occur during the course of an experiment. To correct for this, frequent standard readings were taken, and the data corrected by linear interpolation between standard readings.

At high water contents, the response time of the pressure measuring system was approximately two seconds; however, at low water contents the response time could be as great as two minutes. At low water contents,

---

[4] Consolidated Electrodynamics, 1400 S. Shamrock Ave., Monrovia, California. Type 4 - 312 - 0001 pressure transducer.

[5] Ledex, Inc., 123 Webster St., Dayton, Ohio.

the hydraulic conductivity of the medium used was very low, thus greater time was required for the transmission of water to or from the tensiometers. The hydraulic head values were recorded to nearest mm of water. With careful calibration, the pressure values could be measured with a sensitivity of ± 1.0 mm of water. For a particular experiment, because of thermal drift and minor changes in the calibration, a more realistic estimate of the accuracy would be ± 2.0 mm of water.

C. Water Content Measurement

1. Principles

Water content measurements in a system which is highly transient requires a method which is rapid and non-destructive to the medium. A further requirement for many applications is that the water content be measured over a narrow interval in the direction parallel to the direction of flow. These requirements are best satisfied by gamma-ray absorption techniques. The principles upon which these methods are based, and their application to water content measurements have been described in detail elsewhere [Ferguson and Gardner (1962), Davidson et al (1963)], and therefore will be considered here only briefly.

The attenuation in a beam of gamma radiation caused by its passage through an absorbing material may be expressed by the equation:

$$I = I_o' \ \mathrm{EXP}\ (-\mu\rho l) \qquad (5)$$

where I is the intensity of the transmitted beam, I_o' the intensity of the incident beam, and ρ the density, l the thickness and μ the gamma absorption coefficient of the absorbing material. Equation (5) is strictly valid only for monochromatic radiation. The radiation reaching a detector will be made up of transmitted radiation as well as diffuse radiation. The diffuse radiation will be at a lower energy level than the transmitted, and can be

eliminated by electronic discrimination in the pulse height analyzer. The amount of diffuse radiation reaching the detector is reduced by the detector collimator (Figure 6).

Equation (5) can be extended to multi-component systems. The components in flow column studies generally include the container wall (subscript c), the porous solid matrix (subscript s) and water (subscript w). The effect of the air can be neglected. Equation (5) becomes:

$$I = I_o' \ \text{EXP} \left(-\mu_w \rho_w \theta_x \ -\mu_s \rho_b x \ -\mu_c \rho_c x_c \right) \qquad (6)$$

where x is the path length through the porous medium, ρ_b the bulk density and x_c the container wall thickness. In principle, by using handbook values for the absorption coefficients and densities and a known value of θ to determine I_o', equation (6) can be used directly to calculate θ. In practice, however, because of coincidence losses in the detector and the fact that the transmitted radiation is not monochromatic, the exponential relationship of equation (6) must be verified for the system being used and the absorption coefficients should be measured under conditions approximating as closely as possible, the experimental conditions.

The production of gamma rays within the source is a random process producing statistical variations in the observed counting rates. These variations obey Poisson's law, thus, if the average counting rate is I, one standard deviation (σ) = $\sqrt{I}$ and 95% of the observations (I) will be within $\pm 2\sigma$. At higher counting rates, the statistical component is a smaller proportion of the observation than at lower counting rates. For this reason, more precise measurements can be obtained by using high counting rates. This is particularly important if the counting time is short.

2. Gamma Source and Shield

The source of gamma radiation was 178 mCi of Cs-137 as CsCl powder

sealed in a stainless steel capsule.[6] The source shield shown in Figure 6 has cylindrical geometry and was machined from three different blocks of lead which had previously been moulded to the approximate dimensions required. The source capsule was screwed into the source holder and held in place by an 8-32 set screw in the brass insert shown in Figure 6. The lead collimator was removable so that collimators having different shapes and sizes of apertures could be used. A fourth block of lead was moulded to fit over the collimator when the system was not in use.

3. Gamma Counting System

The gamma counting system was purchased from the Harshaw Chemical Company.[7] A block diagram of the components is shown in Figure 7. The detector consisted of a 2.54 cm diameter x 7.62 cm thallium activated sodium iodide crystal coupled to an RCA-8054 multiplier phototube with a plug-on voltage divider. The detector assembly was shielded and mounted on the movable platform as shown in Figures 6 and 8.

The output from the phototube went through a preamplifier stage (NB-11) to the amplifier (NA-11). The amplifier had a differential linearity of ± 1% or better, and a maximum count rate of 50 KC. By use of the pulse height analyzer (NC-11) it was possible to count only those photons which fell within a specified range on the energy spectrum.

The linear ratemeter (NR-10) gave a visual display of the counting rate on a dial mounted in the front panel. This was used primarily as an

---

[6] U.S. Nuclear Corp., Div. of ICN, 2727 Campus Drive, Irvine, California. Type 375 gamma source capsule.

[7] Harshaw Chemical Co., 6801 Cochran Rd., Solon, Ohio.

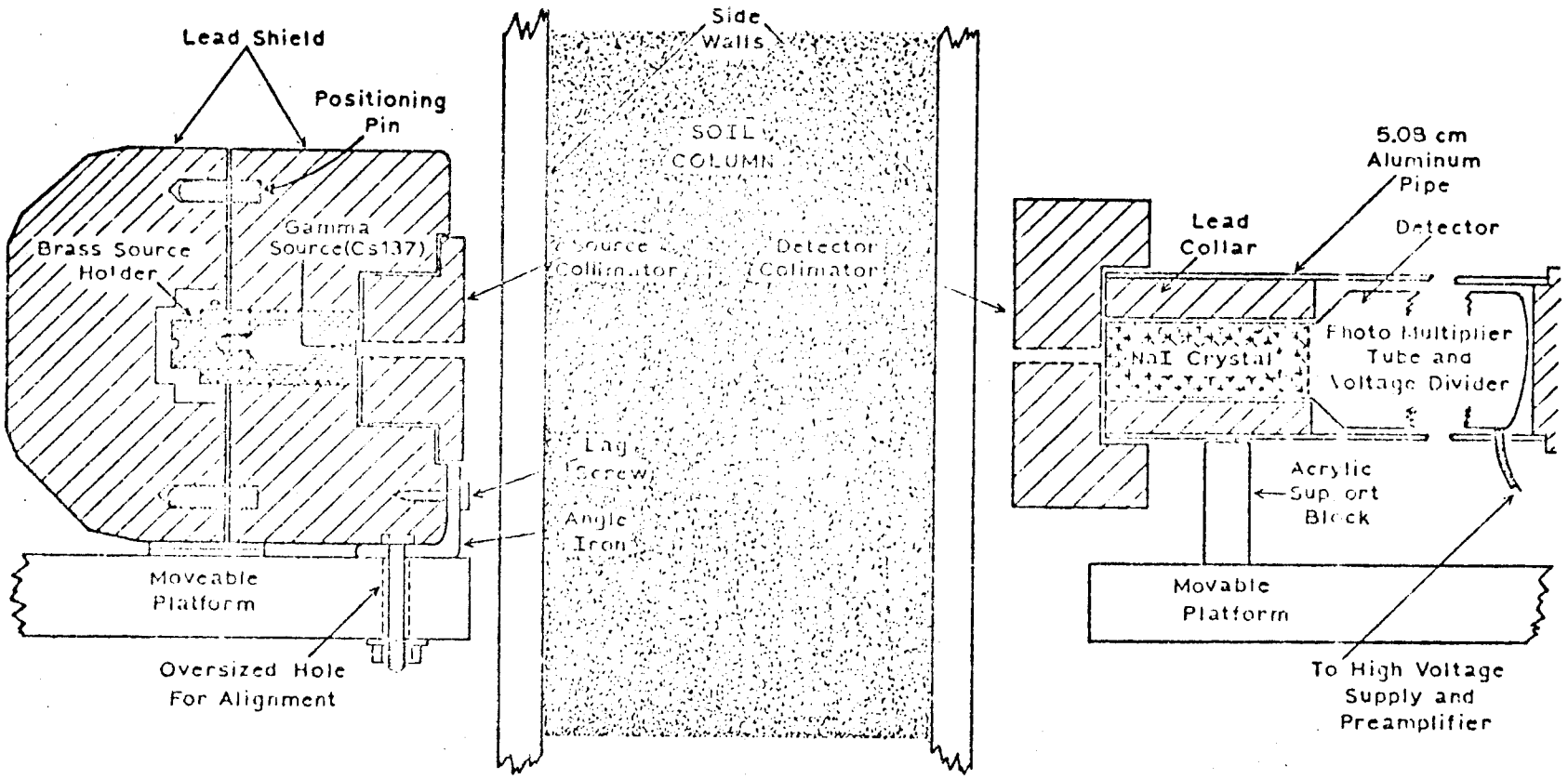

Figure 6. Cross section through gamma source and detector showing lead shielding and positioning relative to the soil column.

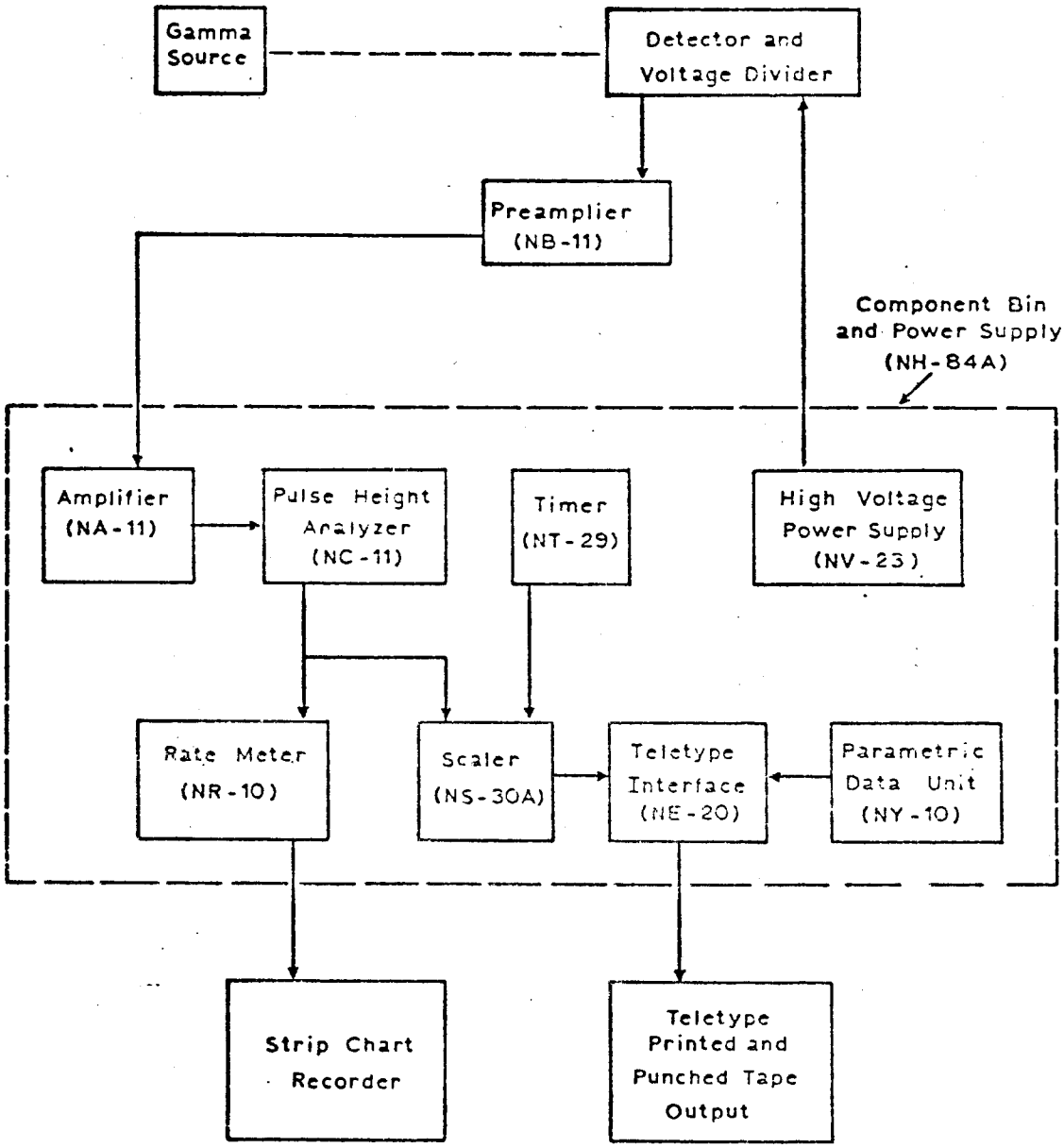

Figure 7. Block diagram of water content measuring system.

indicator during the preliminary adjustments. The ratemeter had an analogue output which was used to drive a strip-chart recorder to give a visual indication of changes in the water content during an experiment. The scaler (NS-30A) was a six-decade scaler having a visual display output in parallel with a six digit BCD output. It could be ordered to START, STOP, or RESET manually or by a remote control unit.

The timer (NT-29) allowed for preset counting times ranging from 0.01 seconds to 999 minutes. The timer operated only while the scaler was counting, and at the end of the counting period stopped the scaler and initiated printout through the interface unit.

The parametric data unit (NY-10) permitted six digits of data to be entered manually. The numbers set on the parametric data unit were printed before each scaler reading, and could be used to indicate elapsed time, position, etc.

The interface unit (NE-20) coupled the counting system to a readout system. Data could be accepted at a number of addresses; however, only two were used in this application, one for the scaler, and one for the parametric data unit. At the end of the counting interval the interface unit scanned all addresses and transmitted the data at those addresses which were in use to a teletypewriter. After all addresses had been monitored, the scaler and timer were ordered to RESET and START. The teletypewriter (model 33-ASR) gave printed as well as punched paper tape output.

4. Lift Mechanism

Throughout the experiment, the column was held in a stationary position, and the source and detector were moved vertically along the column. The mechanism used for this purpose is shown in Figure 8.

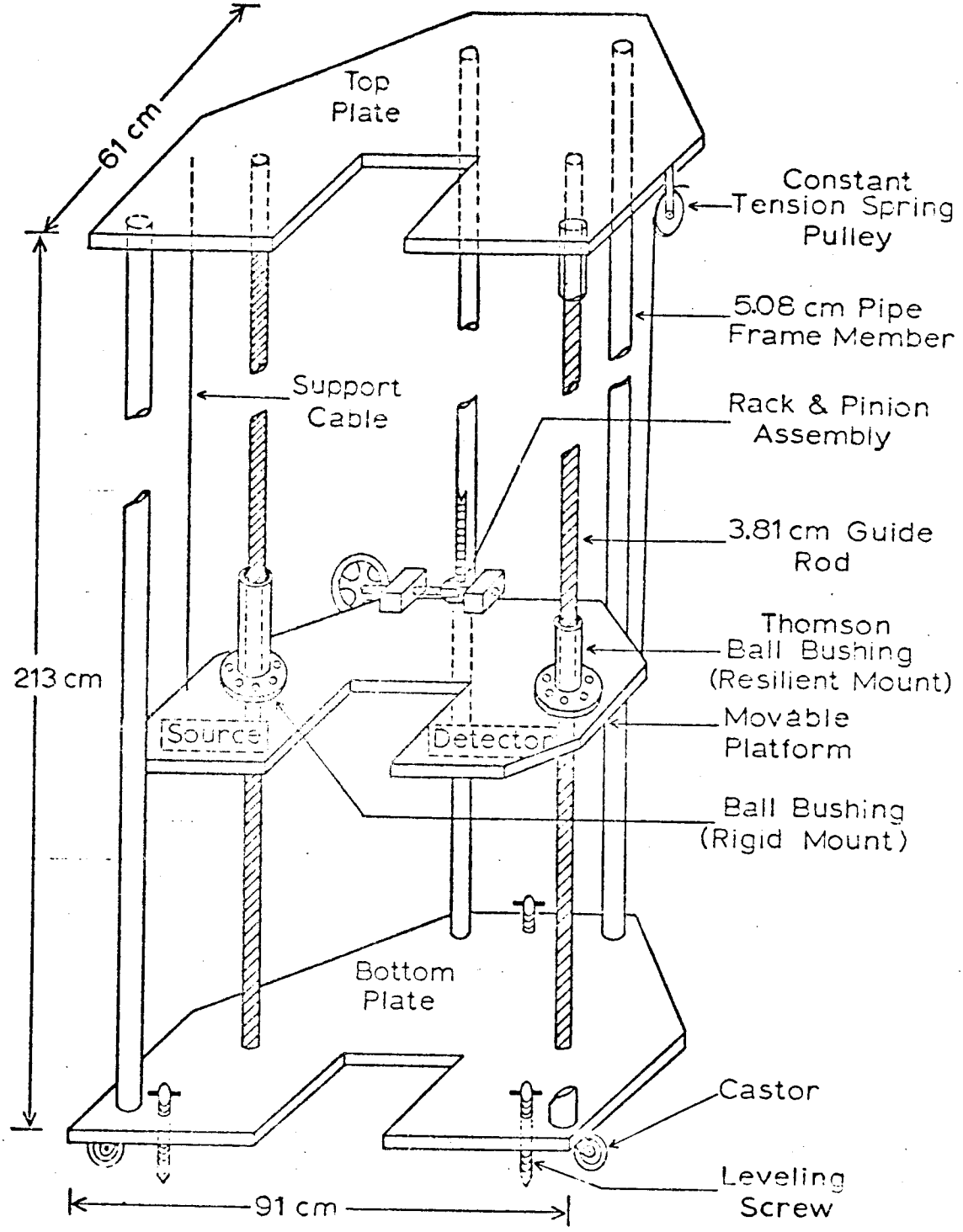

Figure 8. Lift mechanism for transporting the gamma source and detector vertically along the flow column.

The main framework consisted of a top and bottom plate cut from 2.22 cm sheet aluminum bolted on opposite ends of four 5.08 cm steel pipes 2.111 m long. The bottom plate was fitted with four casters and three levelling screws. During operation, the mechanism was supported by the levelling screws which fit into steel plates glued to the floor.

The movable platform, which carried the source and detector was cut from 2.22 cm sheet aluminum. Two ball bushings[8] were set in an aluminum collar which was mounted rigidly near one edge of the platform. A third ball bushing was positioned in a resilient mount near the opposite edge of the platform. The resilient mount was used to avoid stress being applied on the platform as a result of distortion or misalignment in the guide rods. The platform was held in a rigid lateral position by two 3.81 cm dia. case 60, ground steel rods.[9] For alignment purposes, the guide rods were held in adjustable mounts at both top and bottom. A rack gear was attached to one of the support pipes, and the platform was moved manually by means of a hand wheel and pinion attached to the platform. The weight of the platform, source and detector was counterbalanced by four cables attached to "constant" tension spring pulleys. A centimetre scale and a pointer were used to position the platform. The platform moved freely over its entire length of travel with no apparent stress being placed upon it. It could be positioned easily at any desired location within $\pm$ 0.5 mm. It was held in position by tightening a thumb screw on the shaft of the pinion gear. In order to accommodate the column and its supporting equipment, rectangles 21.6 x 22.9 cm were cut from the front edge of the top and bottom plates and the movable platform.

---

8 Thomson Industries, Inc., Manhasset, New York, 11030. Bushing #A-243848.

9 Thomson Industries, Inc., 1060 Steel, 60 case hardened tolerance class "5".

5. Operating Conditions and Calibration

The primary energy peak for Cs-137 occurs at 660 KeV. Initially, the lower level control of the pulse height analyzer was set at 550 KeV to include only the radiation within the primary peak. While continuously monitoring a brass absorber, considerable instability in the counting rate was observed. The amount of drift was reduced to some extent by circulating water at a constant temperature (± 0.01°C) around the detector and enclosing the detector in a Styrofoam box. The only condition which gave a stable counting rate was the setting of the pulse height analyzer to include the entire spectrum except for the initial noise region. (All radiation above 50 KeV was included.) In addition to giving a stable counting rate, inclusion of the entire spectrum gave a higher counting rate and thus greater precision in the water content determinations.

While monitoring a brass absorber, appreciable variation in the counting rate was observed as the movable platform was raised from its extreme lower position to extreme upper position. The variation was not believed to be caused by changes in the source-detector alignment. It was also observed that the maximum counting rates occurred when the platform was near the bottom or top plates of the lift mechanism, or near the adjacent bench top. The amount of variation was reduced, although still appreciable, when only the primary energy peak was included rather than the entire spectrum. The evidence indicated that the increase in the counting rate when the source and detector were in the proximity of some massive object may have been caused by an increase in the number of reflected photons reaching the detector. The problem was not pursued, and a complete explanation is not at hand. In order to minimize any errors introduced by this positional effect, the system was calibrated under conditions similar to those which would be encountered during the experiments.

The ports of the source and detector collimators were shaped and aligned to give the maximum counting rate while keeping the vertical dimension of the gamma beam small. The source collimator port was 2.5 mm in diameter and that of the detector collimator was 2 mm high by 1.5 cm wide. The effective vertical dimension of the gamma beam was determined by passing the beam vertically from air onto a brass absorber. The counting rate in air changed to the counting rate for the brass absorber, as the platform was moved a distance of 3 mm. This indicated that the effective thickness of the gamma beam was 3 mm. Preliminary tests indicated that the counting rates for the saturated and drained column would be approximately 1.3×10^6 and 1.7×10^6 counts per minute respectively.

Since the entire spectrum of Cs-137 was used rather than just the primary peak and since coincidence losses in the detector and electronics can be appreciable at the counting rates used, it was necessary to verify the exponential relation of equation (6). Brass plate absorbers were placed between the source and detector until the counting rate was reduced to a value somewhat greater than the maximum expected during the experiments. Additional brass plates of known thickness were placed in sequence in the beam, and the counting rate determined after the addition of each plate. Plates were added until the counting rate was reduced to a value less than that which would be encountered throughout the study. Log (I_o'/I) vs. l (absorber thickness) gave a linear correlation coefficient of .999996 and an intercept on the ordinate of .00528 verifying the validity of equation (6) over the expected range of counting rates.

Calibration of the gamma system can be accomplished by a number of methods. If, in equation (6), $\rho_b \mu_s x$ and $\mu_c \rho_c x_c$ are considered to be constant at a particular position, they can be combined with I_o' to give I_o. Furthermore, if the remaining parameters are considered to be functions of position

($\bar{z}$) equation (6) becomes:

$$I_{\bar{z}} = (I_o)_{\bar{z}} \text{ EXP} - [(\mu\rho)_w]_{\bar{z}} \times_{\bar{z}} \theta_{\bar{z}} \quad (7)$$

By using measured values of $(x)_{\bar{z}}$ and $(\mu\rho)_w$, I_o can be determined by measuring $I_{\bar{z}}$ at a known water content. $I_{\bar{z}}$ was determined with the experimental column completely saturated. At saturation, the water content is given by:

$$\theta_{\bar{z}} = 1 - (\rho_b)_{\bar{z}}/\rho_s \quad (8)$$

where $(\rho_b)_{\bar{z}}$ is the bulk density of the medium at elevation $\bar{z}$ and ρ_s is the particle density. By the pycnometer method, ρ_s was determined to be 2.640 g/cc. $(\rho_b)_{\bar{z}}$ was determined gravimetrically by sectioning the column at the completion of the experiment. This completed the measurements necessary for calibration of the gamma system.

The measured bulk densities are shown in Figure 9. The bulk densities were determined within an accuracy of $\pm$ 0.04 g/cc; however, this resulted in an I_o value giving calculated volumetric water contents within $\pm$ 0.015. This amount of error was large, but not unreasonable. The scatter in the bulk densities did not appear to be random since in many cases a large value was followed by a low value. This nonrandomness could have been introduced by the procedure used in sectioning the column. From the packing procedure used, one might expect to observe trends in the bulk density values along the column; however, the sharp change between adjacent measuring points does not appear to be realistic. For these reasons, a line of qualitative best fit was drawn through the data points and values of $(\rho_b)_{\bar{z}}$ used to calculate $(I_o)_{\bar{z}}$ were read from the curve.

The bulk density could also have been determined using gamma ray attenuation. The latter procedure requires that the column be scanned while in the air dry condition. As will be described in a subsequent section,

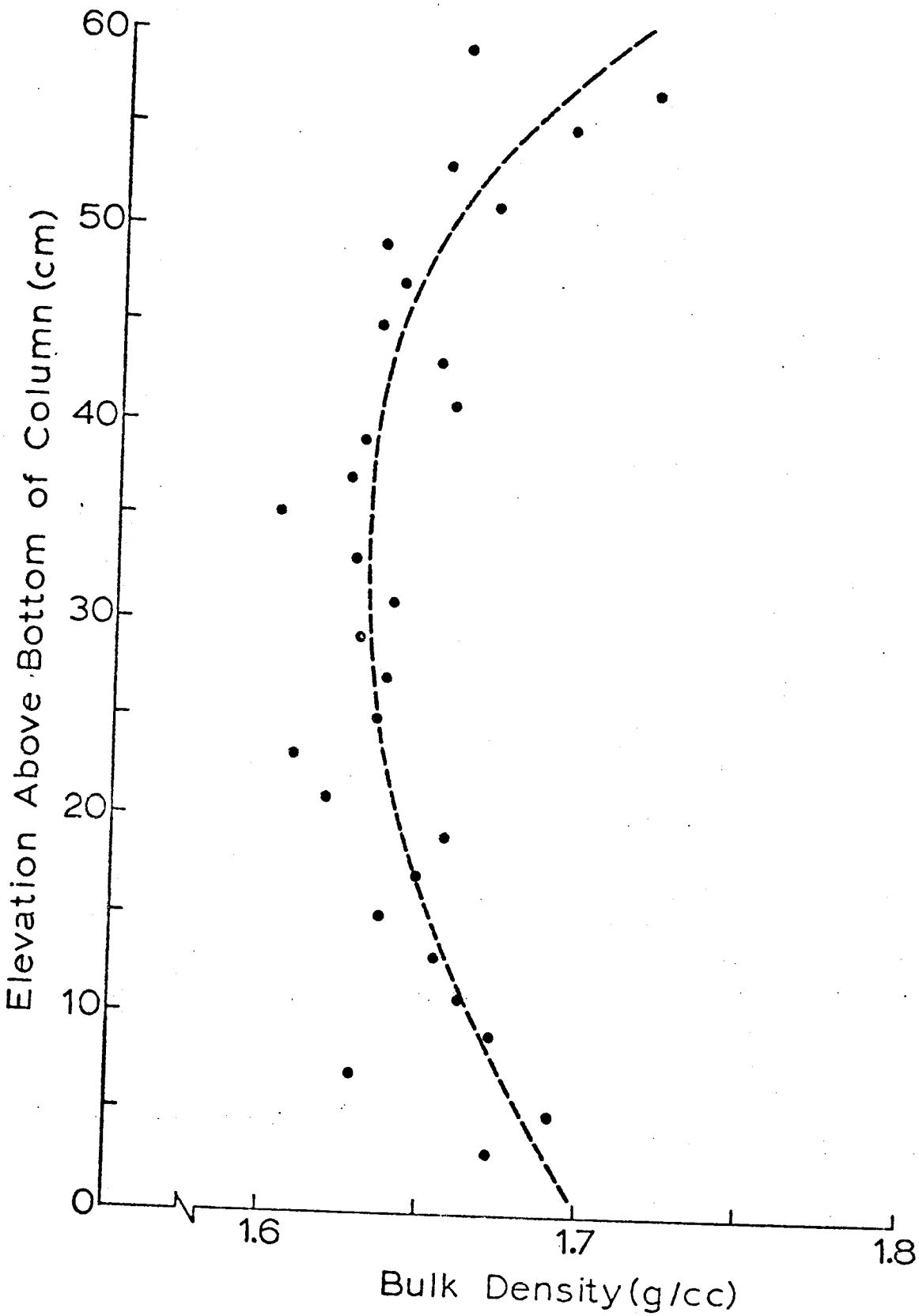

Figure 9. Bulk density of the medium as determined gravimetrically at the conclusion of the experiment.

the column was packed while wet, thus making the alternate method for determining ρ_b impossible. Measurement of the bulk density using the gamma system appears to be advisable since more accurate measurements can be made, and the system can be calibrated at the beginning of the experiment.

In a preliminary experiment, the column was packed and saturated and I_z determined. Then the column was drained, the outflow carefully measured, and a final set of values of I_z determined. From the change in the counting rate, the change in the water content at each position was calculated, and by integration, the total outflow volume was determined. The measured volume of outflow was 337.0 ml and the calculated value 337.8 ml, a difference of less than 0.3%. The value of $(\mu_o)_w$ used was that determined on the water filled column giving considerable confidence in this value. In calculating the change in water content, I_o is not required, and thus the good agreement found does not reflect upon the bulk density determinations.

Another check of the calibration procedure was made at the end of the experiments. Before disassembly, the column was drained to a water content close to the residual water content, and the water content was determined using the gamma system. The column was disassembled and the volumetric water content determined gravimetrically. Precautions were taken to prevent evaporation while sectioning the column. Figure 10 shows the final calculated and measured water contents. At most positions the water content determined by gamma ray attenuation was greater than that determined gravimetrically; however, the agreement was quite good over the major length of the column.

D. Column Preparation

The medium used in this study was a naturally occurring soil taken from a sand dune area near Wray, Colorado. The particle size distribution was determined by sieve analysis and was found to be:

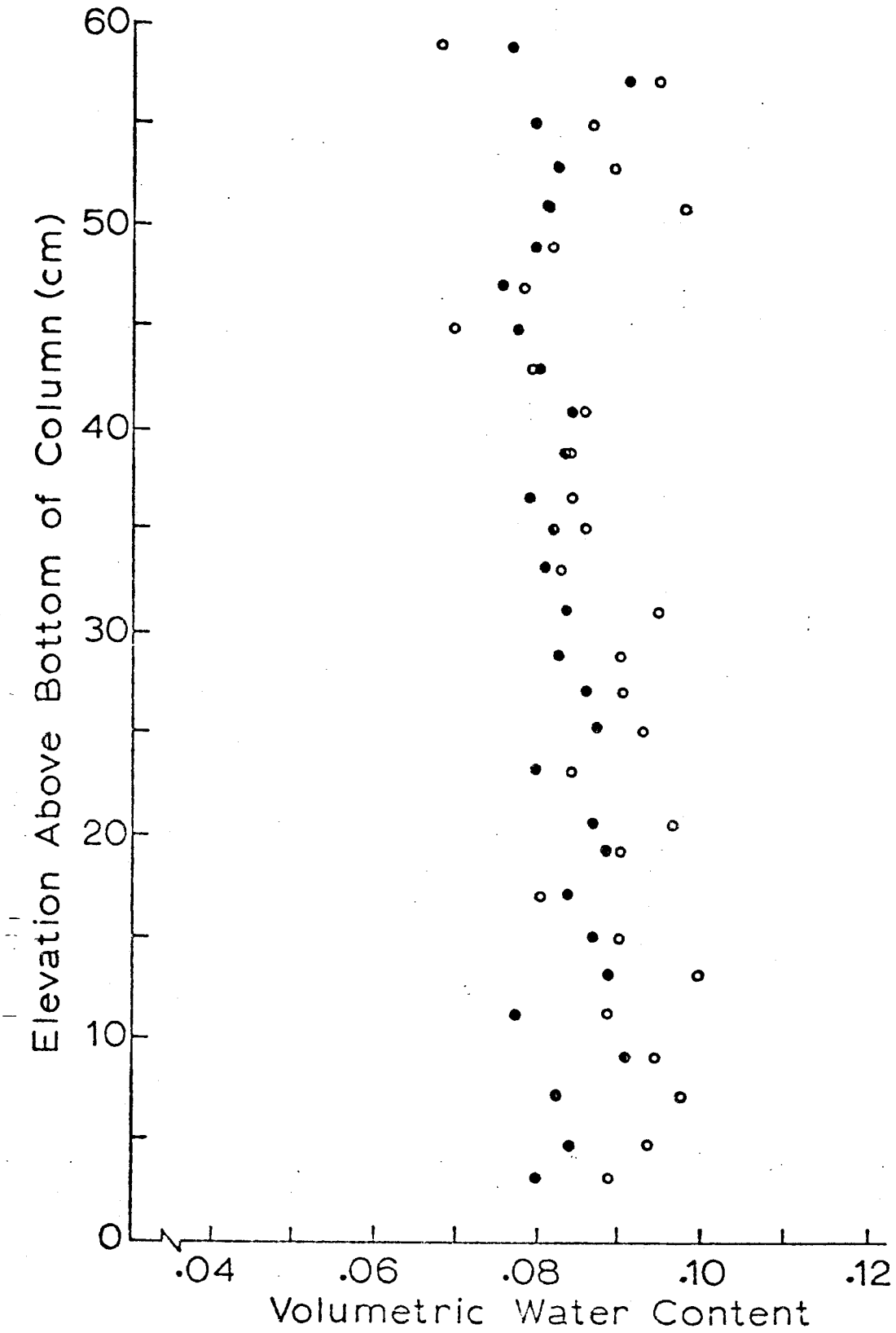

Figure 10. Final water content distribution as determined gravimetrically (●) and by gamma radiation attenuation (o).

PARTICLE DIAMETER (mm)	% PASSING
1.000	98.9
0.589	96.8
0.295	74.2
0.177	36.0
0.104	10.7
0.074	6.8

The solution used in preparing the column and during the experiments contained 0.1 N $CaSO_4$ and 0.1% phenol.

The column was rigidly supported in an upright position by a slotted iron framework, and rested on a wooden box 15 cm high with approximately the same cross sectional dimensions as the column. The inside of the box was cut with grooves to accept brass plate absorbers. These plates were used as a standard to check for drift in the gamma calibration.

Prior to filling the column, the tensiometers were saturated under vacuum then fastened into place. An extension, 25 cm long with the same cross sectional dimensions as the column was fastened to the top of the column. A 1.5 cm i.d. brass tube with a funnel fastened to the top was lowered into the column and filled until the sand level stood in the funnel. The tube was raised slowly and moved back and forth in an attempt to achieve a uniform packing. During filling, the level of sand in the funnel was maintained. The column was filled to the top of the extension then tapped gently until there appeared to be no more settling. The air was flushed from the sand by introducing carbon dioxide at the bottom of the column. Carbon dioxide flowed through the column for approximately 1½ hours, and was followed immediately by deaerated water (solution). The column was flushed with 6 litres of water over a period of 24 hours to ensure that all entrapped bubbles of carbon dioxide would be dissolved and removed from the column, leaving the medium in a condition of complete saturation. The column was tapped again until there appeared to be no more settling. Any change in the packing during

the experiment would alter the hydraulic properties of the medium, but of perhaps greater significance is the effect of changes in the bulk density on the calibration of the gamma system. The bulk density was included in the I_o term of equation (7) and was also used in determining the saturated water content. In both situations, the bulk density was assumed to be constant with respect to time. The objective was to obtain a very dense and presumably more stable packing. When there appeared to be no more settling, the water table was lowered to the bottom of the extension, the extension removed, and the upper barrier fastened into place. The screen, supported by the lucite plate, was held firmly against the upper surface of the sand by the two brass rods passing through the top plate. The tensiometer system was thoroughly flushed to remove all air. At this point brass plates were inserted into the slots of the wooden box beneath the column until the counting rate was within the range expected in the experiments, and an initial standard reading taken. The brass plates were not disturbed for the duration of the experiment.

The bottom tensiometer was connected to a separate transducer and recorder to give a continuous record of the hydraulic head at an elevation one cm above the bottom of the column. This was used as the lower boundary condition for the numerical simulation of the flow experiments. The pressure at the bottom tensiometer was used as the boundary condition rather than the pressure under the barrier to avoid complications caused by barrier impedance. Barrier impedance would have been difficult to incorporate into the analysis since it was time dependent.

E. Sampling Procedure and Data Assimilation

A sampling time of 15 seconds appeared optimum. This was sufficient time for a tensiometer to come to equilibrium (except in regions which were quite dry) and at the counting rates used, gave good precision in the water

content measurements. The average total number of counts in 15 seconds was approximately 4×10^5, giving a standard deviation of 6.3×10^2 or an uncertainty in the calculated volumetric water content of $\pm 3.0 \times 10^{-3}$. Also, for the boundary conditions to be imposed, 15 seconds was considered short enough to map accurately the transient nature of the resulting flow system.

A particular gamma reading was considered to apply at the middle of the 15 second interval over which it was taken. Although the counting time was 15 sec., the dead time, or time for the information to be transmitted to the teletype was 2.23 seconds, giving a total time for each reading of 17.23 seconds. The source and detector were moved from one position to the next during the dead time. The information read onto the punched tape from the parametric data unit included the counting time (15 seconds), the position which was being monitored, and an index to indicate whether or not the reading was a standard reading. The position numbers were all odd; thus, if set to an even number, that reading was to be ignored. This was used to eliminate a reading if counting began before the platform was in position, or if the platform was left in the same position for a period of time during which there would be little change in the water content.

The paper tape printer used to print out the hydraulic head values was driven by a 15 second timer. The value printed was considered to apply at the end of the 15 second sampling period. Immediately after a value was printed, the monitoring system was switched to the next tensiometer to allow as much time as possible for the tensiometer to come to equilibrium. Each hydraulic head value was designated by a sequence number. The first reading (at t = 15 sec.) was numbered 1, the second reading 2, etc. Division of the sequence number by four gave the elapsed time at which the reading was taken. In addition to the sequence number, the location at which the reading was taken was also written on the paper tape.

To initiate an experiment, a clock which displayed the total elapsed time, the scaler and the printer timer were started simultaneously, then the appropriate change in the boundary condition was made. It should be noted that since the measurement periods differed, the water content and hydraulic head values were recorded at different elapsed time values. The large amount of data acquired necessitated the use of a computer to apply corrections to the data and convert gamma counts to water content. Since the hydraulic head data was on printed tape, it had to be hand punched onto computer cards. One data point included the hydraulic head value, a sequence number which could be converted to elapsed time and the location. Frequent standard readings were taken. and the data was corrected by linear interpolation between consecutive standard readings. The elapsed time for a particular reading was simply its sequence number divided by four. The hydraulic head values and their corresponding elapsed time values were sorted by the computer according to position. Since the bottom of the column was selected as the reference elevation, the pressure head was calculated by subtracting the elevation of the tensiometer (its location number) from the hydraulic head values. For each position, the hydraulic head was plotted against elapsed time on microfilm. The microfilm output gave a good visual concept of the changes taking place and was also used to eliminate erroneous data. In addition, the corrected and sorted data was placed on punched cards, a convenient form for future calculations.

The gamma data, which was on punched tape, was transferred to punched cards. Standard readings were taken at approximately one hour intervals and a proportional correction applied to the data:

$$\frac{I}{I_{so}} = \frac{I_t}{I_{st}} \tag{9}$$

where I is the corrected observed counting rate, I_{so} is the initial standard reading, I_t is the observed counting rate at time t, and I_{st} is the standard reading at time t. Since there was negligible drift in the gamma system over periods of one to two hours, the value of I_{st} used in equation (9) was the last standard reading taken before time t. The corrected counting rate was converted to water content using equation (7) and the calibration constants obtained as described above. The elapsed time for a particular reading was determined by multiplying the number of readings taken by the time required for a single reading. The water contents and corresponding elapsed times were sorted according to position and output on both microfilm and punched cards.

F. Flow Experiments

1. Hydraulic Properties of the Medium

The first series of experiments was conducted to determine the hydraulic properties of the medium. The medium was considered to be non-uniform; therefore, the pressure head and hydraulic conductivity were considered to be functions of both water content and position.

To determine the $h(\theta,\bar{z})$ relation, the entire column was first drained from its initial condition of true saturation. By adjusting the needle valve on the flow control system, the rate of drainage was made slow enough that data could be collected to trace out a complete curve of $h(\theta)$ at all locations from the one drainage cycle. Most of the water was drained from the column during a $2\frac{1}{2}$ hour period. Although the outflow rate was very low, the drainage condition was maintained for another four hours, and periodic measurements were taken to ensure that the water content was approaching the residual water content. The $h(\theta,\bar{z})$ relationship so determined was the "initial drainage curve".

The flow control system was next adjusted so that the pressure beneath the bottom barrier slowly became less negative, inducing the column to wet along the "main rewet curve" until all points in the column were at a pressure head equal to or greater than zero. The column was again drained, this time along the "main drainage curve". The main wetting and drainage curves defined the hysteretic region of interest at each location; however, it was still necessary to measure families of scanning curves at each location.

To determine the drying scanning curves, the column was wetted from the bottom along the main wetting curve until the sampling location five cm from the bottom gave a gamma counting rate intermediate between the saturated and drained rates. The boundary condition was then changed to produce drainage. Four such cycles were performed with the reversals approximately equally spaced between the saturated and drained counting rates (water contents). The same procedure was followed taking as the index location, the measuring point 10 cm above the previous index location. During the wetting and drying cycles, gamma data and hydraulic head data were collected at several sampling locations on either side of the index location. Continuing this procedure, a family of drainage scanning curves was traced for each of the 29 measuring locations in the column.

A similar process was used to generate the families of wetting scanning curves, with the medium being drained along the main drainage curves and rewet along wetting scanning curves.

It should be noted that the description of the hysteretic, position dependent $h(\theta)$ function required a myriad of data, the collection of which was very time consuming. Collection of the drainage scanning curve data was particularly time consuming since the water content for a curve at a

particular location had to be reduced to a low water content in order to reverse along the main wetting curve.

As described previously, the raw data was corrected and sorted to give $h(t)$ and $\theta(t)$ at each sampling location. The segments of each set of data corresponding to the scanning curves of interest were separated and read back into the computer. Since the pressure head and water content data were taken on different time axes, in order to determine $h(\theta)$, the pressure head corresponding to the water content at a particular time was determined by linear interpolation on $h(t)$. Although $h(t)$ was not linear, the data points were sufficiently close together that such an assumption would introduce only slight errors. The pressure head and water content were changed to the dimensionless variables, Φ and Θ by dividing the pressure head values by the length of the column (60 cm) and the water content values by the maximum saturated water content (38.7%). Since all positions did not have the same saturated water content, all would not have a dimensionless saturated water content value of one. The $\Phi(\Theta,\bar{z})$ information was placed on punched cards and plotted on microfilm.

$K(\theta,\bar{z})$ was calculated using an adaptation of the transient procedure developed by Watson (1966). For one dimensional flow in the vertical direction, the continuity equation becomes:

$$\frac{\partial\theta}{\partial t} = -\frac{\partial q}{\partial \bar{z}} \tag{10}$$

For $\bar{z} = 0$ at the top of the column and $\bar{z}$ positive in the upward direction equation (10) can be integrated to give the flux q at a position $\bar{z}$:

$$q_{\bar{z}} = q_o + \int_{\bar{z}}^{o} \frac{\partial\theta}{\partial t}\, d\bar{z} \tag{11}$$

where q_o is the flux at the upper end of the column.

For a particular experimental sequence such as the initial drainage, differentiation of $\theta(t,\bar{z})$ for constant values of t, and subsequent integration with respect to $\bar{z}$ yields the last term of the right hand side of equation (11). Thus if the flux at the top of the column is known, the flux at any point $\bar{z}$ in the column can be calculated. From the $H(t,\bar{z})$ data, $\partial H/\partial \bar{z}$ at a given $\bar{z}$ and t can be calculated. Substituting the flux and gradient into the Darcy equation yields the conductivity $K(\theta)$ at a particular time and position. A complete description of the procedure was given by Watson (1966).

In an attempt to verify the assumption that $K(\theta)$ was nonhysteretic, conductivities were calculated for data collected during the initial drainage, the main rewet and the main drainage cycles. For these three flow situations, the flux at the soil surface was equal to zero.

In a drainage experiment designed specifically to determine $K(\theta,\bar{z})$, a porous barrier was used to add water at a measured rate to the top of the column. The flow rates were adjusted such that the outflow rate (at the bottom) was slightly greater than the inflow rate. The integration in equation (11) was performed graphically, introducing the possibility of significant error. By introducing the measured flux at the upper boundary, the effect of the integral on the flux at a position $\bar{z}$ was reduced, hopefully reducing the amount of scatter in the calculated $K(\theta)$ values.

2. Flow Experiments for Checking the Numerical Solution

Three hysteretic flow situations were established for the purpose of comparing measured flow conditions with the predictions of the numerical solution. In all three experiments, the upper boundary condition was zero flux, and the lower boundary condition was a time dependent potential as shown in Figure 11.

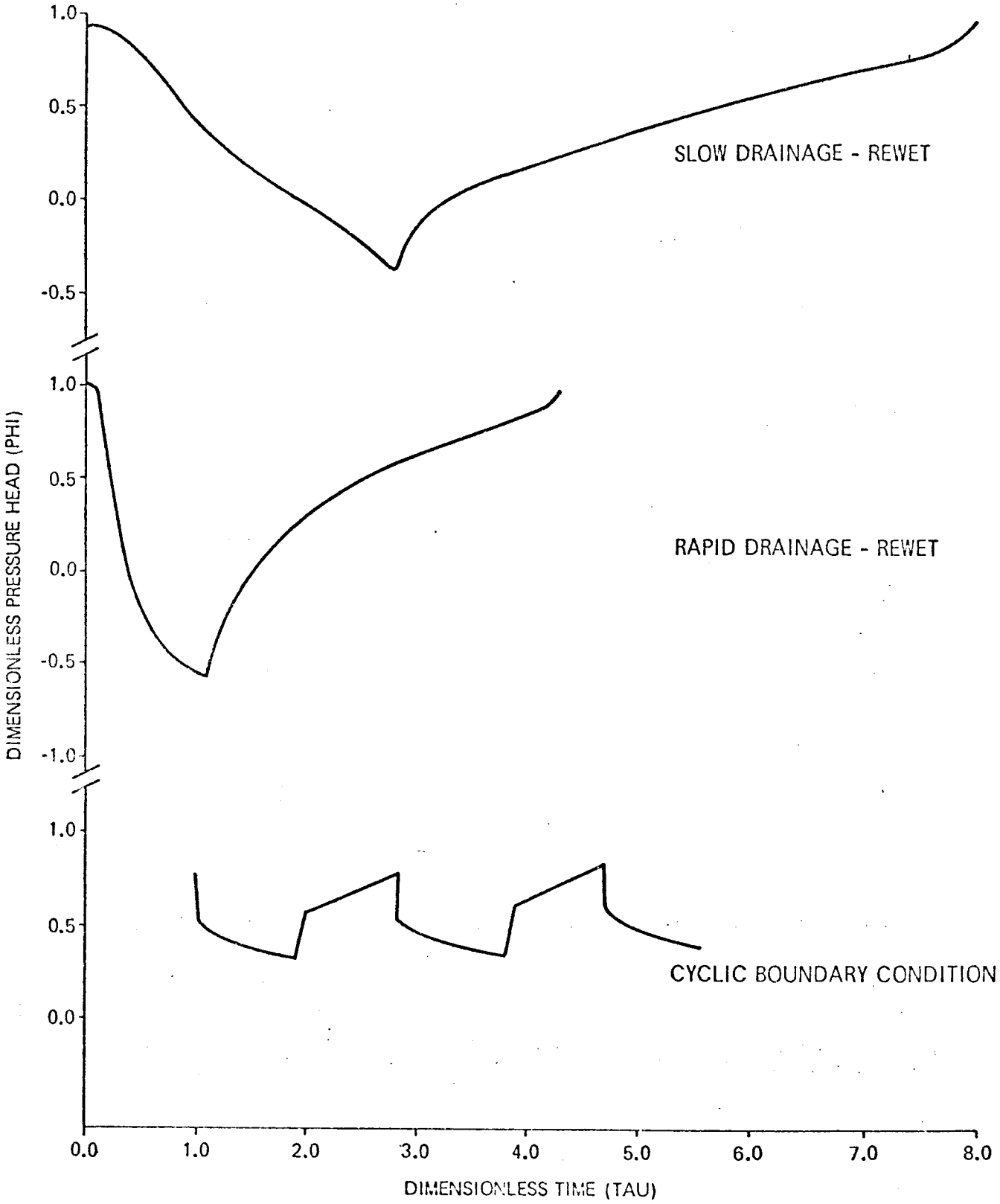

Figure 11. Diagram showing the lower boundary condition for the three flow experiments.

a) Slow Drainage-Rewet

Initially, all regions of the column were at the saturated water content reached by rewetting. The column was then partially drained at a slow rate by gradually reducing the pressure at the bottom, then rewet to a pressure head equal to or greater than zero.

b) Fast Drainage-Rewet

Identical to (a) but the drainage and rewet rates were approximately twice as great.

c) Cyclic Boundary Condition

In the third experiment, equilibrium conditions were established with the water table (h = 0) at an elevation of approximately 26 cm above the bottom of the column. A square wave pressure variation was applied under the bottom barrier. The pressure was initially increased to a constant value which was held for 20 minutes, then reduced to a lower value for the same period of time. Two and one-half such cycles were performed.

G. Numerical Solution

The numerical solution of the flow equation used in this study was written by D. F. Heermann[10] and A. Klute[11]. As yet, the solution has not been published; however, complete details can be obtained from either Heermann or Klute. A very brief description of the solution procedure will be given here.

The dimensionless flow equation (5) was written in finite difference form according to the predictor-corrector formulation of Douglas and Jones

---

[10] U.S.D.A. Agricultural Research Service, Fort Collins, Colorado 80521.

[11] Department of Agronomy, Colorado State University, Fort Collins, Colorado 80521.

(1963) as described by Remson et al (1971). The time-space field was discretized by dividing the dimensionless time axis into increments of $\Delta\tau$. The nodes on the time axis were denoted by m = 1,2,3, ... and for constant $\Delta\tau$, τ can be calculated from $\tau = \Delta\tau(m-1)$. Similarly, the position variable ζ was divided into increments of $\Delta\zeta$ with the position nodes designated by n = 1,2,3, ... The dimensionless pressure head Φ at a position n and time m is thus written as $\Phi_{n,m}$.

In the predictor-corrector formulation the numerical solution is advanced in time by two steps. Solution of the predictor set of algebraic finite difference equations gives $\Phi_{n,m+\frac{1}{2}}$, the pressure head at each position node after one half time step. The corrector set of equations uses the values of $\Phi_{n,m}$ and $\Phi_{n,m+\frac{1}{2}}$ to obtain $\Phi_{n,m+1}$, the pressure head at the end of the time step. Both the predictor and corrector sets of algebraic equations are linear and have a tridiagonal matrix of coefficients. Comparison of the predictor-corrector and iterative Crank-Nicolson procedures [Remson et al (1971)] by Klute and Heermann showed the predictor-corrector method to use considerably less computer time with no apparent loss in accuracy or stability.[12]

The solution process constructed by Heermann and Klute allowed for variable $\Delta\tau$ and $\Delta\zeta$. $\Delta\tau$ was adjusted internally, based upon the rate at which changes in pressure head were occurring within the flow system. In addition, time dependent flux or potential boundary conditions could be applied at the upper and lower boundary.

The dimensionless conductivity $\kappa(\Theta,\bar{z})$, required in the solution of the predictor and corrector equations, was determined from an empirical function:

---

[12] Personal communication.

$$\kappa = \alpha\Theta^{\eta} \tag{12}$$

The parameters α and η are functions of $\bar{z}$ for a nonhomogeneous material. The dimensionless water capacity ν, was determined by calculating the slope of an empirical pressure head function $\Phi = \Phi(\Theta)$. The form of the empirical function used will be discussed in the following section; however, it should be mentioned here that it was necessary to specify four empirical parameters in order to determine ν at a particular value of Φ and $\bar{z}$. After each calculation of $\Phi_{n,m+1}$ a check was made to see if the sign of $\partial\Phi/\partial t$ had changed. A change in sign indicated that a reversal had occurred and that the water capacity had to be calculated from a different hysteresis curve. When a reversal occurred, that time step was not recalculated, but a search was made for the appropriate scanning curve, and the resulting information used in the next time step. The parameters used in describing the $\Phi(\Theta)$ functions were assumed to be position dependent. The formulation of the hysteresis subroutine was dependent upon the characteristics of the empirical form used to represent the measured $\Phi(\Theta)$ functions; therefore, a discussion of that subroutine will be delayed until the appropriate time, in the "Results and Discussion" section.

IV. RESULTS AND DISCUSSION

A. Saturated Conductivity Measurements

The saturated conductivities determined under steady flow conditions are shown in Figure 12. As expected, the conductivity is considerably greater at true saturation than at the water content reached by rewetting the soil to a pressure head equal to or greater than zero. The conductivities determined after rewetting the soil at the beginning of the experiment, and shortly before disassembly of the column, differed as shown in Figure 12. The differences were small and could have been caused by different amounts of air being entrapped during wetting, or by slight changes in the column packing. Figure 12 was interpreted as evidence that little change in the packing occurred over the major length of the column during the course of the experiment. As would be expected, a comparison of Figure 12 with the graph showing bulk density distribution (Figure 9) shows the lowest conductivities to occur at positions having the highest bulk density. Although an attempt was made to pack the column uniformly, Figures 9 and 12 show the packing to be non-uniform in the vertical direction.

B. Hydraulic Conductivity - Water Content Relation

The results of the conductivity calculations for four flow conditions at position 15 are shown in Figure 13. The data of Figure 13 are similar to the data obtained for each of the 29 sampling locations. There was less data for the end positions (3,57,59) and considerably more scatter in it; therefore, there was less certainty in the $K(\theta)$ functions determined at these locations. The scatter in the data of location 15 is typical of the scatter found at most locations and appears to be typical of the calculation procedure [Rogers and Klute (1971)].

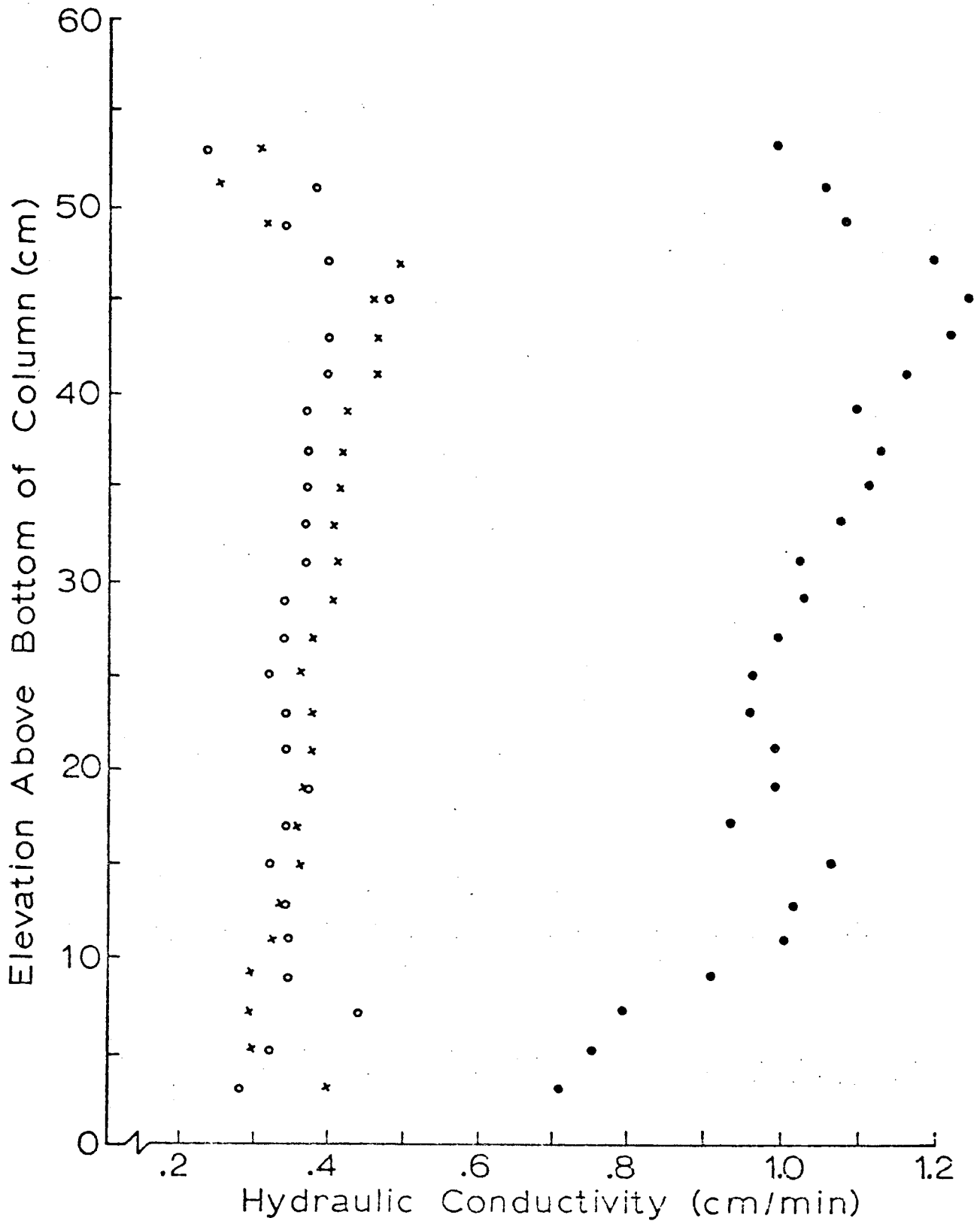

Figure 12. Saturated conductivity distribution determined under conditions of steady flow. (● - true saturation, o - beginning of experiment, x - end of experiment.)

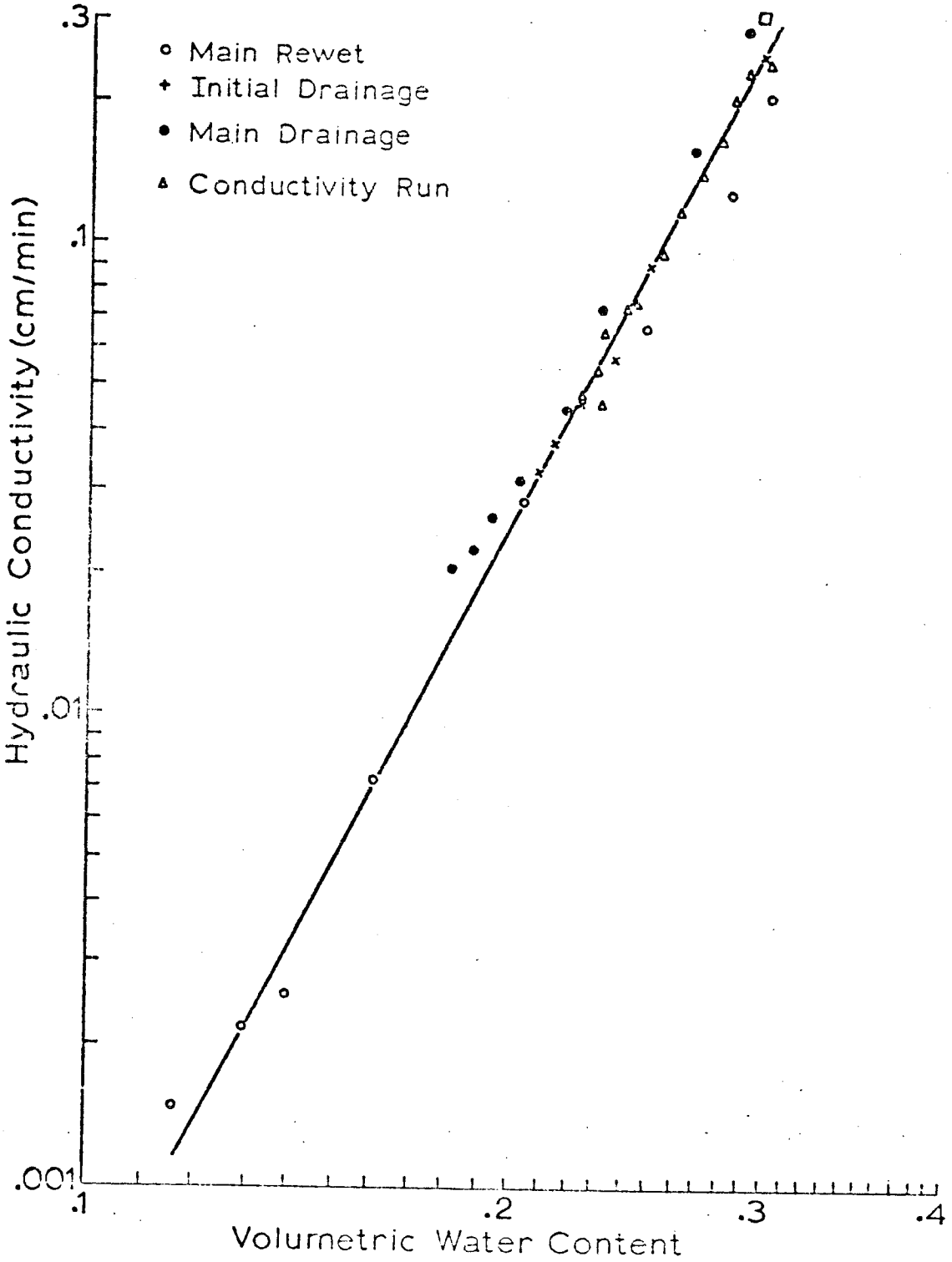

Figure 13. Results of K(θ) determinations at position 15.

A statistical test was not performed; however, the conductivities determined from the main rewet, initial drainage and main drainage flow conditions did not appear to be significantly different from each other. The data shown in Figure 13 suggest that higher conductivities were obtained from the main drainage data; however, this was not consistent when all locations were considered. The evidence indicates that hysteresis in $K(\theta)$, if present, is smaller than the scatter in the data; thus, the assumption of a non-hysteretic $K(\theta)$ function for the medium was justified.

The conductivity run, in which water was supplied to the upper surface at a rate slightly less than it was removed from the bottom, was designed to reduce the amount of scatter in the data. When the data of all positions were considered, this objective did not appear to be achieved. By applying the measured flux at the upper surface, the effect of errors introduced by graphical integration would be reduced; however, the greatest uncertainty was associated with the graphical determination of the gradient $(\partial H/\partial z)_t$. As a result of the column draining at a slower rate, more points could be determined on the $K(\theta)$ curve than could be determined by each of the other three flow conditions.

The regression line of Figure 13 had a linear regression coefficient of 0.976. Thus, $\log_{10}K$ was considered to be a linear function of $\log_{10}\theta$ or

$$\varkappa = \alpha\Theta^{\eta} \tag{13}$$

where $\varkappa$ is the dimensionless conductivity and Θ is the dimensionless water content. The value of K_s used in deriving $\varkappa$ was 1.0 cm/min and the value of θ_s used to calculate Θ was 0.376. The same values of K_s and θ_s were used at all measuring locations. The empirical parameters, α and η, were derived from graphs similar to Figure 13. Since the column was assumed to be non-homogeneous, values of α and η had to be determined at each sampling location.

The values derived are shown in Appendix A, Table 2. Equation (13) was used in the numerical solution to calculate $\varkappa$ from Θ, with α_z and η_z as input information.

C. Pressure Head - Water Content Relationship

1. $\Theta(\Phi,\zeta)$ Data

Figure 14 shows a microfilm plot generated for position number fifteen. The data points represent the initial drainage, main wetting and main drainage curves and three members of the family of wetting scanning curves. Figure 15 shows the initial drainage, main wetting and main drainage curves and four members of the family of drying scanning curves. The data shown is representative of that derived at each of the 29 measuring locations. The amount of scatter and the resulting uncertainty in $\Theta(\Phi)$ was considerably greater at the sampling locations near the ends of the column (positions 3,57 and 59).

During measurement of the initial drainage curves, the column was maintained in a drainage condition for approximately four hours after most of the water appeared to be drained from the column. However, as indicated in Figure 14, the water content did not proceed along the nearly horizontal, low water content portion of the normal drainage curve. It may have been possible to reduce the water content futher by maintaining the column in a drainage condition for a longer period of time, but considering the number of drainage cycles performed, this would have been extremely time consuming and thus impractical. At low water content, the conductivity of the medium becomes very low, resulting in very low drainage rates and thus the slow approach to the residual water content.

As the pressure head became less negative, the medium wet along the main wetting curve to the water content at zero pressure head, Θ_s. Θ_s is

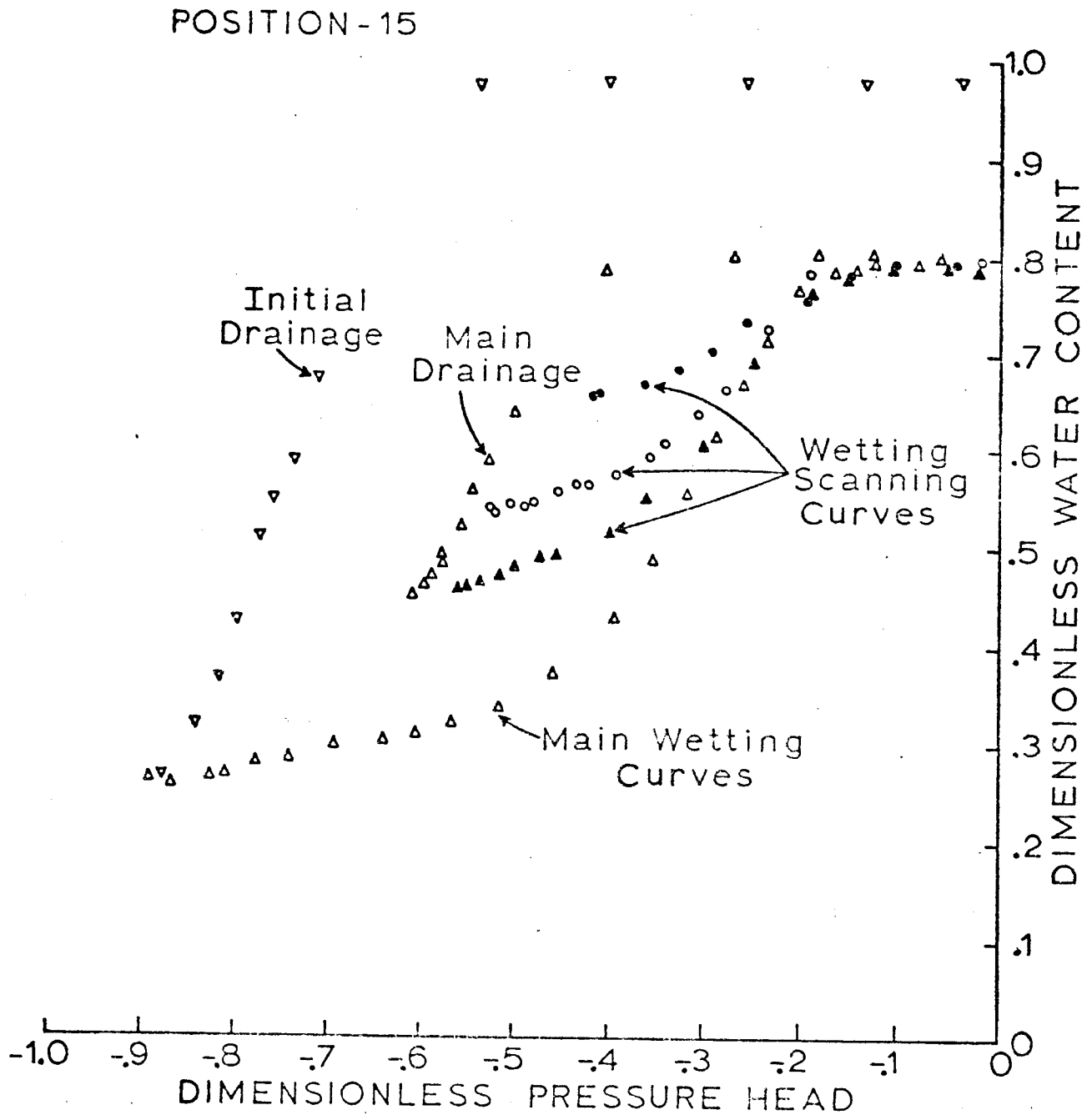

Figure 14. The $\Theta(\Phi)$ relationships obtained for position 15. The initial drainage, main drainage, and several wetting scanning curves are shown.

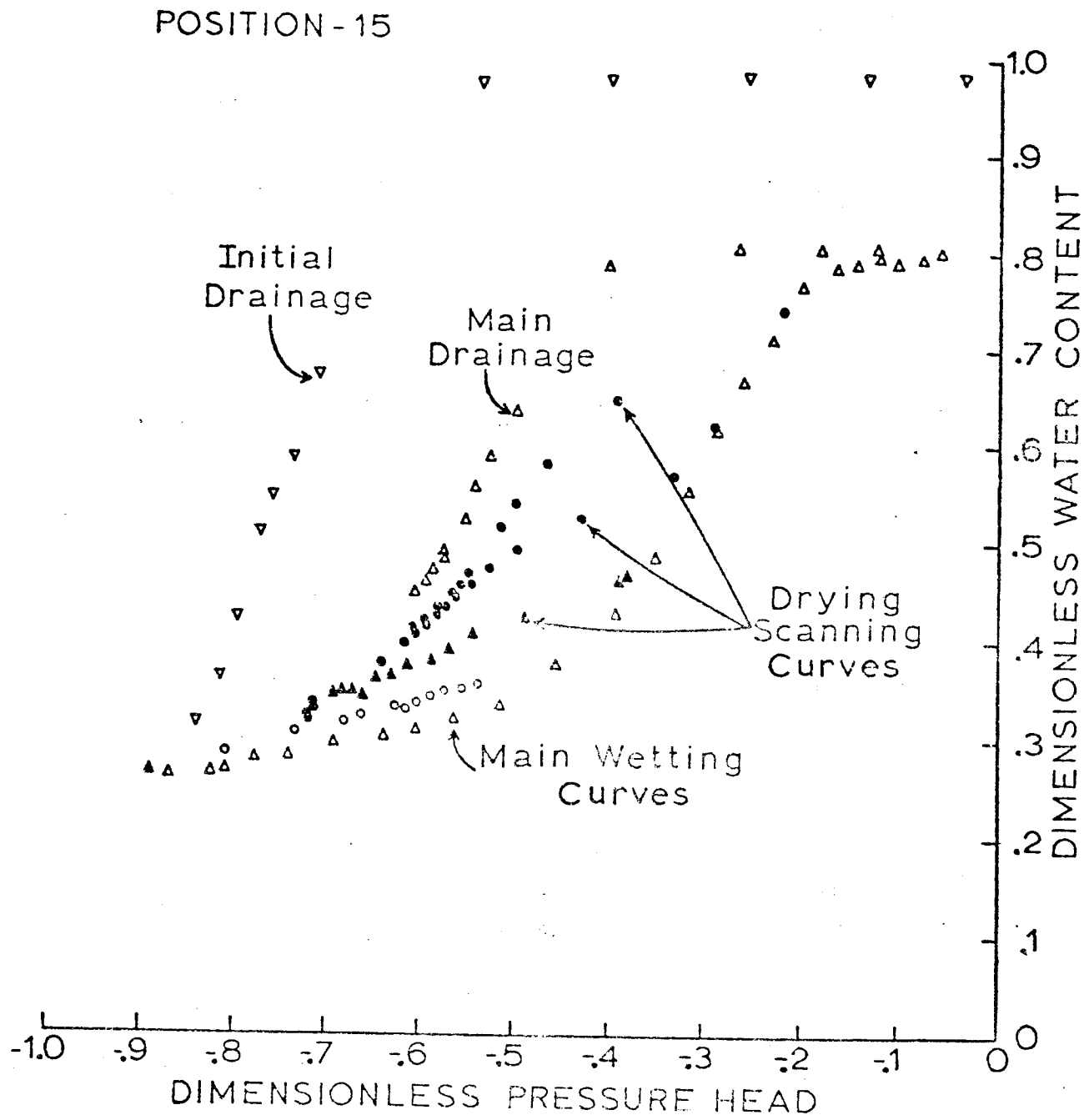

Figure 15. Same as Figure 14, except that drying scanning curves are shown.

less than the water content at true saturation Θ_{st} as a result of air entrapment. The main wetting curve is not unique, but is the lower limit on the hysteretic region of interest. If the medium had been drained along the initial drainage curve to a lower water content before rewetting, a different main wetting curve would have been measured. The main drainage curve departs from the water content axis at Θ_s and is reproducible to the extent that Θ_s is reproducible. Θ_s will be reproducible if the same amount of air is entrapped during each wetting cycle, and the medium is rigid. All of the wetting curves measured at a given position appeared to converge to the same value of Θ_s, at least within experimental error. All flow experiments were conducted in a manner such that the water content-pressure head values would fall on or within the boundary formed by the main drainage and main wetting curves.

The shape of the hysteresis curves varied from position to position. For example, locations near the centre of the column had a much narrower hysteretic region than is shown for position 15. This was further evidence that the column was non-uniform.

2. Empirical Representation of $\Theta(\Phi,\zeta)$

As described previously, the numerical solution of the flow equation requires a value of the water capacity for each Φ calculated. Since the water capacity is $\partial\Theta/\partial\Phi$, the $\Theta(\Phi,\zeta)$ functions must be specified within the computer.

One possible method is to read the hysteresis data into the computer in tabular form. The water capacity at a particular point may then be determined by interpolation (linear or otherwise) between the measured scanning curves. This method requires that a suitable interpolation scheme be devised and in the case of an inhomogeneous medium, would require a large amount of

computer storage.

The procedure used in this study was to represent the scanning curves by empirical equations. A scanning curve could then be described by specifying the parameters of the empirical equation, and the water capacity obtained by differentiation of the equation.

King (1965) showed that a wide range of $\theta(\phi)$ curves could be represented by an equation of the form

$$\theta = \theta_o \left\{ \frac{\cosh\left[(\phi/\phi_o)^{\beta} + \varepsilon\right] - \cosh \varepsilon \left(\frac{\theta_o - \theta_r}{\theta_o + \theta_r}\right)}{\cosh\left[(\phi/\phi_o)^{\beta} + \varepsilon\right] + \cosh \varepsilon \left(\frac{\theta_o - \theta_r}{\theta_o + \theta_r}\right)} \right\} \qquad (14)$$

where θ_o, θ_r, β, ϕ_o and ε are curve fitting parameters. θ_o can be identified with the dimensionless water content at $\phi = 0$. Also, following King (1965), θ_r is greater than zero, ε is equal to or greater than zero, and ϕ_o and β are less than zero. It can readily be shown that as ϕ approaches zero, θ approaches θ_o and as ϕ approaches minus infinity, θ approaches θ_r.

a) Wetting Curves

Representation of a single wetting curve required the selection of θ_o by inspection (θ at $\phi = 0$) and selection of values of the other four parameters (θ_r, β, ϕ_o and ε) by use of a digital computer and a curve fitting routine.

The curve fitting routine assigned five equally spaced values to each of the four parameters resulting in 625 combinations of parameter values. For each set of parameter values equation (14) was solved for each data point on the curve, and the sum of the squared differences between the calculated and measured values of θ was determined. A smaller interval was taken around the parameter values giving the smallest sum of squared differences, and the process repeated. Very little change in the parameter values was realized

by performing a third iteration. This procedure was inefficient since each of the 2 x 625 combinations of parameter values was tested; however, it did not prove to be expensive in terms of computer time, and gave the desired results. The data points and the empirical equation giving the smallest sum of squared differences was plotted on microfilm.

Figure 16 shows the data points and a plot of the empirical equation (solid line) derived for each wetting curve of location 15. The agreement was exceptionally good.

An equation to represent the complete family of wetting curves at a particular location in the column would be most convenient. An examination of the parameter values for each wetting curve at several locations showed that e could be taken as zero and that Θ_r was very nearly the water content at which the curve departed from the main drainage curve. Figure 17 shows the values of the parameters β and Φ_o plotted against Θ_r for the four wetting curves at position 15. As suggested by this plot β and Φ_o were assumed to be linear functions of Θ_r. That is:

$$\begin{aligned} \beta &= S_B \Theta_r + I_B \\ \Phi_o &= S_p \Theta_r + I_p \end{aligned} \qquad (15)$$

where S_B, I_B and S_p, I_p are the slopes and intercepts of the respective linear relations.

Thus, since $e = 0$, equation (14) may be written:

$$\Theta = \Theta_o \left\{ \frac{\cosh\left[\left(\frac{\Phi}{S_p \Theta_r + I_p}\right)(S_B \Theta_r + I_B)\right] - \left(\frac{\Theta_o - \Theta_r}{\Theta_o + \Theta_r}\right)}{\cosh\left[\left(\frac{\Phi}{S_p \Theta_r + I_p}\right)(S_B \Theta_r + I_B)\right] + \left(\frac{\Theta_o - \Theta_r}{\Theta_o + \Theta_r}\right)} \right\} \qquad (16)$$

As pointed out previously, Θ_o can be determined by inspection, and has the same value for all wetting curves at a particular location. Thus, equation

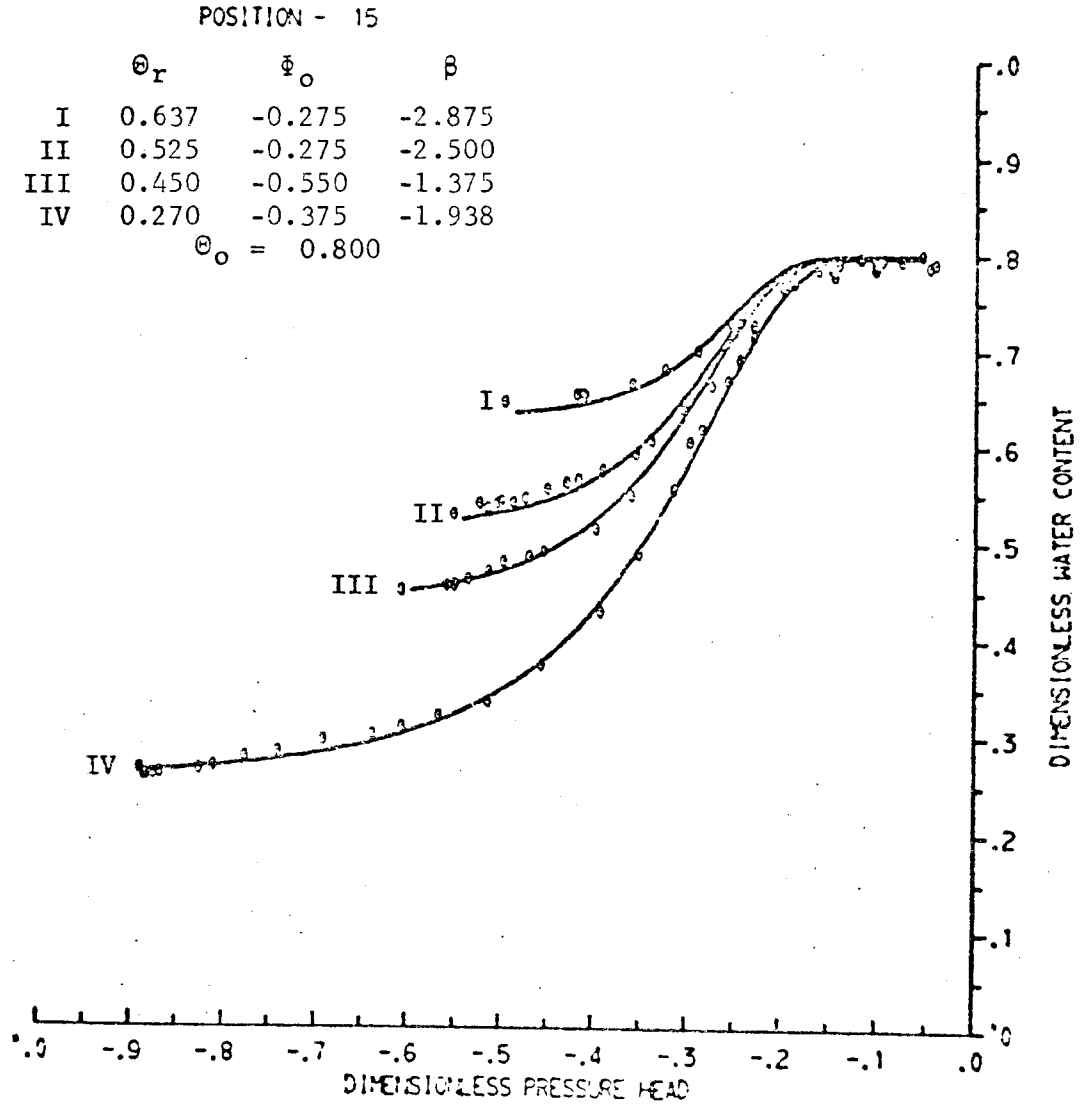

Figure 16. Comparison of experimental data (points) and the fitted empirical function, equation (14), (solid lines) for the wetting scanning curve data at position 15.

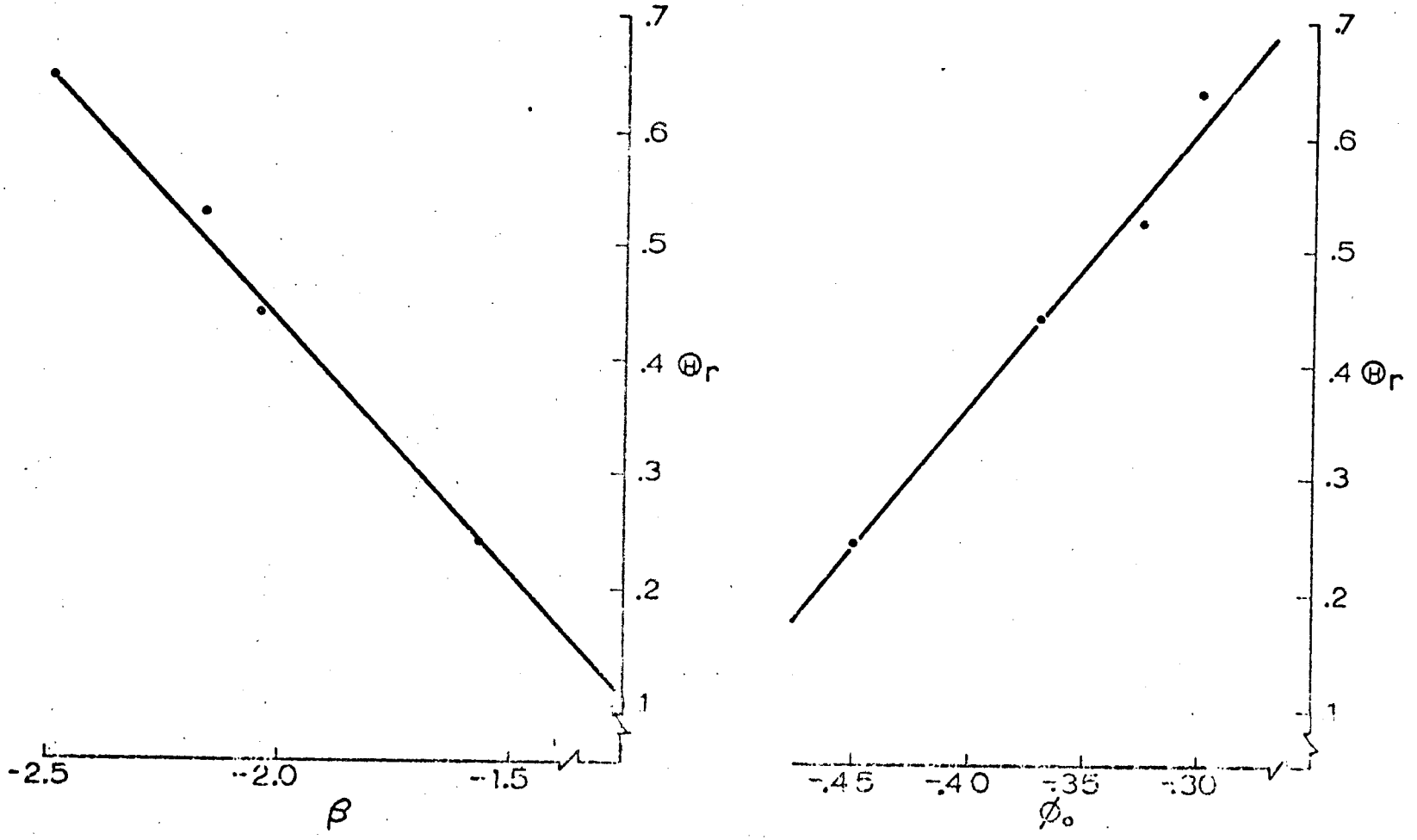

Figure 17. Graph of the parameters β and Φ derived for each wetting curve plotted against the respective values of θ_o for position 15.

(16) is a four parameter equation which gives the scanning curve for each value of θ_r, the water content at which the wetting curve departs from the main drainage curve. That is, equation (16) represents the infinite family of wetting curves at a particular location.

The values of the four parameters (S_B, I_B, S_p, I_p) may be determined graphically as the slopes and intercepts of straight lines similar to those shown in Figure 17. Alternatively a curve fitting technique similar to that described for selecting the parameters of equation (14) was used. For each set of values of the parameters, (S_B, I_B, S_p, I_p) equation (16) was solved for each point of each experimental curve and the total sum of squared differences between the experimental and calculated values determined. In fitting equation (16) to the family of experimental curves, the appropriate value of θ_r for each curve in the family was used. Figure 18 shows the experimental points for position 15 and their empirical representation derived by using equation (16) and the parameter values giving the smallest sum of squared differences. Again, the agreement between the data points and the empirical representation is very good. It should be emphasized that the four parameters (S_B, I_B, S_p, I_p) define the entire family of wetting scanning curves, and a single curve is defined by these four parameters plus θ_r. Since the column was assumed to be non-uniform, a set of parameters was derived for each measuring location. The parameter values for the main wetting curve at each location in the column are shown in Appendix A, Table I.

The parameters S_B, I_B, S_p and I_p can be determined by fitting equation (16) to the data for one wetting curve; then, other wetting curves can be generated by substituting different values of θ_r into equation (16). By this procedure, the main wetting curve of position 15 was used to generate the parameter values, and an empirical representation of the remaining

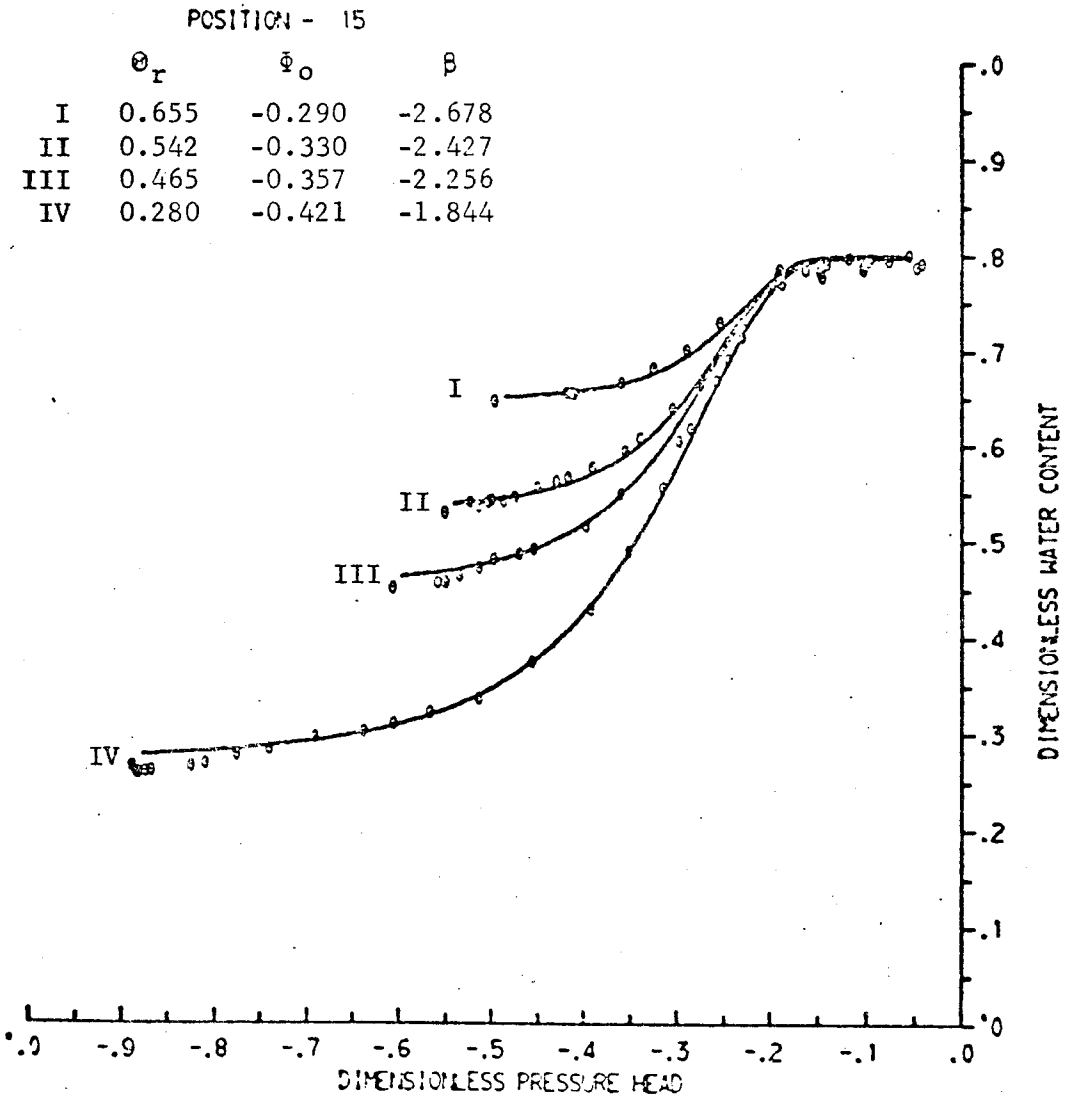

Figure 18. The empirical representation of the family of wetting curves compared with the measured data. The data of all measured curves was used to derive the curve fitting parameters.

experimental curves was subsequently derived. The results are shown in Figure 19. The good agreement between the experimental curves and their empirical representation strongly suggests the possibility of being able to generate the family of wetting scanning curves from a single experimentally determined curve. Since only one material was used in this study, it is recognized that the results may have been fortuitous. In light of the tremendous savings to be made in time and effort required to experimentally measure a family of scanning curves, the method appears to be worthy of further investigation.

b) Drying Curves

Empirical representation of the drying curves proved to be more difficult. In applying equation (14), preliminary studies showed that ϵ could be assumed to be zero and that Θ_r was the water content to which all members of a family of drying curves appeared to converge. The value of Θ_o used was the water content at which the extrapolated drainage curve reached a dimensionless pressure head of zero. This left only two parameters to be evaluated (β and Φ_o). A curve fitting routine similar to that described for fitting equation (14) to an individual wetting curve was used to evaluate β and Φ_o.

Figure 20 shows the drainage scanning curves of location 15 fitted using equation (14). The empirical curves represented most of the data quite well; however, one problem region was evident. For curves having Θ_o values between approximately 0.55 and 0.75, the empirical curves departed from the main wetting curve with a smaller slope than did the experimental curves, then broke more sharply to rejoin the experimental curves.

Allowing ϵ to take on non zero values did not improve the agreement between the empirical and experimental curves. A reduced sum of squared

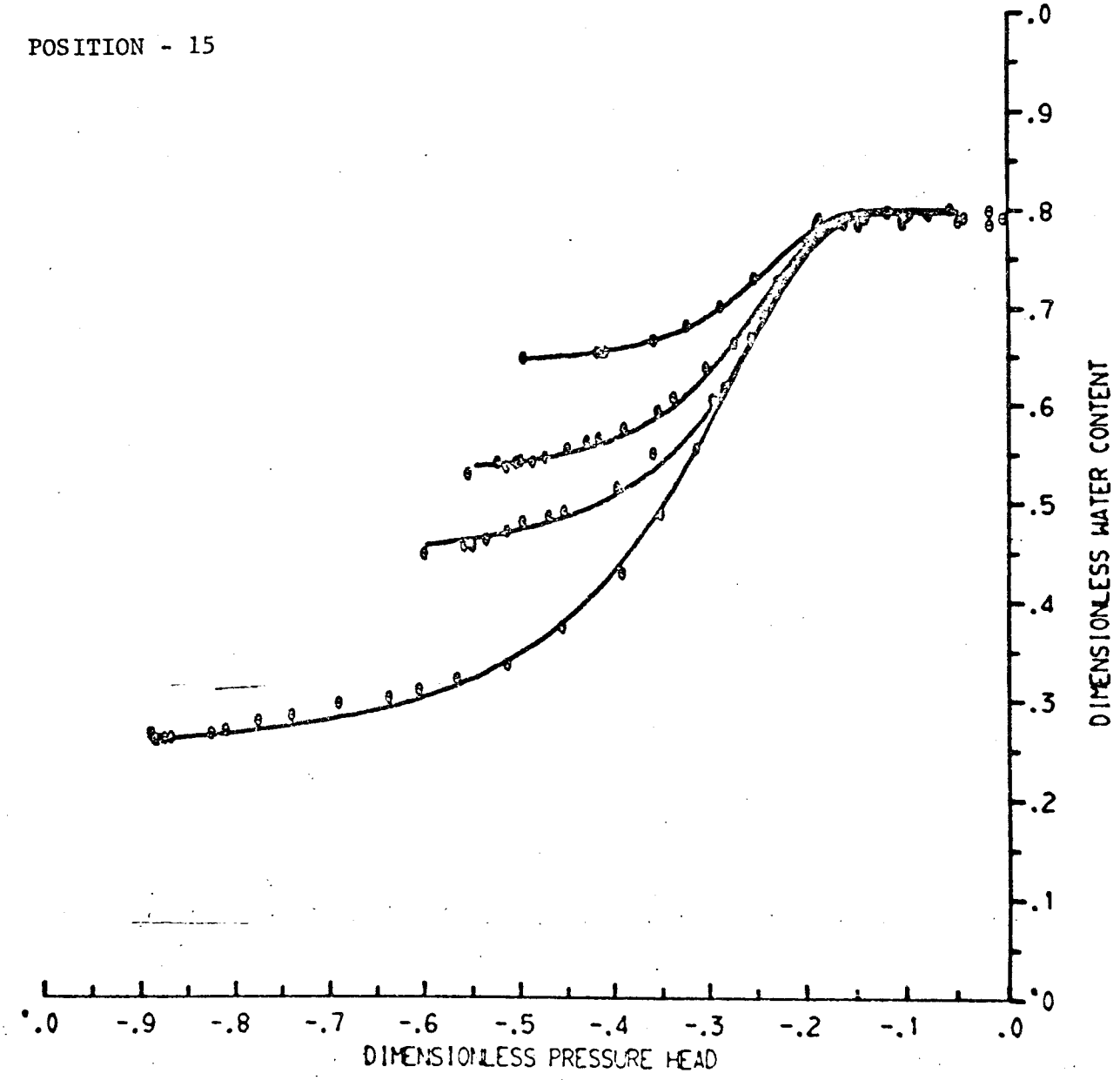

Figure 19. Figure 19 is identical to Figure 18, except the parameter values were obtained from only the data of the main wetting curve.

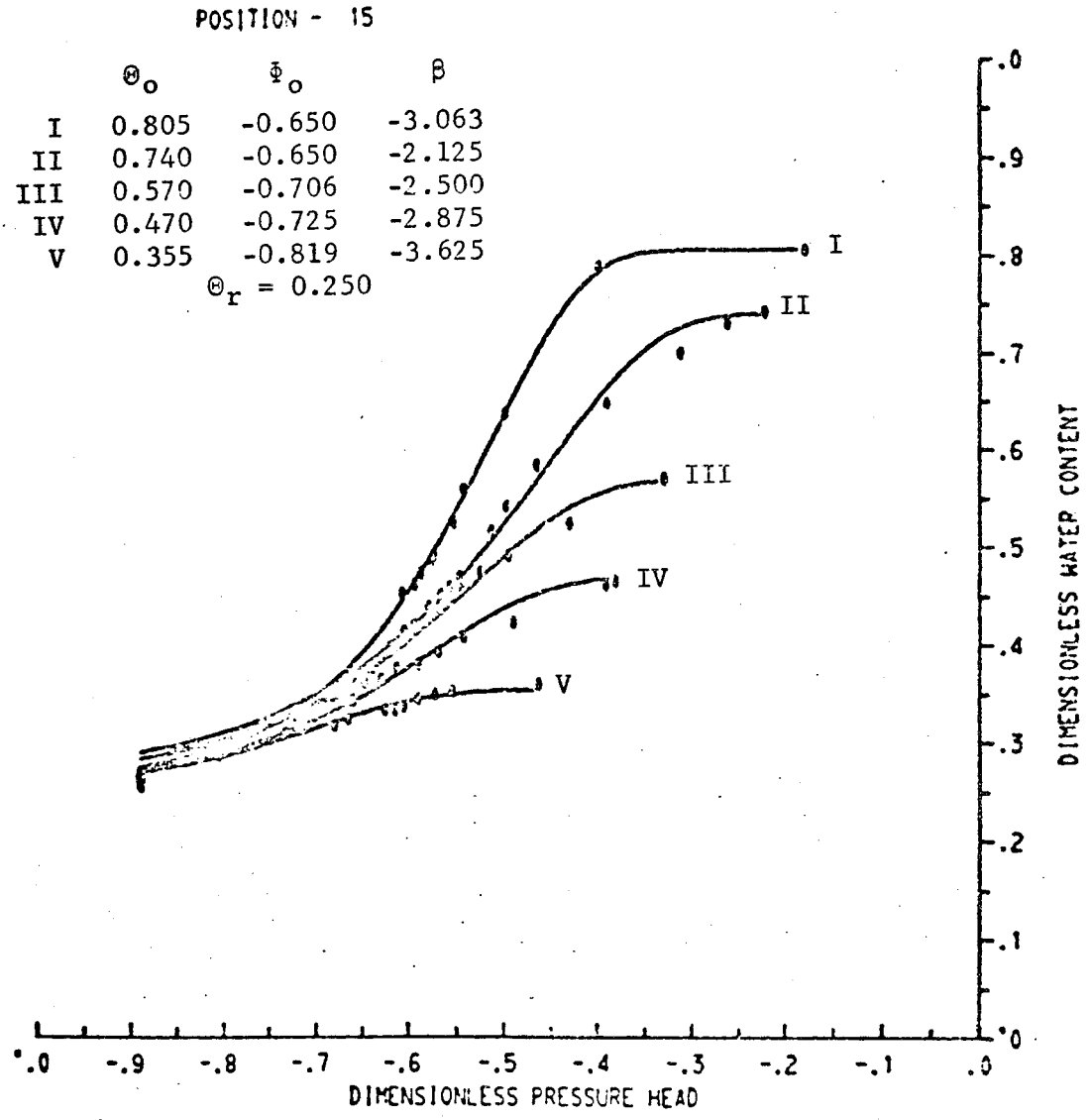

Figure 20. Comparison of experimental data (points) and the fitted empirical function, equation (14), (solid lines) for the drying scanning curve data at position 15.

differences could be obtained by treating Θ_o and Θ_r as parameters rather than by selecting them by inspection of the data; however, in most cases this resulted in poorer agreement between the empirical curves and the data curves in the high water content regions. Undoubtedly this is a consequence of the sum of squared differences criterion being weighted by the greater number of data points in the low water content region. After considerable testing, it was concluded that selection of Θ_o and Θ_r by inspection and searching for the values of β and Φ_o which gave the smallest sum of squared differences, consistently gave the best agreement between the empirical and experimental curves.

As indicated in Figure 21, there did not appear to be a linear relationship (or any simple functional relationship) between the parameter values of β and Φ_o and Θ_o. For this reason, the parameter values for an unmeasured curve were determined by linear interpolation between the measured curves bracketing the required curve. In order to represent accurately a family of drainage curves, there must be a sufficient number of points (β, Θ_o) and (Φ_o, Θ_o) such that linear interpolation between points would not introduce significant errors.

In many instances, inspection of the hysteresis information indicated that adjacent positions were similar to each other. For these situations the data were pooled, and for each group of data, a graph similar to Figure 21 was constructed. An examination of these graphs indicated that the functions $\beta = \beta(\Theta_o)$ and $\Phi_o = \Phi_o(\Theta_o)$ could each be approximated by three (or fewer) straight line segments and consequently could be specified by four values of (β, Θ_o) and (Φ_o, Θ_o). The parameter values for the main drainage curve at each location are shown in Appendix A, Table I.

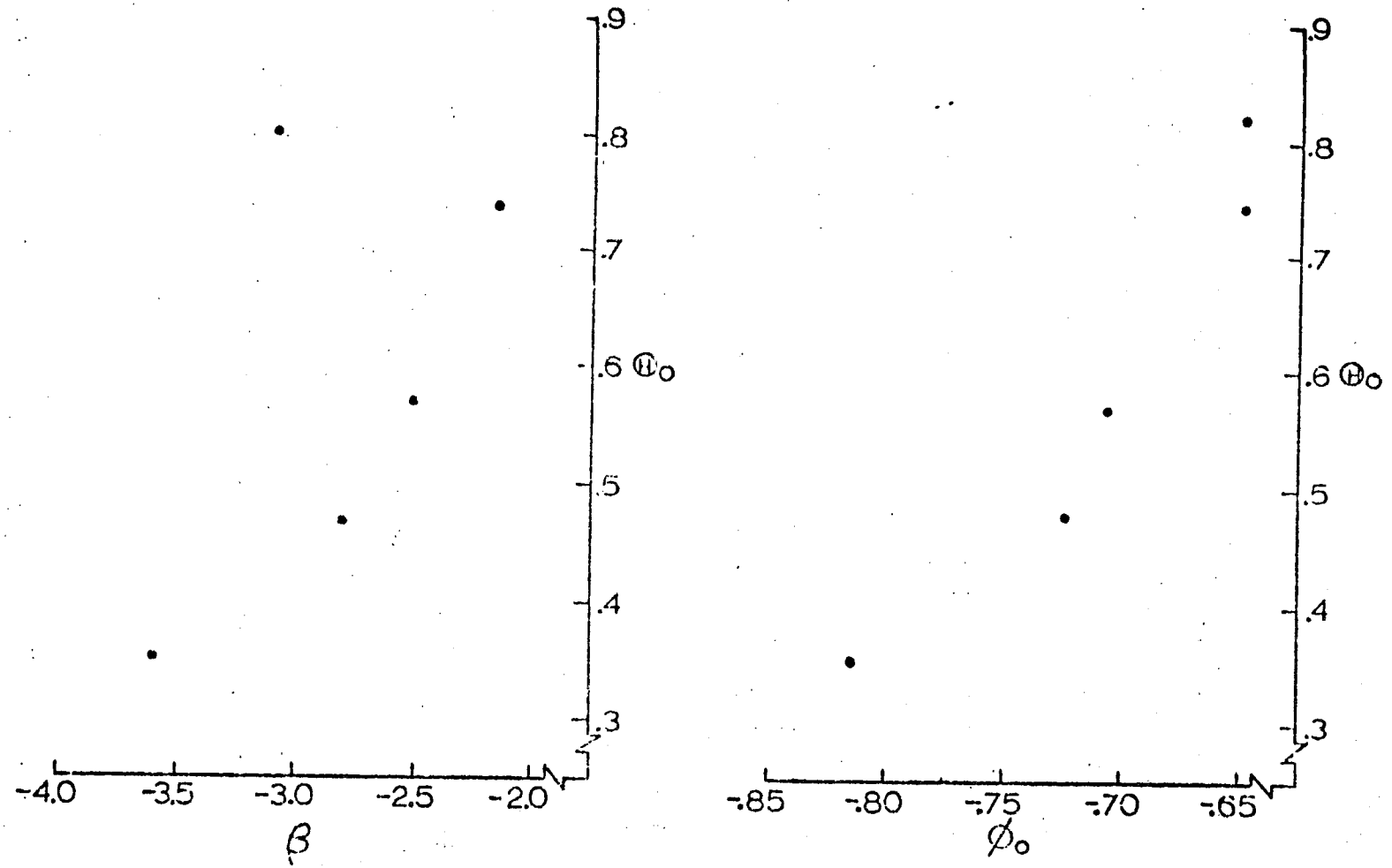

Figure 21. The parameters β and ϕ_o derived for each measured drying scanning curve at position 15 plotted against θ_o.

Since there was no simple relation between the parameters (β and Φ_o) and Θ_o, there was no apparent method for generating the family of drying curves from a single measured curve. The simple representation of a family of wetting curves is undoubtedly the result of the similarity in shape among members of the family. Drying curves, on the other hand go through a transition from sharp breaking curves for values of Θ_o near Θ_s to more gradually breaking curves for lower values of Θ_o.

In addition to the families of primary wetting and drying scanning curves there are families of secondary scanning curves. A curve which departs from a primary curve rather than a main curve is a secondary curve. For this study, if a reversal occurred (change in the sign of $\partial\Theta/\partial\tau$) at a point (Φ,Θ) other than on one of the main curves, the appropriate $\Theta(\Phi)$ function for determining the water capacity was assumed to be the primary scanning curve which passed through the reversal point.

3. Hysteresis Subroutine

In order to calculate the pressure head at a particular point in the space-time grid $(\Phi_{n+1}, m+1)$, the predictor-corrector formulation of the flow equation required that the water capacity at the previous time step $(\Phi_{n,m})$ be specified.

The slope of $\Theta(\Phi)$, γ, can be determined by differentiating equation (14) to give:

$$\gamma = \frac{d\Theta}{d\Phi} = \left\{ \frac{\dfrac{2\beta\Gamma\Theta_o}{\Phi_o}\left(\dfrac{-\Phi}{-\Phi_o}\right)^{\beta-1}\sinh\left(\dfrac{-\Phi}{-\Phi_o}\right)^{\beta}}{\left[\cosh\left(\dfrac{-\Phi}{-\Phi_o}\right)^{\beta}+\Gamma\right]^2} \right\} \qquad (17)$$

where $\Gamma = (\cosh e)\left[\dfrac{\Theta_o - \Theta_r}{\Theta_o + \Theta_r}\right]$.

When calculating $\Phi_{n+1,\, m+1}$, $\Phi_{n,m}$ is known, thus equation (17) can be solved for $\gamma_{n,m}$, provided β, Φ_o, Θ_o, Θ_r and ϵ are known. As discussed previously, ϵ could be assumed equal to zero for the medium used in this study.

While a particular region continues to wet, it does so along the $\Theta(\Phi)$ curve specified by the appropriate values of the parameters β, Φ_o, Θ_o and Θ_r. If the region commences to drain, however, the water content proceeds along a new $\Theta(\Phi)$ function which must be specified by a new set of parameter values. The hysteresis subroutine was entered each time a reversal (change in the sign of $\partial\Theta/\partial\tau$) was detected. Its purpose was to select the new values of β, Φ_o, Θ_o and Θ_r to be used until the next reversal was detected.

Each position node n was assigned a hysteresis index of +1 if it was draining, or -1 if it was wetting. When a reversal was detected, the sign of the hysteresis index was changed, and the hysteresis subroutine called. If the hysteresis index was + 1, the hysteresis subroutine would search for the appropriate drying curve parameters and similarly, if -1, a set of wetting curve parameters would be derived.

The hysteresis subroutine searched for the scanning curve which passed through (Φ_n, Θ_n), the pressure head and water content calculated at the time step before the reversal was detected. To locate the appropriate wetting curve, equation (16) can be solved for Θ_r by substituting (Φ_n, Θ_n) and the values of S_B, I_B, S_p, I_p and Θ_o which apply to node n. Since equation (16) is implicit in Θ_r, an iterative search procedure was used to find the value of Θ_r which satisfied (16). Knowing Θ_r, new values of β_n and $(\Phi_o)_n$ were calculated from equation (15), and control returned to the main programme.

Selection of drainage curve parameters was less straight forward.

The hysteresis subroutine must provide values of Θ_o, and Φ_o corresponding to a drainage curve passing through a reversal point (Θ_n, Φ_n). Θ_n was taken as an initial estimate of Θ_o. Values of β and Φ_o corresponding to the estimated Θ_o were determined by interpolation in the table of values of β and Φ_o versus Θ_o described above (p. 66). Equation (14) was solved for Θ at Φ_n using these parameters. A new estimate of Θ_o was made based upon the difference between Θ_n and the calculated value of Θ. The process was repeated until the calculated value of Θ was sufficiently close to Θ_n.

Selection of wetting curve parameters for a particular node required that values of Θ_o, S_B, I_B, S_p and I_p for that node be stored in the computer. Selection of drying curve parameters required that Θ_r and four sets of (Θ, β, Φ) be stored for each node. Since the column had 29 nodes, 29 x 18 = 522 storage locations were required for the complete description of the hysteretic $\Theta(\Phi)$ function in the non-uniform column.

D. Comparisons Between Predicted and Measured Results

1. Slow Drainage - Rewet Experiment

Figure 22 is a print of the microfilm output showing the relation between predicted and measured dimensionless pressure head (PHI) at positions 31 and 33 for the slow drainage - rewet experiment. The symbols indicate the measured pressure head values while the solid lines trace the numerically predicted pressure heads. Only two positions are shown; however, the degree of accuracy demonstrated in Figure 22 was typical of most locations in the column. There is near perfect agreement between the measured and predicted results during the drainage phase of the experiment, although, as the time of reversal was approached, the predicted

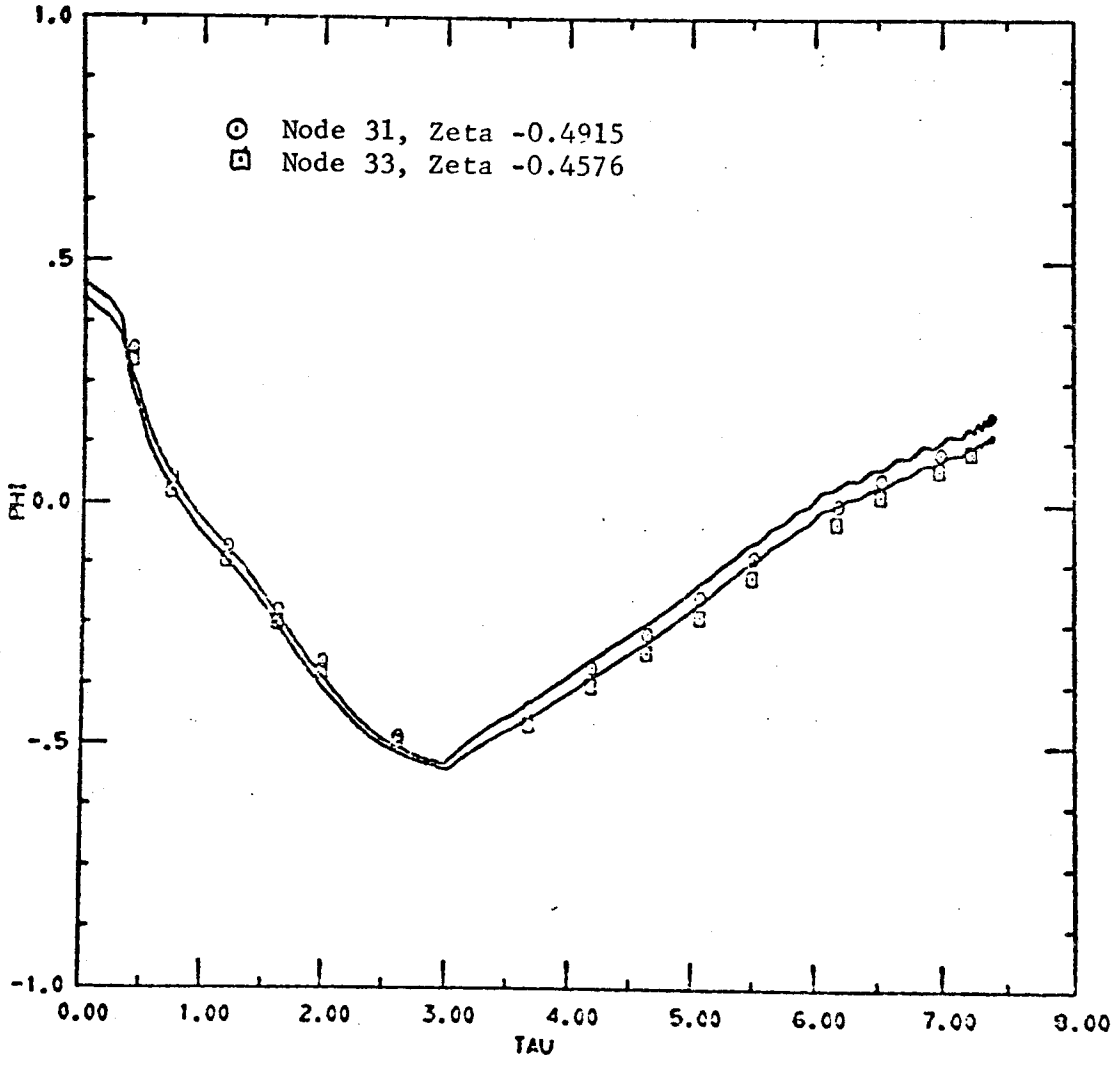

Figure 22. Comparison of the measured (symbols) and predicted (solid lines) dimensionless pressure head versus time at positions 31 and 33 for the slow drainage - rewet experiment.

pressure heads were slightly more negative than those measured. During the wetting phase, the predicted pressure head was consistently higher than the measured values.

Figure 23 shows the measured and predicted pressure head profiles in the column at $\tau = 0$ and at four arbitrarily selected values of $\tau > 0$. $\Phi(\bar{Z})$ at $\tau = 0$ represents the initial condition (static equilibrium). At $\tau = 2$ all positions in the column were draining, at $\tau = 3$ the portion of the column above an elevation of 27 cm continued to drain while the lower portion was wetting, at $\tau = 4$ only that portion of the column above an elevation of 45 cm continued to drain, and at $\tau = 5.5$ all parts of the column were saturated or were wetting.

As indicated previously, the numerical solution tended to predict pressure heads more negative than those measured during drainage and less negative than those measured during wetting. The greatest differences occurred at the upper end of the column (above an elevation of 51 cm). During collection of the hysteresis data, changes in the bulk density in this region introduced errors into the water content data. This resulted in uncertainties in the form of the $\Theta(\Phi)$ functions and consequently greater errors in the predicted values of Φ at the upper end of the column. Neglecting the data for $\tau = 0$, the average difference between the predicted and measured pressure heads was $\Delta\Phi = 1.24 \times 10^{-2}$ ($\Delta h = 0.75$ cm) and if the positions above an elevation of 51 cm were ignored, 95% of the predicted values were within $\Delta\Phi = 2.0 \times 10^{-2}$ ($\Delta h = 1.2$ cm) of the measured values.

The numerical solution is an approximation of the true solution; furthermore, the hydraulic functions $\Theta(\Phi)$ and $\kappa(\Theta)$ used in the numerical solution were empirical representations of the actual functions and consequently, subject to some error. For these reasons, perfect agreement

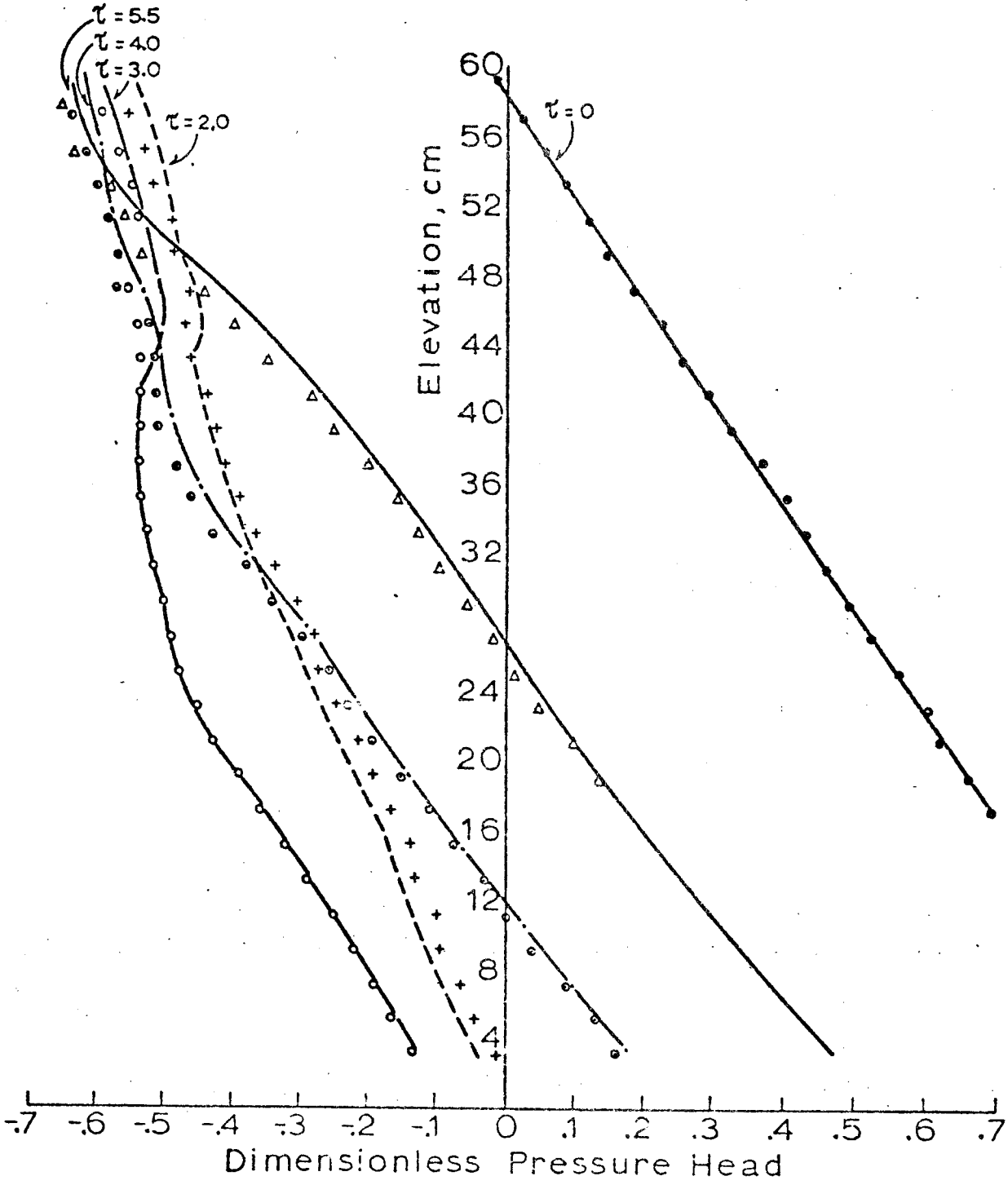

Figure 23. Graph showing measured and predicted dimensionless pressure head profiles for selected values of elapsed time during the slow drainage - rewet experiment.

between the measured and predicted pressure heads could not be expected. Considering the good agreement between measured and predicted results as demonstrated by Figures 22 and 23, a detailed study of the cause of the differences did not appear to be warranted. Since the slow drainage-rewet experiment, and the experiments performed to collect the hysteresis information were conducted at approximately the same rates, a possible rate dependence of $\Theta(\Phi)$ was not considered to be a factor in accounting for the differences between the predicted and measured Φ values.

Figure 24 is similar to Figure 21 except $\Theta(\tau)$ for positions 31 and 33 have been plotted rather than $\Phi(\tau)$. Similarly, Figure 24 shows the $\Theta(Z)$ profiles corresponding to the $\Phi(Z)$ profiles of Figure 23. There appears to be considerably more scatter of the measured water content data about the predicted curves (Figure 25) than in the case of the measured and predicted pressure heads (Figure 23). Some of this apparent scatter is caused by the expanded scale used in plotting Θ. If, for the data of Figure 24, the initial condition ($\tau = 0$) and positions above an elevation of 51 cm are neglected, the average difference between the predicted and measured values of Θ is 1.7×10^{-2}, or in terms of volumetric water content, a difference of approximately 6.5×10^{-3}. Also, 95% of the predicted values of Θ were within 3.0×10^{-2} of the measured values.

The differences between the observed and predicted water contents are probably the result of several factors. The predicted Θ values were calculated from the predicted Φ values by using the appropriate $\Theta(\Phi)$ function. As a result of the steepness of the $\Theta(\Phi)$ curves, small errors in Φ could produce large errors in Θ. As an approximation, if the steep portion of a drainage curve is considered the average difference between the measured and predicted Φ values (1.25×10^{-2}) could result in differences

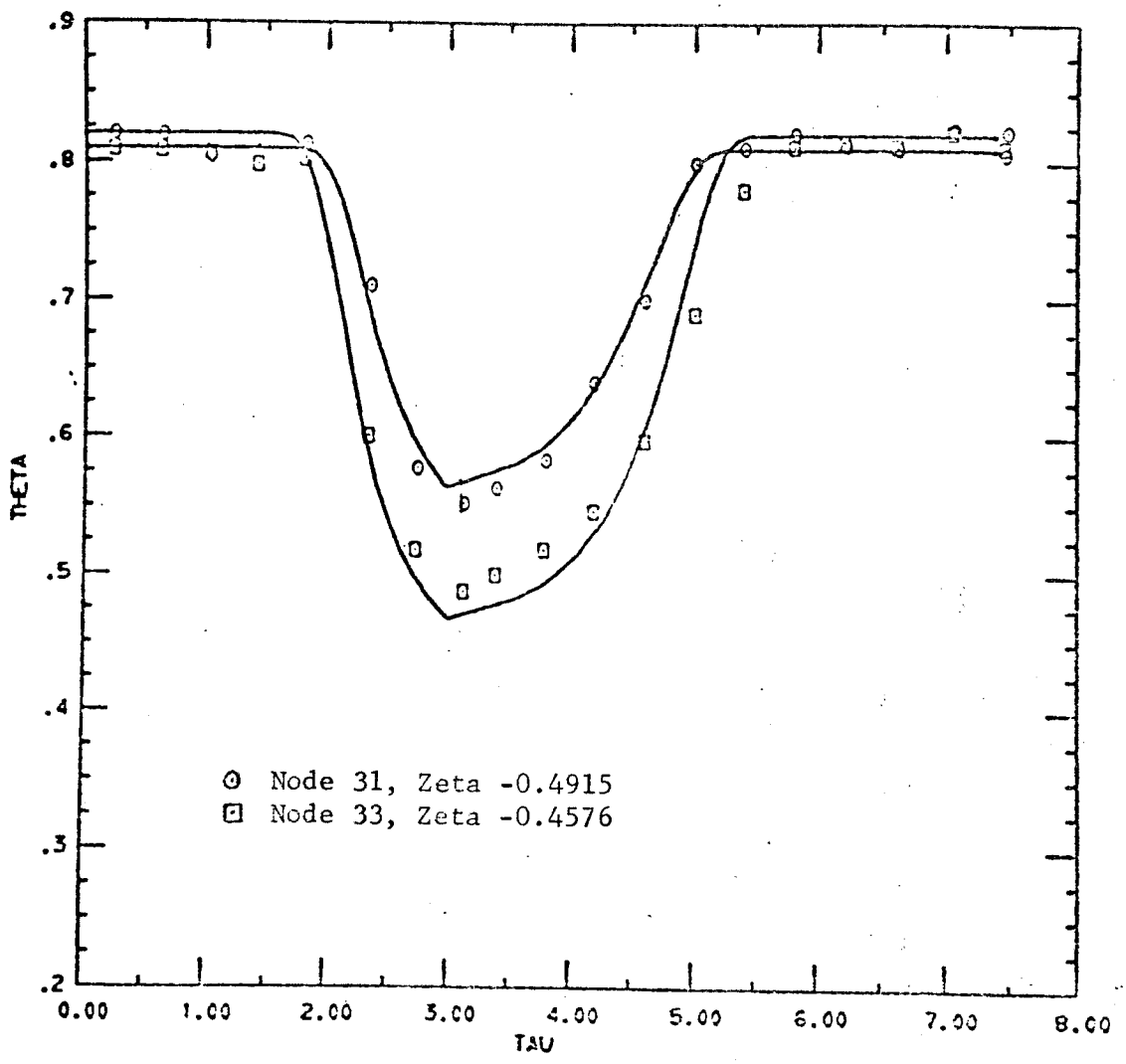

Figure 24. Comparison of the predicted (solid lines) and measured (symbols) dimensionless water content versus time at positions 31 and 33 for the slow drainage - rewet experiment.

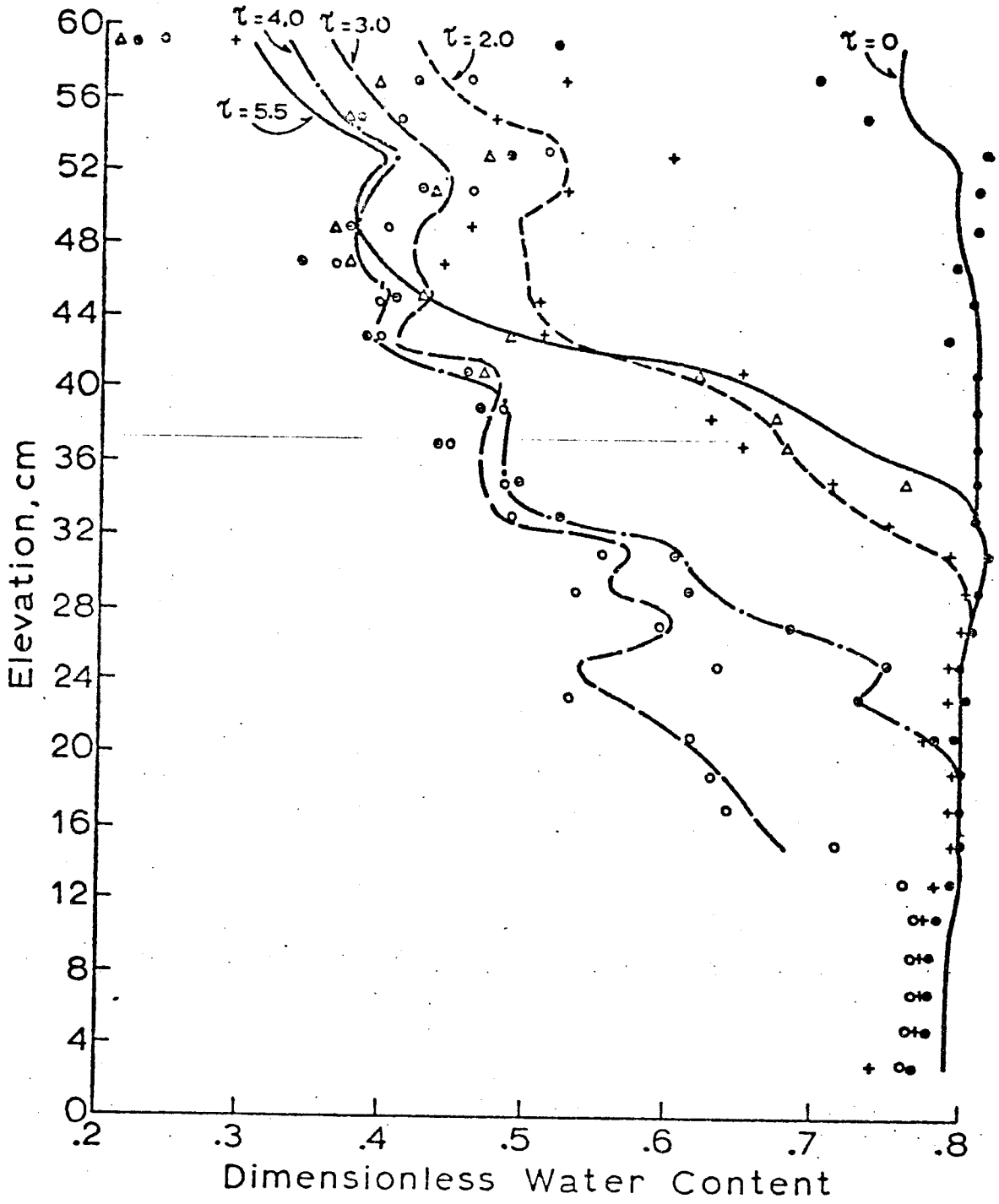

Figure 25. Comparison of measured (symbols) and predicted (solid lines) water content profiles at selected values of the elapsed time during the slow drainage - rewet experiment.

between predicted and measured θ values of 2.6×10^{-2}. The average observed difference was approximately one half this value. Following the trends observed in the pressure head profiles, the predicted water contents should be lower than those measured when drying and higher than those measured during wetting. Although this trend can be seen in Figure 25, the scatter of the measured θ values about those predicted suggests the influence of other factors. An incorrect empirical representation of the $\theta(\Phi)$ functions would result in erroneous θ values since θ is calculated from $\theta(\Phi)$.

The measured values of θ can also be questioned. The uncertainty in θ resulting from statistical variations in the observed gamma counting rate is $\theta \pm 0.008$ and therefore, could not be a major cause of the scatter indicated in Figure 25. Furthermore, if the difference between measured and predicted θ values was the result of counting statistics, the measured water content data should vary randomly about the predicted values for any node. As exemplified by Figure 24, this was not the case. On the other hand, a change in the bulk density of the medium of 0.05 g/cc would give rise to an error in the measured values of θ of 0.05. Changes in the packing at the upper end of the column were undoubtedly the cause of the large differences between predicted and measured θ values in this region. In several instances, the measured θ values at a particular value of $\bar{z}$ differed in a consistent manner from the predicted values. As examples, in Figure 25, all the measured values at position 51 were higher than the predicted values, while at position 47, the measured values were less than those predicted. This would be consistent with an increase in the bulk density of the medium at position 51 and a decrease at 47. Although considerable effort was made to obtain a stable packing before calibrating

the gamma system, small but significant changes in the bulk density could have occurred.

The irregular shape of the computed water content profiles of Figure 25 is a consequence of the non-uniform nature of the medium.

The results of the slow drainage-rewet experiment indicate the predictor-corrector formulation of the flow equation to be a valid method for solving unsaturated flow problems (subject to the limitations of the flow equation). The results further demonstrate the usefulness of the empirical forms used to represent the $\kappa(\Theta)$ and $\Theta(\Phi)$ functions for a non-uniform medium. The medium used in this study was relatively uniform; therefore, further tests should be conducted using media consisting of layers with large textural differences.

2. Rapid Drainage - Rewet Experiment

Figure 26 shows the measured (symbols) and predicted (solid lines) pressure heads at positions 27 and 33 for the rapid drainage - rewet experiment. As in the slow drainage experiment, the numerical solution predicted pressure heads greater than the measured values during the wetting phase of the experiment.

As demonstrated in Figure 27, for four arbitrarily selected values of τ, the numerical solution predicted the measured pressure head profiles quite accurately. The average difference between the predicted and measured values of Φ was 1.66×10^{-2}, or an average difference in head of 1.0 cm of water.

The measured and predicted water content profiles corresponding to the pressure head profile of Figure 27 are shown in Figure 28. The average difference between measured and predicted values of Θ was 2.9×10^{-2}, or in terms of volumetric water content, 1.16×10^{-2}. Although the average

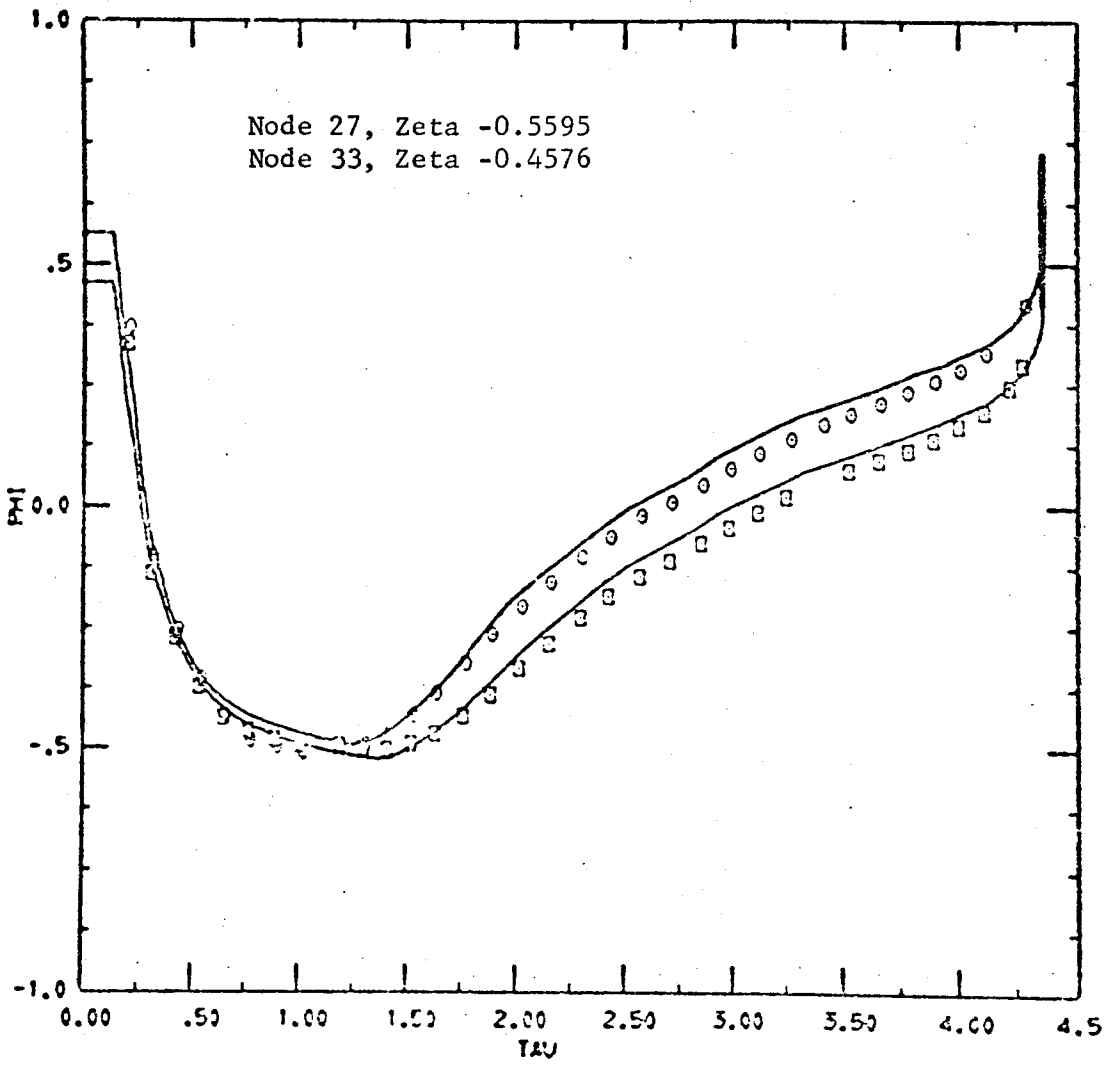

Figure 26. Comparison of the measured (symbols) and predicted (solid lines) dimensionless pressure head versus time at positions 27 and 33 during the rapid drainage - rewet experiment.

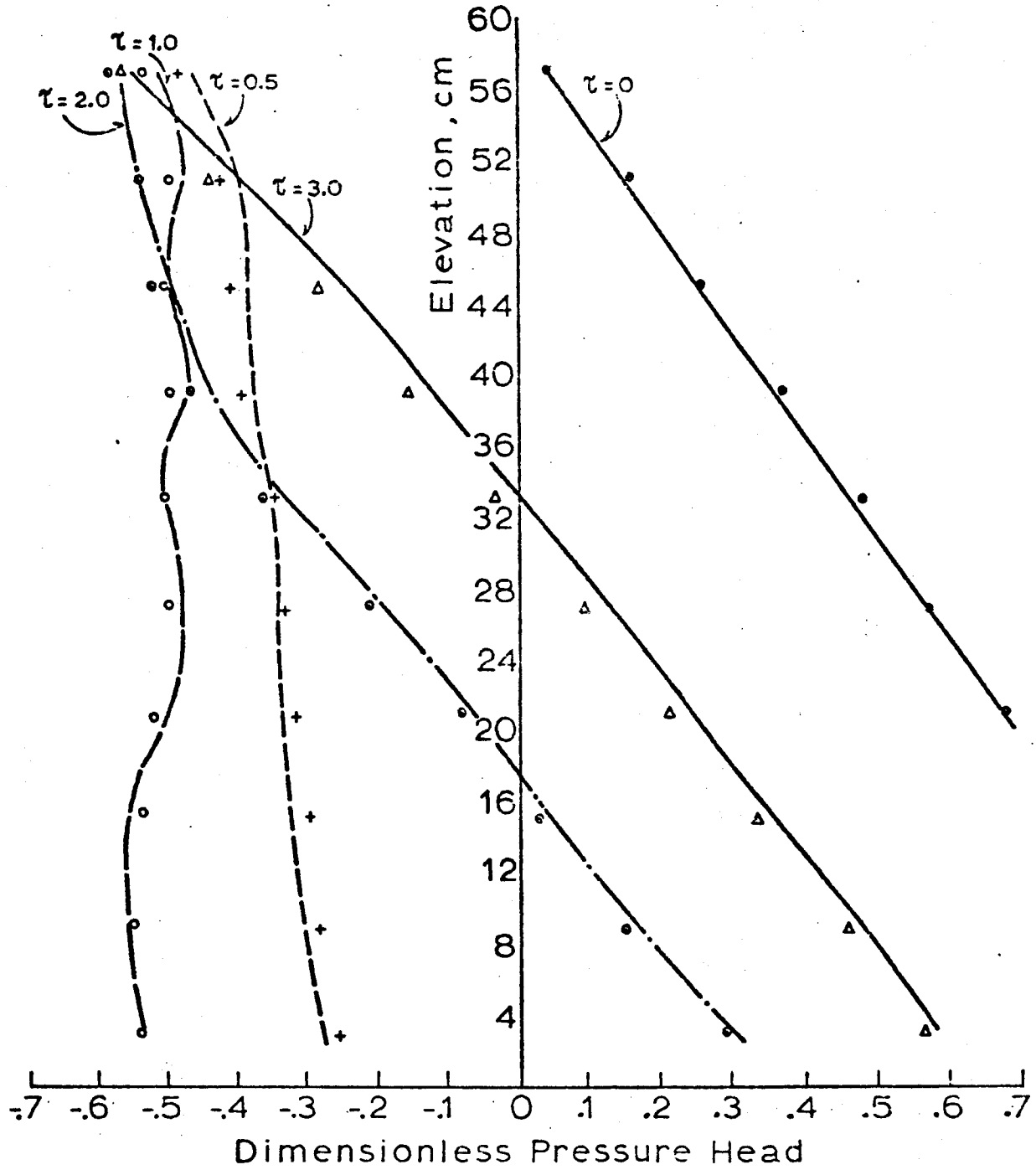

Figure 27. Comparison of the predicted (solid lines) and measured (symbols) pressure head profiles at selected values of the elapsed time during the rapid drainage - rewet experiment.

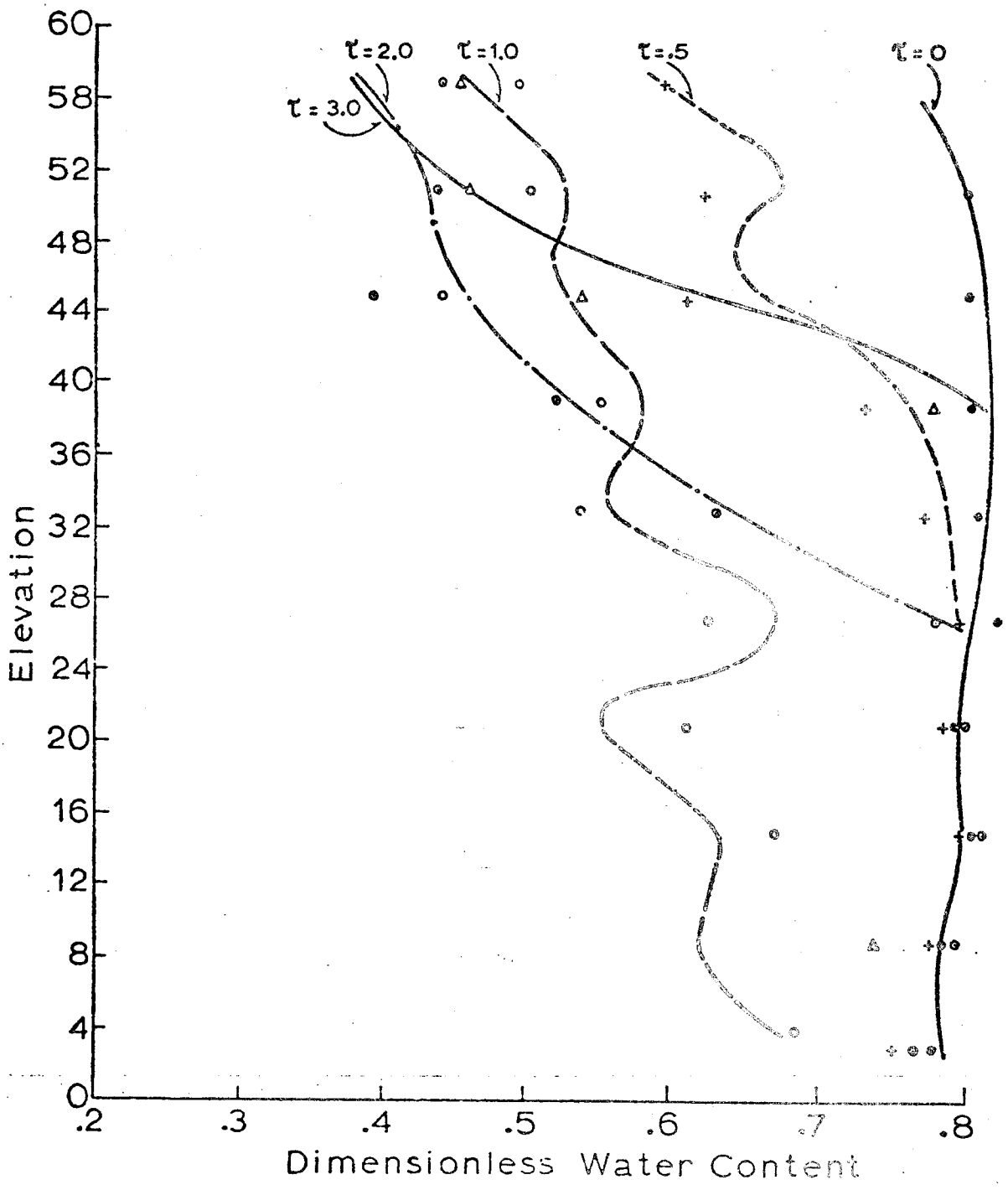

Figure 28. Comparison of measured (symbols) and predicted (solid lines) water content profiles at selected times during the rapid drainage - rewet experiment.

difference is not unreasonable, differences in Θ of as much as 4.8×10^{-2} were observed. The greatest differences were observed for the $\tau = 1.0$ profile.

The average difference between measured and computed values of Φ and Θ for the rapid drainage - rewet experiment were 25% and 100% respectively, greater than for the slow drainage experiment. A portion of the increased difference found in the rapid drainage experiment could be attributed to a greater uncertainty in the measured data. The response time of the tensiometers, although short at high water contents, could introduce small errors in measured Φ values in a rapidly changing system. Similarly, the water content calculated for a 15 second counting interval was assumed to apply at the mid point of the interval. This assumption is valid if the water content is a linear function of time; however, errors would be introduced if $d^2\Theta/d\tau^2$ is not equal to zero. Although $d^2\Theta/d\tau^2$ was generally greater in the rapid drainage - rewet experiment than in the slow drainage - rewet experiment, it seems unlikely that this would contribute significantly to the greater difference between measured and predicted Θ values.

In the rapid drainage experiment, the column was drained at a rate approximately twice that at which the hysteresis information was collected. If $\Theta(\Phi)$ is rate dependent, the empirical equations used to represent $\Theta(\Phi)$ may not be applicable to the rapid drainage situation and consequently, could introduce errors into the predicted pressure head and water content values.

The difference between the predicted and measured water contents could be attributed primarily to the differences in the profiles at $\tau = 1.0$ (Figure 28). An explanation is not evident; however, it is possible that

the differences observed at $\tau = 1.0$ are the result of an anomalous drainage pattern caused by the drainage of the medium adjacent to the lower porous barrier.

Considering the greater stress placed upon the numerical solution by a rapidly changing system, as well as the greater uncertainty in the measured data, the agreement between the measured and predicted results for the rapid drainage - rewet experiment were considered to be quite good. A time dependence of $\Omega(\Phi)$, if present, did not appear to seriously limit the predictive capability of the numerical solution.

3. Cyclic Boundary Condition Experiment

Figures 29 and 30 show the measured and predicted pressure head and water content respectively at positions 39 and 45 during the cyclic boundary condition experiment. As indicated in Figure 29, the predicted pressure heads were consistently lower than those measured. In initiating the experiment, the column was drained until the water table was at an elevation of 26 cm and maintained in this condition until a state of static equilibrium was approached. As shown by Topp et al (1967), in going from a transient condition to one of static equilibrium, the water content corresponding to a particular pressure head can decrease. When the cyclic boundary condition was applied in this experiment, the column may have commenced to drain along some curve other than the main drainage curve. It could be argued that this would result in predicted pressure heads which were lower than those measured; however, after the first drainage cycle, position 45 (Figure 29) rewet to a pressure head of almost 0.0 or, was in the saturated condition and would proceed along the main drainage curve during the next drainage cycle. The second drainage was predicted with no greater accuracy than was the first. In addition, at positions where

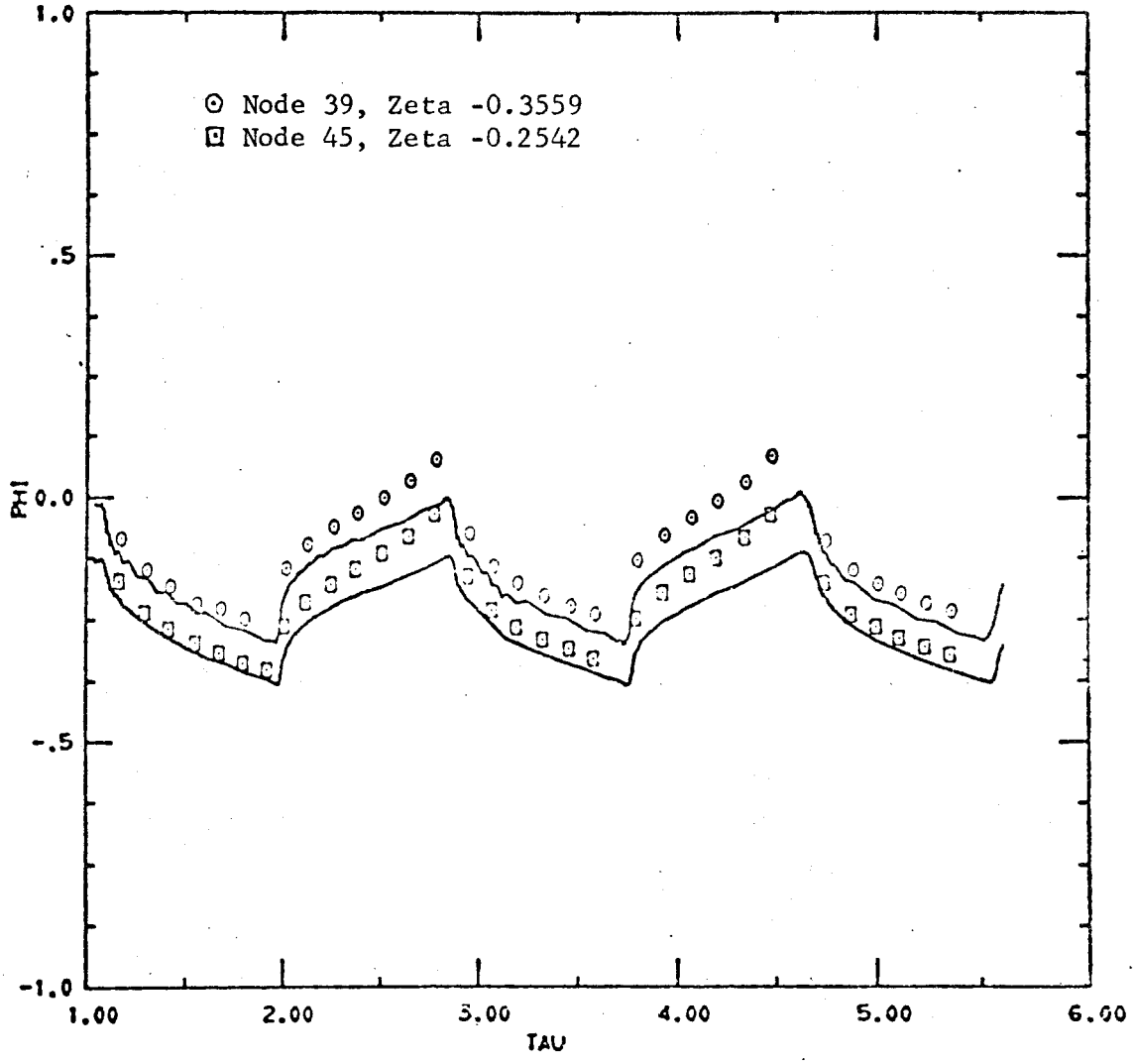

Figure 29. Comparison of measured (symbols) and predicted (solid lines) dimensionless pressure head versus time during the rapid drainage - rewet experiment.

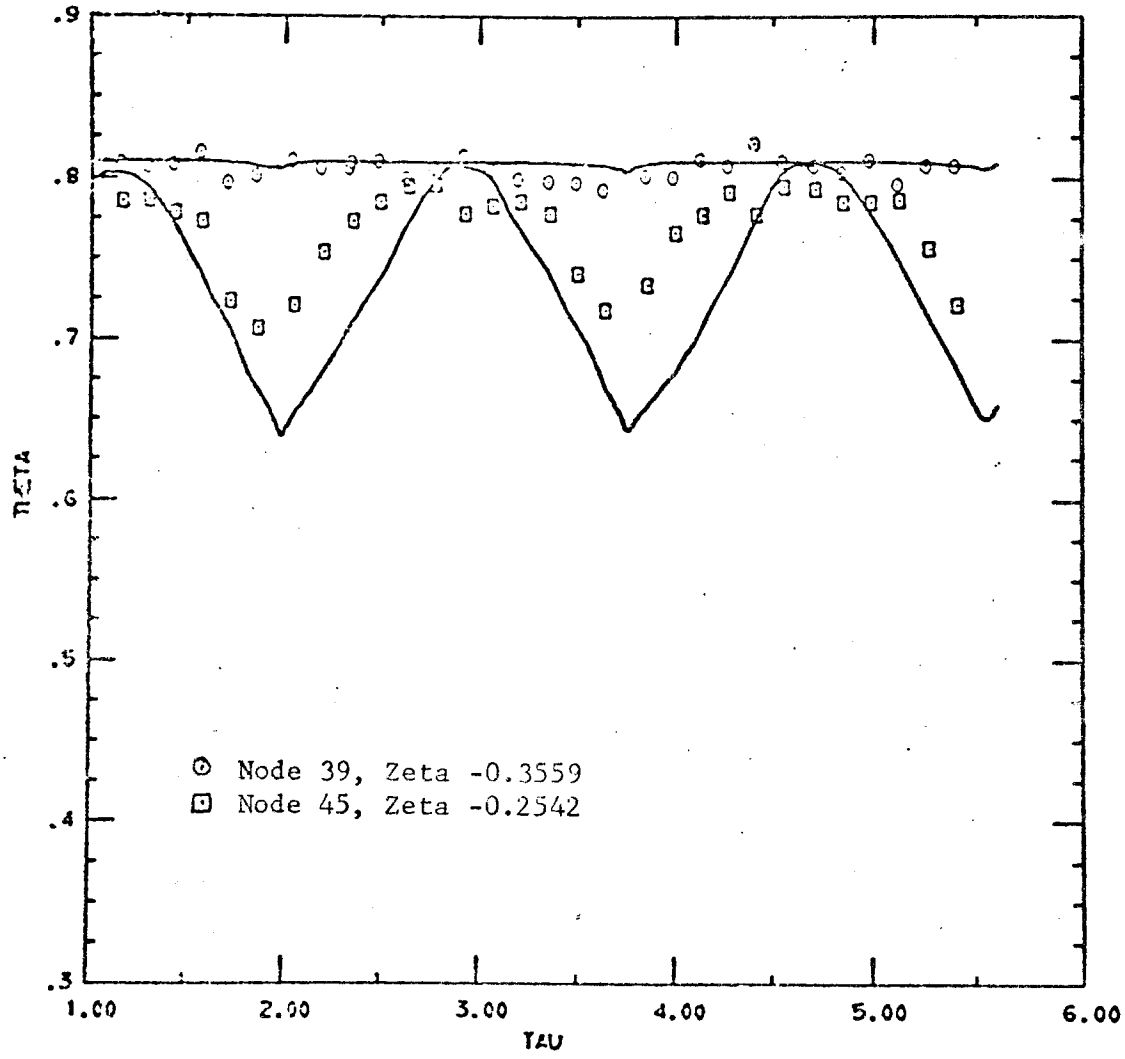

Figure 30. Comparison of measured (symbols) and predicted (solid lines) dimensionless water content versus time at positions 39 and 45 for the cyclic boundary condition experiment.

there was no drainage (position 39 and lower), the pressure heads were predicted with no greater accuracy than at positions where drainage did occur. This suggests that the difference between predicted and measured pressure heads was not caused by a time dependence of $\Theta(\Phi)$ during initiation of the experiment.

The consistently low predicted pressure heads resulted in consistently low predicted water contents (Figure 30). Both the numerical and measured results indicate little or no drainage at position 39. Although differences between predicted and measured results were as great as $h = 6.0$ cm and $\theta = 0.03$ (volumetric water content), it must be remembered that a cyclic step change at the boundary induces a strongly hysteretic flow system and consequently, a very difficult situation to simulate numerically.

In the cyclic boundary condition experiment, during the first cycle, the column would drain and wet along the main drainage and primary wetting scanning curves respectively. Additional cycles would proceed along secondary and consecutively higher orders of families of scanning curves. The fact that the agreement between predicted and measured results did not become worse as more cycles were performed suggests that the use of only the primary scanning curves is a reasonable approximation.

4. Non-hysteretic and Uniform Medium Simulations

In the previous sections, it was shown that if the medium was considered to be non uniform and $\Theta(\Phi)$ hysteretic, then the numerical solution could predict $\Theta(\bar{z}, \tau)$ and $\Phi(\bar{z}, \tau)$ for the drainage-rewet experiments quite accurately. Although not a major objective of this study, some consideration was given to the completeness with which $\Theta(\Phi, \bar{z})$ and $\kappa(\Theta, \bar{z})$ must be specified in order to obtain reasonably accurate predicted results.

In addition to the hysteretic and non-uniform case discussed previously, two additional simulations of the slow drainage-rewet experiment were performed:

1) $\Theta(\Phi)$ was assumed to be non-hysteretic. Only the main drainage curve at each position in the column was specified. As a result, when the rewet phase of the experiment was encountered, the water capacity and subsequently Θ, continued to be calculated using the main drainage curve rather than the appropriate wetting curve.

2) The medium was assumed to be uniform. The position dependent conductivity $\kappa(\Theta, \bar{z})$ was described by specifying different values of the parameters α and η (see equation 13) for each position. The values of α and η for all positions were averaged, resulting in an average $\kappa(\Theta)$ function which was assumed to apply over the entire column. Similarly, average sets of the parameters needed to describe the wetting and drying scanning curves were determined.

The difference between the measured and each predicted result including the hysteretic non-uniform case was found to be:

	*Average Difference Between Measured and Predicted Results			
	Pressure Head		Water Content	
	Φ	h(cm)	Θ	θ
Hysteretic Non-Uniform	1.2×10^{-2}	0.72	1.7×10^{-2}	6.5×10^{-3}
Non-Hysteretic Non-Uniform	1.2×10^{-2}	0.72	5.6×10^{-2}	2.2×10^{-2}
Hysteretic Uniform	3.1×10^{-2}	1.26	4.4×10^{-2}	1.8×10^{-2}

*The average was calculated using the difference between measured and predicted values at τ = 2,3,4 and 5.5. Positions above node no. 51 were excluded.

The three methods of simulating the slow drainage - rewet experiment all predicted the measured values of pressure head with a high degree of accuracy. The difference between measured and predicted Φ values was no greater when the medium was assumed to be non-hysteretic than when assumed to be hysteretic. This result was unexpected. No comparison of hysteretic and non-hysteretic predicted pressure heads was found in the literature. The water capacity determined at a particular Φ value on the main drainage curve would be quite different from that determined at the same Φ value on a wetting curve. Furthermore, the water content determined from the drainage curve, and subsequently $\kappa(\Theta)$ would be greater than that determined from the wetting curve. It is possible that during the wetting phase of the drainage - rewet experiment, the error in the water capacity was compensated by the error in the conductivity, the net result being good agreement between the measured Φ values and those predicted by the non-hysteretic simulation. Since only one material was considered, and one experimental situation, it is not suggested that the predicted pressure heads are generally independent of hysteresis.

When the column was considered to be uniform, the difference between measured and predicted Φ values was greater than that found for the hysteretic non-uniform simulation. Nevertheless, the agreement between measured and predicted results was quite good. The degree of non-uniformity in the medium did not appear to affect seriously the predicted Φ values.

Significantly greater difference was found between measured and predicted values of Θ for the non-hysteretic and uniform medium simulations than was exhibited by the hysteretic non-uniform case. Figure 31 shows the measured $\Theta(Z)$ and three computed $\Theta(Z)$ profiles corresponding to the three simulations for $\tau = 3$ and $\tau = 5.5$. The average difference between measured

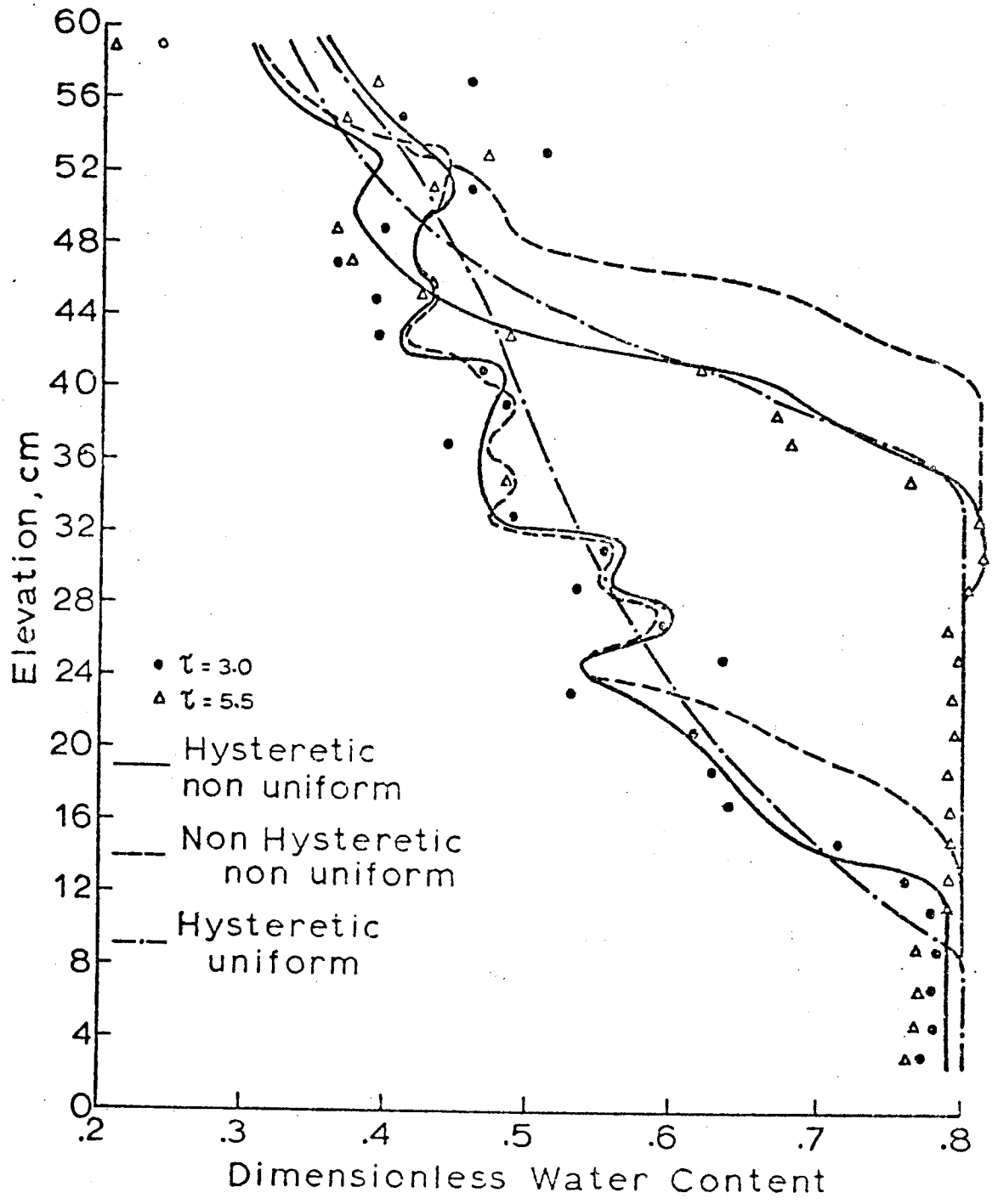

Figure 31. Water content profiles for the three simulations of the slow drainage-rewet experiment. The symbols show the measured data for two selected values of time while the lines show the results of the simulations.

Θ values and those predicted by the non-hysteretic similation was 5.6 $\times 10^{-2}$; however, as indicated in Figure 31, differences greater than 2.0 $\times 10^{-1}$ were observed during the wetting phase of the experiment. (At $\tau = 3$, positions below 27 were wetting, while at $\tau = 5.5$, all positions in the column were wetting.) As expected, from a consideration of the shapes of the main drainage curve and the wetting scanning curves, during the wetting phase of the experiment, the non-hysteretic solution predicted water contents considerably greater than those measured.

In contrast to the non-uniform simulation, the uniform simulation predicted uniform $\Theta(\bar{Z})$ profiles (Figure 31). As indicated in the previous table, the average difference between measured and predicted Θ values was greater when the column was considered to be uniform rather than non-uniform. Since an attempt was made to pack the column uniformly, it appears that what might be considered a minor non-uniformity in a natural flow system could produce quite significant errors in predicted water content values.

V. CONCLUSIONS

1. The conductivity measurements indicated that for the material used, Wray Dune Sand, $\kappa(\Theta)$ was not significantly hysteretic.
2. The good agreement found between the predicted and measured values of Φ and Θ for the slow drainage - rewet experiment indicated that under the conditions of this experiment:
   a) The unsaturated flow equation is an adequate description of the flow process.
   b) The numerical solution used was an adequate solution of the flow equation for a non-uniform medium. The scale of the non-uniformity in the medium used was rather small. It is not necessarily true that the procedure used would work equally well for a medium having zones with large textural differences.
3. Conclusion 2(b) implies that the empirical forms used, adequately represented the hydraulic functions $\kappa(\Theta)$ and $\Theta(\Phi)$ for the non-uniform medium. In the empirical equation used to represent the hysteretic $\Theta(\Phi)$ function, equation 14, e was found to be equal to zero. For wetting curves, β and Φ_o were found to be linear functions of Θ_r, while for drainage curves there did not appear to be any simple functional relationship between β, Φ_o and Θ_o. Further studies are needed to assess the generality of the methods used to describe the families of wetting and drying scanning curves.
4. The agreement between the predicted and measured results of the rapid drainage - rewet experiment was considered to be adequate although not as good as for the slow drainage experiment. The decreased accuracy could not be traced to a rate dependence of $\Theta(\Phi)$.

5. The cyclic boundary condition experiment did not indicate that secondary scanning curves should be incorporated into a description of the hysteretic $\Theta(\Phi)$ function. The poor agreement between measured and predicted results for this experiment could have resulted from the collection of insufficient data in regions where changes were occurring most rapidly, or by an inadequate flow control system.
6. The non-hysteretic simulation of the slow drainage - rewet experiment predicted the pressure head distribution with as great an accuracy as did the hysteretic simulation. This could have considerable significance in the solution of flow problems where the head distribution is the question of greatest interest. Further experimentation needs to be conducted in order to test the generality of this result. The non-hysteretic simulation resulted in large errors in the predicted water content values.
7. The hysteretic uniform medium simulation suggested that small non-uniformities in the medium could cause significant errors in the predicted water content values.

LIST OF REFERENCES

Collis-George, N. and M. J. Rosenthal. 1966. Proposed outflow method for the determination of the hydraulic conductivity of unsaturated porous materials. Austral. Jour. Soil Res. 4:165-180.

Davidson, J. M., J. W. Biggar and D. R. Nielsen. 1963. Gamma radiation intensity for measuring bulk density and transient water flow in porous materials. Jour. Geophysical Res. 68:4777-4783.

Ferguson, J. and W. H. Gardner. 1962. Water content measurement in soil columns by gamma-ray absorption. Soil Sci. Soc. Amer. Proc. 26:11-14.

Freeze, R. Allan. 1969. The mechanism of natural ground-water recharge and discharge. 1. One dimensional, vertical, unsteady, unsaturated flow above a recharging or discharging ground-water flow system. Water Resources Res. 5:153-171.

Freeze, R. Allan and James Banner. 1970. The mechanism of natural ground-water recharge and discharge. 2. Laboratory column experiments and field measurements. Water Resources Res. 6:138-155.

Hanks, R. J., A. Klute and E. Bresler. 1969. A numeric method for estimating infiltration, redistribution, drainage and evaporation of water from soil. Water Resources Res. 5:1064-1069.

Hanks, R. J. and S. A. Bowers. 1962. Numerical solution of the moisture flow equation for infiltration into layered soils. Soil Sci. Soc. Amer. Proc. 26:530-534.

Ibrahim, H. I. and W. Brutsaert. 1968. Intermittent infiltration into soils with hysteresis. Jour. of Hydraulics Div., ASCE 94:113-137.

King, L. G. 1965. Description of soil characteristics for partially saturated flow. Soil Sci. Soc. Amer. Proc. 29:359-362.

Klute, A. 1971. Soil water flow theory and its application in field situations. Presented as part of a symposium on the Field Soil Moisture Regime, Soil Sci. Soc. Amer., August 1971, New York, N.Y. In press.

Klute, A. and D. B. Peters. 1966. Hydraulic and pressure head measurement with strain gauge pressure transducers. International Association of Scientific Hydrology Proceedings of the Wageningen Symposium - Water in the Unsaturated Zone, 156-165.

Philip, J. R. 1969. Theory of infiltration. Advances in Hydroscience 5: 216-291.

Poulovassilis, A. 1962. Hysteresis of pore water, an application of the concept of independent domains. Soil Sci. 93:405-412.

Remson, Irwin, G. M. Hornberger and F. J. Molz. 1971. Numerical methods in subsurface hydrology. Wiley-Interscience, N.Y.

Richtmyer, R. D. 1957. Difference methods for initial value problems. Interscience Publisher, New York.

Rogers, J. S. and A. Klute. 1971. The hydraulic conductivity - water content relationship during nonsteady flow through a sand column. Soil Sci. Soc. Amer. Proc. 35:695-700.

Rubin, J. 1967. Numerical method for analyzing hysteresis-affected, post-infiltration redistribution of soil moisture. Soil Sci. Soc. Amer. Proc. 31:13-20.

Rubin, J. and R. Steinhardt. 1963. Soil water relations during rain infiltration. I. Theory. Soil Sci. Soc. Amer. Proc. 27:246-251.

Smiles, D. E., G. Vachaud and M. Vauclin. 1971. A test of the uniqueness of the soil moisture characteristics during transient, nonhysteretic flow of water in a rigid soil. Soil Sci. Soc. Amer. Proc. 35:534-539.

Staple, W. J. 1970. Predicting moisture distributions in rewetted soils. Soil Sci. Soc. Amer. Proc. 34:387-392.

Staple, W. J. 1969. Comparison of computed and measured moisture redistribution following infiltration. Soil Sci. Soc. Amer. Proc. 33:840-847.

Topp, G. C. 1969. Soil-water hysteresis measured in a sandy loam and compared with the hysteretic domain model. Soil Sci. Soc. Amer. Proc. 33: 645-651.

Topp, G. C., A. Klute and D. B. Peters. 1967. Comparison of water content-pressure head data obtained by equilibrium, steady state and unsteady state methods. Soil Sci. Soc. Amer. Proc. 31:312-314.

Topp, G. C. and E. E. Miller. 1966. Hysteretic moisture characteristics and hydraulic conductivities for glass bead media. Soil Sci. Soc. Amer. Proc. 30:156-162.

Vachaud, G. and J. L. Thony. 1971. Hysteresis during infiltration and redistribution in a soil column at different initial water contents. Water Resources Res. 7:111-127.

Watson, K. K. 1966. An instantaneous profile method for determining the hydraulic conductivity of unsaturated porous materials. Water Resources Res. 2:709-715.

Whisler, F. D. and A. Klute. 1965. The numerical analysis of infiltration, considering hysteresis, into a vertical soil column at equilibrium under gravity. Soil Sci. Soc. Amer. Proc. 29:489-494.

APPENDIX A

Table I. Main drainage and main wetting curve parameters assigned to the various positions for the numerical calculations.

Positions	Θ_o	Θ_r	Main drainage Φ_o	Main drainage β	Main wetting Φ_o	Main wetting β
(1-8)	0.790	0.220	-0.6864	-3.800	-0.4438	-1.489
(9-10)	0.795	0.260	-0.7106	-3.650	-0.4828	-1.495
(11-12)	0.795	0.230	-0.6714	-3.647	-0.4483	-1.700
(13-14)	0.798	0.265	-0.6916	-4.695	-0.4509	-1.663
(15-22)	0.800	0.250	-0.6610	-2.985	-0.4333	-1.778
(23-24)	0.800	0.240	-0.6427	-2.568	-0.3910	-1.787
(25-26)	0.800	0.240	-0.6711	-2.120	-0.4141	-1.867
(27-28)	0.810	0.240	-0.6711	-2.517	-0.4368	-1.618
(29-30)	0.810	0.240	-0.6518	-2.740	-0.3976	-1.788
(31-32)	0.810	0.250	-0.6823	-2.517	-0.4406	-1.636
(33-34)	0.820	0.255	-0.6040	-2.458	-0.3970	-1.789
(35-36)	0.810	0.255	-0.6142	-2.422	-0.3980	-1.789
(37-38)	0.810	0.220	-0.6402	-2.311	-0.3585	-1.740
(39-40)	0.810	0.220	-0.6402	-2.311	-0.3969	-1.711
(41-42)	0.810	0.180	-0.6511	-2.311	-0.4157	-1.622
(43-46)	0.810	0.180	-0.5876	-2.032	-0.3642	-1.622
(47-48)	0.800	0.180	-0.5912	-1.979	-0.3570	-1.700
(49-50)	0.800	0.200	-0.6009	-1.979	-0.3570	-1.750
(51-52)	0.800	0.200	-0.6184	-2.120	-0.3732	-1.833
(53-54)	0.790	0.250	-0.6313	-2.120	-0.3672	-1.944
(55-60)	0.760	0.250	-0.5338	-2.300	-0.3774	-2.187
Average Parameters	0.800	0.240	-0.6451	-2.850	-0.4010	-1.756

Table 2. Conductivity function parameters assigned to the various positions for the numerical calculations.

Positions	η	κ_o
(1-4)	4.979	1.039
(5-6)	5.031	1.319
(7-8)	4.711	1.147
(9-10)	5.023	1.012
(11-12)	5.459	1.298
(13-14)	6.227	1.252
(15-16)	5.680	1.047
(17-18)	5.604	1.215
(19-20)	5.585	1.360
(21-22)	5.723	1.371
(23-24)	5.875	1.221
(25-26)	6.250	1.309
(27-28)	6.043	1.126
(29-30)	5.431	1.306
(31-32)	5.569	1.058
(33-34)	5.073	1.061
(35-36)	5.400	1.241
(37-38)	5.803	1.314
(39-40)	6.095	1.382
(41-44)	6.250	1.310
(45-46)	4.936	1.020
(47-48)	4.910	1.136
(49-50)	4.822	1.368
(51-52)	5.414	1.079
(53-54)	6.100	1.108
(55-60)	5.830	1.437
Average Parameters	5.561	1.225